VILNIUS UNIVERSITY
CENTRE FOR PHYSICAL SCIENCES AND TECHNOLOGY

ARŪNAS TUZIKAS

NICHE APPLICATIONS OF SOLID-STATE LIGHTING WITH CONTROLLABLE COLOUR-RENDITION, SPATIAL, PHOTOCHEMICAL, AND PHOTOBIOLOGICAL PROPERTIES

Doctoral thesis
Materials science (08T)

Vilnius, 2014

The research work has been carried out in 2010-2014 at the Semiconductor Physics Department and the Institute of Applied Research, Vilnius University.

Scientific supervisor:

Prof. habil. dr. Artūras Žukauskas (Vilnius University, Technological Sciences, Materials Science – 08T).

Consultant:

Prof. dr. Rimantas Vaicekauskas (Vilnius University, Physical Sciences, Informatics – 09 P).

VILNIAUS UNIVERSITETAS
FIZINIŲ IR TECHNOLOGIJOS MOKSLŲ CENTRAS

ARŪNAS TUZIKAS

KIETAKŪNIO APŠVIETIMO SU VALDOMOMIS SPALVŲ PERTEIKIMO, ERDVINĖMIS, FOTOCHEMINĖMIS IR FOTOBIOLOGINĖMIS SAVYBĖMIS NIŠINIAI TAIKYMAI

Daktaro disertacija
Medžiagų inžinerija (08T)

Vilnius, 2014

Disertacija rengta 2010-2014 metais Vilniaus universiteto Puslaidininkių fizikos katedroje ir Taikomųjų mokslų institute.

Mokslinis vadovas:

Prof. habil. dr. Artūras Žukauskas (Vilniaus universitetas, technologijos mokslai, medžiagų inžinerija – 08T).

Konsultantas:

Prof. dr. Rimantas Vaicekauskas (Vilniaus universitetas, fiziniai mokslai, informatika – 09 P).

Reziumė

Nors šviesos diodo (toliau šviestuko) atsiradimo istorija siekia 1907 metus, kai Henry Joseph Round žurnale *Electrical World* aprašė silicio karbido kristalo švytėjimą [1] kuris, kaip išaiškėjo vėliau, buvo sąlygotas injekcinės elektroliuminescencijos, tačiau tik pastarąjį dešimtmetį šviestukų taikymai bendrojo ar specializuoto apšvietimo srityse įgavo didelį mastą. Dėl didelio efektyvumo bei mažų matmenų šiandien jie tapo nepakeičiami vaizduoklių gamyboje (tiek mobiliuosiuose įrenginiuose, tiek kompiuterių monitoriuose bei televizoriuose) ir ima vyrauti tokiose taikymuose kaip biuro, gyvenamųjų gamybinių ir sandėliavimo patalpų, prekių, reklaminis, architektūrinis bei lauko apšvietimas.

Galimybė komponuoti šviesos spektrinės galios skirstinį iš siaurą spektrinę juostą turinčių šviestukų komponenčių daro tokį apšvietimą labai universaliu. Pavyzdžiui tos pačios spalvinės temperatūros ir šviesos srauto apšvietimas gali būti realizuojamas naudojant begalę skirtingą ar tą patį spalvį turinčių (metamerinių) spektrinės galios skirstinių, pasižyminčiu: a) skirtingomis spalvų perteikimo savybėmis: sodrinimu, blukinimu ar aukšta spalvų atgava; b) skirtingu fotocheminiu poveikiu apšviečiamų paviršių pigmentams; c) skirtingu fotobiologiniu poveikiu žmogaus cirkadiniam ritmui; d) skirtingu šviesos veiksmingumu ir kt. Šviesos šaltinis, sudarytas iš tiesioginės emisijos bei konversijos fosfore šviestukų telkinio kartu su mikrokontrolerine valdymo sistema, gali būti derinamas siekiant išryškinti vieną ar kitą minėtą savybę. Tokį šviestuvą papildžius ryšio moduliu galima būtu realizuoti išmaniąsias apšvietimo sistemas, pavyzdžiui gatvių apšvietimo instaliacijas, gebančias prisitaikyti prie eismo srauto bei klimatinių sąlygų, kas leistų taupyti daugiau elektros energijos.

Nepaisant naujų galimybių, kurias teikia kietakūnė technologija, daugelyje nišinių taikymų sričių, tokių kaip dailės kūrinių apšvietimas ar gatvių apšvietimas, kol kas ne visos jos yra panaudojamos dėl sunkumų, susijusių su spektrinio galios skirstinio parinkimu bei optimizavimu pagal konkrečius apšvietimo kokybei keliamus reikalavimus ar apšvietimo erdvinio skirstinio

parinkimu, užtikrinančiu geriausią balansą tarp elektros energijos taupymo ir tokių subjektyvių įverčių kaip pėsčiojo saugumo jausmas gatvėje.

Šis darbas yra skirtas ištirti kietakūnio apšvietimo su valdomomis spalvų perteikimo, erdvinėmis, fotocheminėmis ir fotobiologinėmis savybėmis galimus taikymus kai kuriose nišinėse srityse. Kaip nišinių taikymų pavyzdžiai, kuriuose ryškiausiai atsiskleidžia valdomo apšvietimo privalumai, buvo pasirinkti dailės kūrinių apšvietimas ir gatvių (lauko) apšvietimas.

Plačiausiai naudojamas apšvietimo spalvinės kokybės įvertis – Tarptautinės apšvietimo komisijos pasiūlytas bendrasis spalvų atgavos rodiklis – nėra tinkamas visapusiškam kietakūnio šviesos šaltinio (paprastai pasižyminčio siauromis spektrinėmis linijomis) charakterizavimui [2], nes jo pateikiamas įvertis parodo tik testuojamo šviesos šaltinio atitikimą etaloniniam (nesukeliančiam spalvinių iškraipymų) šaltiniui ir neįvertina šviesos šaltinio sukeliamų spalvinių pokyčių pobūdžio. Šiame darbe pritaikius statistinę apšvietimo spalvinės kokybės vertinimo metodiką [3], buvo parodyta galimybė realiu laiku valdyti kokybinius apšvietimo spalvinius parametrus – susietąją spalvinę temperatūrą ir sodrinimo/blukinimo gebą ar spalvų atgavos tikslumą. Šios savybės leido atlikti visą eilę subjektyvaus apšvietimo įverčio tyrimų, kurie padėjo identifikuoti pirmenybinio apšvietimo sąlygas įvairiems apšviečiamiems objektams, tokiu būdu validuojant statistinį apšvietimo spalvinės kokybės vertinimo metodą.

Tiriant pirmenybinių apšvietimo sąlygų pasirinkimą įvairiems dailės kūriniams buvo nustatytos pirmenybinės susietosios spalvinės temperatūros vertės bei spalvų sodrinimo gylis trims skirtingos technikos bei tematikos dailės kūriniams ir parodyta, kad pirmenybinės apšvietimo sąlygos priklauso ne tik nuo apšviečiamo objekto savybių bet ir nuo stebėtojo (žiūrovo) kultūrinės kilmės.

Disertacijoje taip pat buvo atsižvelgta į apšvietimo fotocheminį poveikį apšviečiamiems paviršiams. Esant fiksuotai apšvietai (pagal dailės kūrinių apšvietimo reikalavimus), šviesos žalingas poveikis dailės kūrinių pigmentams kinta keičiant kokybinius apšvietimo parametrus. Pavyzdžiui, didinat spalvinę temperatūrą šviesos žalingas poveikis gali išaugti iki dviejų kartų. Šiame darbe

buvo pasiūlytas sprendimas fiksuoti fotocheminę žalą, keičiant išmanaus šviestuvo parametrus ir pademonstruota tokio fiksavimo įtaka muziejinių eksponatų vizualizavimui.

Nagrinėjant šviestukais grįsto apšvietimo pritaikymą gatvių apšvietimui buvo išnagrinėti šie aspektai: a) priimtiniausio apšvietimo erdvinio skirstinio nustatymas pėsčiųjų zonoje; b) žemos spalvinės temperatūros kietakūnio šaltinio naudojimas mezopinėmis sąlygomis.

Atsižvelgiant į tokius kriterijus kaip saugumo ir komforto jausmas buvo parodyta kad pėsčiųjų zonai priimtiniausiam apšvietimo erdviniam skirstiniui didžiausia įtaką daro arčiausiai stebėtojo esantis šviestuvas, kai tuo tarpu apšvietos lygis už 100 m nuo stebėtojo jam yra praktiškai nereikšmingas. Tokie rezultatai yra svarbus projektuojant dinamiškai valdomą apšvietimą pėsčiųjų zonose.

Sumodeliavus ir sukūrus žmogaus miegą mažai trikdantį žemos spalvinės temperatūros kietakūnį šviesos šaltinį, buvo ištirtas tokio šaltinio panaudojimo galimybės lyginant jį su dabar plačiausiai naudojamais gatvių šviesos šaltiniais. Buvo parodyta, kad toks apšvietimas pasižymi visa eile privalumų: geresne spalvų atgava, mažesniu melatonino sekrecijos slopinimu, mažesne šviesos tarša.

Acknowledgments

I would like to gratefully acknowledge the support of my supervisor prof. Artūras Žukauskas and consultant prof. Rimantas Vaicekauskas during this work.

My special thanks goes to prof. Michael Shur for hosting my internships at Rensselaer Polytechnic Institute.

Also I thank dr. Pranciškus Vitta for valuable discussions and advice. I would like to thank all my friends and colleagues for help.

Separately I would like to thank co-authors of my publications for great team work and multidisciplinary collaboration during the research and publication preparation process.

I would like to express my heartfelt thanks to my parents, wife and daughter for their constant support and encouragement through the duration of my studies.

This work has been supported in part by the Research Council of Lithuania and by the National Science Foundation of the U.S.A. under the Engineering Research Centers Program.

Table of Contents

List of abbreviations

CCT	Correlated colour temperature
CDI	Colour dulling index
CFI	Colour fidelity index
CIE	Commission Internationale de l'Éclairage (International Commission on Illumination)
CL_A	Photopic "circadian light" of a light source normalized to that of the CIE standard illuminant A
CQS	Colour quality scale
CRI	Colour rendition index
CSI	Colour saturation index
F-M	Fransworth-Munsell
FWHM	Full width at half maximum
GAI	Gamut area index
HDI	Hue distortion index
ipRGC	Intrinsically photosensitive retinal ganglion cells
LDI	Lightness distortion index
LED	Light-emitting diode
LER	Luminous efficacy of radiation
LPS	Low pressure sodium lamp
MCLI	Mesopic circadian light index
MFII	Mesopic filtered instrumental index
MGVI	Mesopic general visual index
MLYI	Mesopic eye lens yellowing index
MMSI	Mesopic melatonin suppression index
pc	Phosphor converted
PLC	Power line communication
PWM	Pulse width modulation
Q_f	Colour fidelity scale
Q_g	Colour gamut scale
R_a	CIE general colour rendition index
RDF	Relative damage factor
SDS	Semantic differential scale
SPD	Spectral power distribution
SSL	Solid-state lighting

1. Introduction

The history of the discovery of light emitting diodes seeks 1907, when in his paper in *Electrical World* [1], Henry Joseph Round described the "bright glow" of a silicon carbide crystal on applying voltage. As it turned out later, this glow was due to injection electroluminescence. However only in the past decade, the applications of LEDs in the general or special lighting applications reached colossal scale. Nowadays, due to the high efficacy and small dimensions, LEDs have become indispensable in applications such as display backlighting (in mobile phones, computer displays, etc.) and is becoming the dominant technology in office, residence, industrial, warehouse, commercial, advertisement, architectural, and outdoor lighting. However, such properties as the ability to control the SPD and spatial pattern as well as the advantages offered by dynamic control are still not realized to full extent. Moreover, the application of solid-state lighting raised new challenges related to the general colour rendition index, which is not suitable for predicting the colour-rendering rank order of LED based light sources [2], as well as to circadian and photochemical action of light, etc.

Main goal:

The thesis is aimed at the investigation of niche applications of solid-state lighting with controllable colour-rendition, spatial, photochemical, and photobiological properties.

In order to employ the controllability of LED based lighting technology, we focussed our research on such niche applications as artwork illumination and street (outdoor) lighting. The illumination of artworks must meet conservation requirements and pursue adequate visual impression. The latter aspect is also related to the selection an adequate metric for the assessment of colour rendition. For street lighting, the dynamic tracking the traffic participants, implemented using different dimming scenarios and lighting patterns around a traffic participant, must be applied and the SPD must be optimized for low human circadian action.

Main objectives:

- Validate the statistical metric of the colour rendition of illumination using a solid-state source of light with continuously tuneable SPD.
- Investigate preferences to colour rendition for subjects with different cultural background and for paintings with different familiarity level to subjects participating in the experiment.
- Evaluate the effect of the controlled photochemical impact of light on visual impression from artworks while varying the parameters of the colour quality of illumination, such as CCT, saturation factor and chromaticity deviation from the Planckian locus.
- Establish the main subjective assessment factors of intelligent outdoor lighting and optimize the luminance distribution around a pedestrian within an intelligent street lighting system.
- Assess a LED-based light source with the SPD optimized for low-circadian-action outdoor lighting by quantifying photobiological and light-pollution properties and by investigating reaction time, threshold detection of luminance contrasts, and colour discrimination under mesopic vision conditions.

Novelty and importance

By using the statistical approach to the colour quality of illumination, preferential illumination conditions for familiar objects such as fruits and vegetables have been established.

The preferences to the colour quality of illumination for subjects with different cultural background when illuminating paintings with the different level of the familiarity of the content has been investigated.

The algorithm of light dimming for keeping the photochemical damage irradiance over illuminated surfaces constant while varying the qualitative parameters of lighting has been introduced and the effect of such dimming on the visualization of artworks has been demonstrated.

The optimal luminance distribution for pedestrian areas has been investigated using a smart street lighting installation and the main factors for the subjective preference to the assessment of such a distribution have been established.

A blue-amber ("firelight") LED cluster with low circadian action has been introduced and its photometric, colorimetric, colour rendition, photobiological, light-pollution, and psychophysical properties have been assessed.

Statements to defend

- A smart colour rendition engine with continuously tuneable tetrachromatic SPD can be used for the validation of statistical colour rendition metric by subjective distinguishing between illumination conditions that provide high colour fidelity, increased or decreased chromatic saturation, and subjectively preferential colour quality.
- The preferential CCT and colour rendition quality of artwork illumination subjectively established using the colour rendition engine depends on the content of particular artwork as well as on the cultural background of observers.
- The dimming functionality introduced into the smart colour rendition engine for maintaining constant photochemical damage irradiance, while varying the chromaticity and colour rendition properties of the generated light, results in the noticeable alteration of visual impression from artworks.
- When assessing intelligent outdoor lighting installations for pedestrians in a moderately urbanized area, the major factor to be considered is the subjective feeling of well-being and the minor factor is related to the physical properties of the environment. The first factor primarily depends on the luminous flux of the nearest luminaire, whereas the luminous fluxes of the remote luminaires are less important.
- A balanced approach to the energy saving and performance of solid-state lighting for outdoor environments can be implemented using a blue-amber ("firelight") LED sources with ultralow CCT (1800-1900 K), which have

acceptable properties in terms photobiological hazard, light pollution, and psychophysical functioning under mesopic conditions.

Layout of the thesis

The thesis consists of five chapters divided into sections. The introduction, list of publications, main goal and objectives, novelty, and statements to defend are presented in Chapter 1.

The original results of the thesis are presented in Chapters 2-5. These chapters contain sections presenting a survey on the existing knowledge on the subject under study, existing knowledge gaps, and specific objectives of the original research. The main results in each of these chapters are concluded in the last subchapter.

In Chapter 2, the existing colour rendition metrics are overviewed and a smart colour rendition engine, which allows for continuously tuning metameric spectra with different colour rendition properties, is introduced. The results on the subjective validation of the statistical colour rendition metric using the colour rendition engine are presented.

In Chapter 3, the main requirements for artwork illumination are overviewed and the application of the intelligently controlled colour rendition engine in artwork illumination is investigated in two aspects: a) the establishment of subjective needs in colour quality of illumination as a function of the contents of artworks and the observers' cultural background and b) the effect of the control of photochemical damage irradiance on the visual impression from artworks, while adjusting the chromaticity and colour rendition properties of the illuminant.

Chapter 4 is focused on the application of solid-state technology for outdoor lighting. Here, the results on the optimization of the luminance distribution within an intelligent lighting installation for pedestrian areas using the identification of subjective impressions by Likert scale and SDS are presented.

In Chapter 5 the low-circadian action LED source for outdoor lighting is introduced and the results on the assessment of photometric, colorimetric,

colour-rendition, photobiological, and light-pollution properties as well as on psychophysical performance (reaction time, contrast and colour discrimination) are presented.

The concluding summary is presented at the end of the thesis.

Author's contribution

Author essentially contributed to the development, calibration, and functionalization of the smart colour rendition engine, which is the main instrument for the validation of the statistical colour rendition metric and for the investigation of artwork illumination. Psychophysical research on the investigation of subjective and cultural preferences to artwork illumination was carried out by author during his internship at the Rensselaer Polytechnic Institute (Troy, NY, USA). Author developed the intelligent outdoor lighting system within the Vilnius University campus and participated in psychophysical research on the optimization of luminance distribution for pedestrians. Also, he developed the equipment for the psychophysical investigation of "firelight" LED cluster and participated in research on the assessment of this light source. He also performed a significant portion of work related to the processing of the data of the psychophysical experiments. The interpretation of the results was discussed with the co-authors of the publications and with scientific supervisor prof. A. Žukauskas. The author has prepared the drafts for publications [P9,P11,P14-P18] and personally presented the results of the work at 11 scientific conferences [C1,C5,C7,C10,C12,C15-C17,C23-C25].

List of publications related to the thesis

List of technical papers, conference proceedings and patent applications

P1. A. Žukauskas, R. Vaicekauskas, **A. Tuzikas**, and M. S. Shur, "Solid-state lighting with tailored colour quality," in *Proceedings of the 12th International Symposium on Science and Technology of Light Sources and 3rd International Conference on White LEDs and Solid State Lighting*, M. Haverlag, G. M. W. Kroesen, and T. Taguchi, eds. (FAST-LS, 2010), pp. 363–364.

P2. A. Žukauskas, R. Vaicekauskas, **A. Tuzikas**, P. Vitta, and M. S. Shur, "Statistical approach to color rendition properties of solid state light sources," Proc. SPIE **8123**, 81230X (2011).

P3. P. Vitta, R. Stanikūnas, **A. Tuzikas**, I. Reklaitis, A. Stonkus, A. Petrulis, H. Vaitkevičius, and A. Žukauskas, "Energy-saving approaches to solid state street lighting," Proc. SPIE **8123**, 81231H (2011).

P4. P. Vitta, **A. Tuzikas**, A. Žukauskas, R. Vaicekauskas, A. Petrulis, and M. S. Shur, "Lighting engine for art and museum display," in *Proceedings of the 13th International Symposium on Science and Technology of Lighing*, R. Devonshire and G. Zissis, eds. pp. 343–344 (2012).

P5. A. Žukauskas, R. Vaicekauskas, P. Vitta, **A. Tuzikas**, A. Petrulis, and M. S. Shur, "Color rendition engine," Opt. Express **20**, 5356–5367 (2012).

P6. P. Vitta, L. Dabašinskas, **A. Tuzikas**, A. Petrulis, D. Meškauskas, and A. Žukauskas, "Concept of intelligent solid-state street lighting technology," Electron. Electrotech. **18**, 37–40 (2012).

P7. A. Žukauskas, R. Vaicekauskas, P. Vitta, **A. Tuzikas**, and M. S. Shur, "Polychromatic solid-state light sources for the control of colour saturation of illuminated surfaces," PCT Publ. No WO2013009157 (2013).

P8. A. Žukauskas, R. Vaicekauskas, P. Vitta, **A. Tuzikas**, A. Petrulis, and A. Zabiliūtė, "Solid-state sources of light for preferential colour rendition, " Patent App. No. PCT/LT2013/000004 (2013).

P9. **A. Tuzikas**, A. Liu, A. Žukauskas, R. Vaicekauskas, P. Vitta, A. Petrulis, and M. S. Shur, "Displaying artwork with tunable colour quality," in

Proceedings of the 12th Congress of the International Colour Association, L. MacDonald, S. Westland, and S. Wuerger eds., vol. 1, pp. 43–46 (2013).

P10. A. Liu, **A. Tuzikas**, A. Žukauskas, R. Vaicekauskas, P. Vitta, and M. Shur, "Color preferences revealed by statistical color rendition metric," Proc. SPIE **8835**, 883508 (2013).

P11. A. Liu, **A. Tuzikas**, A. Žukauskas, R. Vaicekauskas, P. Vitta, and M. S. Shur, "Cultural preferences to color quality of illumination of different artwork objects revealed by a color rendition engine," IEEE Photonics J. **5**, 6801010 (2013).

P12. A. Žukauskas, R. Vaicekauskas, **A. Tuzikas**, A. Petrulis, R. Stanikūnas, A. Švegžda, P. Eidikas, and P. Vitta, "Firelight LED source: Toward a balanced approach to the performance of solid-state lighting for outdoor environments," IEEE Photonics J. **6**, 8200316 (2014).

P13. V. Viliūnas, H. Vaitkevičius, R. Stanikūnas, P. Vitta, R. Bliumas, A. Auškalnyte, **A. Tuzikas**, A. Petrulis, L. Dabašinskas, and A. Žukauskas, "Subjective evaluation of luminance distribution for intelligent outdoor lighting," Lighting Res. Technol. **46**, 421– 433 (2014).

P14. A. Žukauskas, R. Vaicekauskas, **A. Tuzikas**, P. Vitta, A. Petrulis, "Daugiaspalviai kietakūniai šviesos šaltiniai skirti fotochemiškai jautrių objektų apšvietimui," (2014) (Patent Application subbmited to Lithuanian Patent Bureau).

P15. **A. Tuzikas**, A. Žukauskas, R. Vaicekauksas, A. Petrulis, P. Vitta, and M. S. Shur, "Artwork visualization using a solid-state lighting engine with controlled photochemical safety," Opt. Express **22**, 16802–16818 (2014).

P16. **A. Tuzikas**, A. Žukauskas, R. Vaicekauskas, A. Petrulis, P. Vitta, and M. Shur, "Smart lighting engine for artwork-specific illumination with controlled photochemical safety," in *Proceedings of the 14th International Symposium on Science and Technology of Lighing* (2014).

P17. A. Petrulis, **A. Tuzikas**, P. Vitta, R. Vaicekauskas, and A. Žukauskas, "Validation of the Kruithof rule in an outdoor environment using a smart solid-state lighting engine," in *Proceedings of the 14th International Symposium on Science and Technology of Lighing* (2014).

List of conference presentations

C1. P. Vitta, **A. Tuzikas**, A. Žukauskas, R. Vaicekauskas, and M. S. Shur, "Colour rendition engineering by a tetrachromatic solid-state lamp," *7th International New Exploratory Technologies Conference* (Turku, Finland, October 19-21, 2010). *Conference Proceedings*, p. 89 (oral presentation).

C2. R. Stanikūnas, A. Švegžda, H. Vaitkevičius, P. Vitta, **A. Tuzikas**, I. Reklaitis, and A. Žukauskas, "Visual search strategies in the contrast sensitivity task in mesopic and photopic conditions," *16th European Conference on Eye Movements* (Marseille, France, August 21-25, 2011), *J. Eye Mov. Res.* **4**(3), p. 160 (poster presentation).

C3. A. Žukauskas, R. Vaicekauskas, **A. Tuzikas**, P. Vitta, and M. S. Shur, "Statistical approach to color rendition properties of solid state light sources," *11th International Conference on Solid State Lighting SPIE Optics+Photonics* (San Diego, California, USA, August 22-24, 2011). *Optical Engineering+Applications, Technical Summaries*, p. 30 (poster presentation).

C4. P. Vitta, R. Stanikūnas, **A. Tuzikas**, I. Reklaitis, A. Stonkus, A. Petrulis, H. Vaitkevičius, and A. Žukauskas, "Energy-saving approaches to solid state street lighting," *11th International Conference on Solid State Lighting SPIE Optics+Photonics* (San Diego, California, USA, August 22-25, 2011), *Optical Engineering+Applications, Technical Summaries*, p. 24 (poster presentation).

C5. **A. Tuzikas**, "Color rendition engineering," *13th International Conference-School Advanced Materials and Technologies* (Palanga, Lithuania, August 27-31, 2011). *Programme and Abstract Book*, p. 85 (poster presentation).

C6. P. Vitta, **A. Tuzikas**, D. Meškauskas, I. Reklaitis, R. Stanikūnas, H. Vaitkevičius, A. Žukauskas, "Energijos taupymo būdai naudojant sumanų kietakūnį gatvių apšvietimą", *39-oji Lietuvos nacionalinė fizikos*

konferencija (Vilnius, Lithuania, October 6-8, 2011). *Programa ir pranešimų tezės*, p. 33 (oral presentation).

C7. **A. Tuzikas**, R. Vaicekauskas, P. Vitta, A. Petrulis, A. Žukauskas, M. S. Shur, "Apšvietimo spalvinės kokybės valdymas kietakūniu šviesos šaltiniu", *39-oji Lietuvos nacionalinė fizikos konferencija* (Vilnius, Lithuania, October 6-8, 2011). *Programa ir pranešimų tezės*, p. 28 (oral presentation).

C8. P. Vitta, **A. Tuzikas**, A. Žukauskas, R. Vaicekauskas, A. Petrulis, and M. S. Shur, "Lighting engine for art and museum display," *13th International Symposium on the Science and Technology of Lighting* (Troy, NY, USA, June 24-29, 2012). *Conference Program and Paper Abstracts*, p 32 (oral presentation).

C9. P. Vitta, **A. Tuzikas**, A. Petrulis, A. Žukauskas, R. Vaicekauskas, and M. S. Shur, "Illumination with tuneable polychromatic LED clusters: Finding individual preferences to colour rendering," *9th International Symphosium on Semiconductor Light Emitting Devices* (Berlin, Germany, July 22-27, 2012). *Programme and Abstract Book*, p. 141 (oral presentation).

C10. **A. Tuzikas**, P. Vitta, A. Petrulis, A. Žukauskas, R. Vaicekauskas, and M. S. Shur, "Solid-state lighting for conserving and intelligent art display," *9th International Symphosium on Semiconductor Light Emitting Devices* (Berlin, Germany, July 22-27, 2012). *Programme and Abstract Book*, p. 178 (oral presentation).

C11. A. Žukauskas, R. Vaicekauskas, **A. Tuzikas**, A. Petrulis, A. Zabiliūtė, and P. Vitta, "Solid- state sources of light for mesopic illumination with minimized circadian action," *Renewable Energy and the Environment Optics and Photonics Congress* (Eindhoven, Netherlands, November 11-14, 2012). *Programme and Abstract Book*, p. JT5A.4 (oral presentation).

C12. A. Liu, **A. Tuzikas**, P. Vitta, R. Vaicekauskas, A. Žukauskas, and M. S. Shur, "Cultural effect on the preferred color quality of illumination revealed by a color rendition engine," *Renewable Energy and the*

Environment Optics and Photonics Congress (Eindhoven, Netherlands, November 11-14, 2012). *Programme and Abstract Book*, p. JT5A.3 (oral presentation).

C13. A. Zabiliūtė, R. Vaicekauskas, P. Vitta, **A. Tuzikas**, A. Petrulis, and A. Žukauskas, "Kietakūniai šviesos šaltiniai, pasižymintys pirmenybine spalvų atgava", *40-oji Lietuvos nacionalinė fizikos konferencija* (Vilnius, Lithuania, June 10-12, 2013). *Programa ir pranešimų tezės*, p. 95 (poster presentation).

C14. A. Petrulis, P. Eidikas, P. Vitta, **A. Tuzikas**, R. Vaicekauskas, R. Stanikūnas, A. Švegžda, A. Žukauskas, "Kietakūniai mezopiniai šviesos šaltiniai, skirti fotobiologiškai draugiškam apšvietimui", *40-oji Lietuvos nacionalinė fizikos konferencija* (Vilnius, Lithuania, June 10-12, 2013). *Programa ir pranešimų tezės*, p. 171 (poster presentation).

C15. **A. Tuzikas**, A. Liu, A. Žukauskas, R. Vaicekauskas, P. Vitta, A. Petrulis, M. S. Shur, "Dailės kūrinių eksponavimas, esant derinamai apšvietimo spalvinei kokybei", *40-oji Lietuvos nacionalinė fizikos konferencija* (Vilnius, Lithuania, June 10-12, 2013). *Programa ir pranešimų tezės*, p. 9 (oral presentation).

C16. **A. Tuzikas**, A. Liu, A. Žukauskas, R. Vaicekauskas, P. Vitta, A. Petrulis, and M. S. Shur, "Displaying artwork with tuneable colour quality," *12th Congress of the International Colour Associacion* (Newcastle upon Tyne, UK, July 8–12, 2013). *Book of Abstracts*, p. 20 (oral presentation).

C17. **A. Tuzikas**, A. Žukauskas, and R. Vaicekauskas, "Enhancing aesthetic pleasure for paintings with tuneable colour quality," *15th International Conference - School Advanced Materials and Technologies* (Palanga, Lithuania, August 27-31, 2013). *Programme and Abstract Book*, p. 98 (poster presentation).

C18. A. Žukauskas, V. Viliūnas, H. Vaitkevičius, R. Stanikūnas, P. Vitta, R. Bliumas, A. Auškalnytė, **A. Tuzikas**, A. Petrulis, and L. Dabašinskas, "Investigation of the subjective factors for the assessment of luminance distributions of intelligent outdoor lighting installations," *10th Biennial*

Conference on Environmental Psychology (Magdeburg, Germany, September 22-25, 2013). *Time Schedule & Abstracts*, pp. 199–200 (poster presentation).

C19. A. Žukauskas, R. Vaicekauskas, P. Vitta, **A. Tuzikas**, A. Petrulis, P. Eidikas, A. Zabiliūtė, R. Stanikūnas, and A Švegžda, "Photobiologically safe and psychophysically acceptable firelight LEDs for outdoor lighting," *10th Biennial Conference on Environmental Psychology* (Magdeburg, Germany, September 22-25, 2013). *Time Schedule & Abstracts*, p. 63 (poster presentation).

C20. P. Vitta, A. Žukauskas, R. Vaicekauskas, P. Eidikas, A. Zabiliūtė, R. Stanikūnas, A. Švegžda, **A. Tuzikas**, and A. Petrulis, "Extra low colour temperature solid-state sources for artificial night lighting," *1st International Conference on Artificial Light at Night* (Berlin, Germany, October 28-30, 2013). *Abstract Book*, p. 111 (oral presentation).

C21. A. Zabiliūtė, R. Vaicekauskas, P. Vitta, **A. Tuzikas**, A. Petrulis, and A. Žukauskas, "Phosphor converted light-emitting diodes with advanced color rendition properties," *Conference on LED and Its Industrial Applications* (Pacifico Yokohama, Japan, April 22-24, 2014). *Extended Abstracts*, p. 24p-LEDp6-32 (poster presentation).

C22. A. Petrulis, **A. Tuzikas**, P. Vitta, R. Vaicekauskas, and A. Žukauskas, "Validation of the Kruithof rule in an outdoor environment using a smart solid-state lighting engine," *14th International Symposium on the Science and Technology of Lighting* (Como, Italy, June 22-27, 2014). *LS14 Conference Program*, CP117 (poster presentation).

C23. **A. Tuzikas**, A. Žukauskas, R. Vaicekauskas, A. Petrulis, P. Vitta, and M. Shur, "Smart lighting for artworks with controlled photochemical safety," *14th International Symposium on the Science and Technology of Lighting* (Como, Italy, June 22-27, 2014). *LS14 Conference Program*, CP75 (poster presentation).

C24. P. Vitta, R. Vaicekauskas, P. Eidikas, A. Zabiliūtė, R. Stanikūnas, A. Švegžda, **A. Tuzikas**, and A. Žukauskas, "Fire-light LEDs for blue-

balanced outdoor lighting," *13th International Conference on Solid State Lighting and LED-based Illumination Systems SPIE Optics+Photonics* (San Diego, California, USA, August 17-21, 2014). *Conference Program*, Paper 9190-13 (oral presentation).

C25. **A. Tuzikas**, A. Petrulis, R. Vaicekauskas, M. S. Shur, and A. Žukauskas, "Smart restorative illumination of artwork and museum exhibits," *13th International Conference on Solid State Lighting and LED-based Illumination Systems SPIE Optics+Photonics* (San Diego, California, USA, August 17-21, 2014). *Conference Program*, Paper 9190-23 (oral presentation).

2. Control and assessment of colour rendition

So far, the assessment and control of the colour rendition quality of illumination remains a problem with no ultimate solution. Despite a large number of colour rendition metrics proposed, their validation usually lacks confidence due to the use of unsystematic sets of light sources with fixed SPDs and due to the difficulties in interpreting subjective judgements on the colour quality of illumination based on ranking of these light sources. In this chapter, we discuss the most important colour rendition metrics and introduce an approach to the assessment of an advanced colour rendition metric (statistical method) based on a smart tetrachromatic light source, which allows for continuously tuning metameric spectra with different colour rendition properties and subjectively selecting the desired colour quality [P1,P2,P5,P8,C1,C3,C5,C7,C9,C13].

2.1. Colour rendition metrics

Since the introduction of advanced fluorescent lamps, the only widely recognized metric for ranking the colour quality of artificial light sources has been the CRI recommended by the CIE [4]. The general CRI (R_a) is based on estimating colour differences within the $U^*V^*W^*$ colour space for 8 test colour samples when a reference standard illuminant (blackbody or daylight phase) is replaced by the SPD of a source under assessment (for sources with chromaticity somewhat different from the reference illuminant, a chromatic adaptation transform based on the von Kries hypothesis [5] is applied). This figure of merit increases toward 100 as the magnitude of the colour differences is reduced to nearly zero, i.e. CRI measures colour fidelity in respect of the reference illuminant. One of the drawbacks of the CRI metric is an inaccurate estimation of the colour differences due to the lack of uniformity of the colour space and the limited accuracy of the chromatic adaptation transform used [6]. Numerous colour spaces with improved perceptual uniformity have been suggested for the refinement of the CRI metric (see [7] and references therein). The most accurate colour-difference estimations are based on the CIECAM02 colour appearance model [6,8].

However starting with the introduction of CRI in 1964, it has been criticized not only for the reduced accuracy, but also for the disregard of subjective preferences to colour rendition. Such preferences are related to the ability of light sources to make colours of illuminated objects appear "vivid" and easy to discriminate. To that end, numerous approaches that consider this aspect of colour quality of lighting, such as the flattery index [9] colour-discrimination index [10], colour-preference index [11], visual clarity approach [12,13], colour-rendering capacity [14], impression of colourfulness [15], index on feeling of contrast [16], and GAI [17] (which measures the area of the polygon embraced by the chromaticity points of the same eight test colour samples used in the general CRI), have been introduced. Basically, these approaches rely on the perceptually positive impact of the increased chroma of rendered colours (colour saturating effect).

Solid-state lighting technology based on both narrow-band (direct-emission) and wide-band (phosphor converted) LEDs dramatically improved the versatility of composing the SPDs of light sources [18]. This inspired numerous experiments on subjective preferences to colour quality of illumination using various solid-state sources of light [2,15,19-25]. These experiments have shown that the CRI-based ranking of light sources contradicts the subjective visual ranking, when solid-state sources of light are compared to other light sources (and to each other) and when white LED light sources are among the light sources used to illuminate an array of coloured objects. As a result, the CIE concluded that CRI is not applicable to predict the CRI rank order of a set of light sources when white LED lamps are involved in the set [2], and recommended the development of a new colour rendering index, or a set of colour rendering indices.

The failure of CRI stimulated a search for advanced colour rendition metrics that would be able to quantify both colour fidelity and subjective preferences to the colour saturating effect. A reasonable approach is the two-metric system, which comprises the general CRI and GAI [17]. An alternative approach is an attempt to quantify the ability of a light source to render object colours with high

fidelity and to discriminate colours within an integral figure of merit, the general CQS [25,26]. This approach is based on the disregard of the colour saturating component in the colour shifts of 15 test colour samples. It also contains numerous refinements, such as the use of more perceptually uniform CIELAB colour space, improved scaling and averaging procedures, CCT factor, and an advanced chromatic adaptation transform. The CQS metric is supplemented by additional scales, such as colour fidelity scale (Q_f , which is the refinement of the general CRI), gamut area scale (Q_g , which is the refinement of GAI), and colour preferences scale (Q_p). The latter scale differs from the general CQS in having additional rewards for increased chroma. Both the two-metric system and CQS suffer from a small number of test colour samples (8 and 15, respectively), which cover a negligible portion of the colour space and make the assessment results dependent on the chosen sample set. The use of a large number of test colour samples requires advanced metrics with the output format different from averaging colour shifts and measuring gamut area.

An example of an advanced colour rendition metric is the colour rendition icon, which graphically condenses information on both the magnitude and direction of the colour shifts for a large number (≥215) of test colour samples [27,28]. However, it might be too tricky to understand for the end-user and is difficult to apply when optimizing and designing light sources with required colour rendition properties.

2.2.Statistical metric of colour rendition

For our investigations, the statistical metric of colour rendition [3] developed by Vilnius university and Rensselaer Polytechnic Institute scientists was selected. Similarly to colour rendition icon [28], the statistical metric is based on a large and systematic set of test colour samples. In spectrophotometrically calibrated Munsell palette of 1269 samples the colour-shift vectors are employed. This statistical metric relies on several novel principles:

- Colour-shift vectors are not more continuously quantified in magnitude and direction, but are rather discretely grouped with respect to particular indices that score certain colour rendition properties;
- The colour-shift vectors are directly compared to known data on chromaticity and luminance discrimination (instead of measuring colour-shift vectors in the coordinates of model colour spaces, which approximate the perceptually uniform colour space with limited accuracy);
- The rating of light sources is presented in explicit numbers that are easy to understand for end-users and can be used for designing sources with predetermined and optimized colour rendition properties.

The statistical metric works as follows. For each of 1269 colour-shift vectors, a colour discrimination shape is built as an elliptical cylinder [3,29] in a three-dimensional chromaticity-luminance space and the colour-shift vector is scored to a particular colour rendition index depending on its behaviour in respect to the shape. The cross-section of the cylinder is a triple-sized MacAdam ellipse [30] which is the region of the just-perceivable chromaticity difference (for a constant luminance of ~48 cd/m^2 used in the definition of the MacAdam ellipses.) The half-height of the shape is three times the just-perceivable luminance difference (0.7%) [5]. Such a shape can be built for any test colour sample by extrapolation of the original MacAdam data for 25 colours. (This metric is independent of the model colour space used.)

Each shape is centred at the colour point of a test colour sample under a reference illuminant. Then the reference illuminant is replaced by the SPD of a light source under assessment and the resulting colour-shift vector is attributed to a particular group. (For sources having chromaticity coordinates that do not exactly match those of the reference illuminant, chromatic adaptation transform similar to that used in CRI [4] or CQS [27] can be applied.) If the colour-shift vector resides within the shape (samples 2, 3, 4, 5, 6, 9, 11, 17 in Fig. 2.1), the colour of the test colour sample under a light source appears as almost indistinguishable from that under the reference illuminant. In this case, the sample is scored up to the statistical Colour Fidelity Index (CFI).

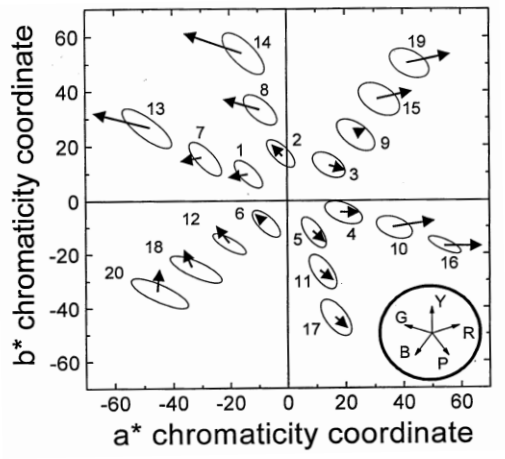

Fig. 2.1. Chromaticity diagram with 20 test colour samples represented by elliptical regions. Each elliptical region contains all colours visually indistinguishable from a colour at the centre of the region. The insert shows the five hue directions that are close to the principle Munsell directions (red, yellow, green, blue and purple). The vectors show colour shifts of the samples when a reference light source is replaced by that under test. Samples 2, 3, 4, 5, 6, 9, 11, 17 score to colour fidelity index; samples 8, 10, 13, 14, 15, 16, 19 score to colour saturation index; samples 12, 18, 20 score to colour dulling index [P7].

Once a vector escapes from the shape, the sample is scored up to one or more other indices, depending on the direction of the vector. When the vector has an excess component directed towards increased chromatic saturation (samples 8, 10, 13, 14, 15, 16, 19 in Fig. 2.1), the sample is scored up to the CSI. Alternatively, when the vector is directed towards decreased chromatic saturation (samples 12, 18, 20 inFig. 2.1) the sample is scored up to the CDI. Other indices, such as HDI or LDI, can be introduced in a similar way, i.e. by scoring up the samples having colour- shift vectors with excess components directed along the hue and lightness axes, respectively.

Of the above statistical indices introduced, two indices (CFI) and (CSI) are directly related to the two criterions, which base the subjective rating of colour rendition, colour fidelity and colour saturating [17]. Other statistical indices for practical light sources are correlated with CFI and CSI and can be used as supplementary ones. For instance, CDI is negatively correlated with CSI, whereas HDI and LDI are negatively correlated with CFI.

The statistical indices are obtained computationally in the single format, which is the percentage of test colour samples scored up to each group. For instance for a light source that keeps 800 vectors out of 1269 within the shapes and draws 200 vectors out of the shapes in the direction of increased chromatic

saturation, CFI is 63% and the CSI is 16%, respectively. Such a format has a very clear meaning and is easy to understand for the end-user. In contrast to the CQS metric and graphical icon, the explicit indices are easy to use in target functions for optimizing the SPDs of light sources with desired colour rendition properties (as was previously done using CRI [31]).

Table 2.1 compares the main features of different colour rendition metrics.

Table 2.1. Comparison of colour rendition metrics [P2].

Metric	Number of samples	Model colour space	Method	Main Output
CIE CRI	8/14	*U*V*W**	Averaging colour shifts	Derivate index (the general CRI)
Two-metric CRI/GAI system	8	*U*V*W**	Averaging colour shifts and estimating gamut area	Two derivate indices (CRI and GAI)
CQS	15	CIELAB	Averaging colour shifts with the colour-saturating component disregarded	Implicit derivative index (CQS) supplemented by other indices
Colour Rendition Icon	215-5600	CIELAB	Condensing data on colour-shift vectors	Graphical icon
Statistical method	1269	Avoided	Grouping on colour-shift vectors	Explicit percentage of test samples for any colour rendition property

However, the psychophysical assessment of the statistical colour rendition metric is difficult because of immense versatility in composing the SPDs of solid-state sources of light. Subjective side-by-side comparison of a large number of light sources is complex technically and exhausting for the subjects. Another problem is the lack of methods for the optimization of light sources in terms of subjective preferences to colour quality. Commonly, the psychophysical experiments on colour rendition preferences that involve solid-state lamps [2,15,19-21,23,24] rely on the ranking of light sources within a particular limited set rather than on finding the globally most preferred SPDs. Meanwhile, manual search of preferred SPDs [P1,22,26] lacks a systematic approach. An important attempt to resolve this problem is the computational optimization of LED clusters using the memory colour preference metric [24,32].

In this chapter, we present a concept of a solid-state source of light with continuously tuneable colour rendition properties. The source was used for the examination of the psychophysical validity of the general CRI, two-metric system, CQS, and statistical approach. This source allowed for a psychophysical optimization of the SPD for meeting subjective preferences to colour quality.

2.3. Colour rendition engine

The concept of colour rendition engineering is based on the sensitivity of chromatic distortions of illuminated objects to the ratio of spectral power between the yellow and red regions of the spectra. The statistical analysis of colour-shift vectors for a high number of test colour samples [29,33] has shown that light sources that have the balanced spectral components in the wavelength ranges of both 530-610 nm and beyond 610 nm can render most colours with small distortions of chroma and, therefore, provide high-fidelity illumination. Meanwhile lamps that lack spectral power in the 530-610 nm wavelength range render many colours with increased chroma, i.e. they exhibit the colour-saturating effect. Alternatively, the lack of spectral power at wavelengths beyond 610 nm results in a decrease of chroma of many rendered colours, i.e. lamps with such SPDs are colour-dulling. These regularities can also be traced in numerous estimations of the gamut area provided by different SPDs [25,27,34,35] and experiments on subjective assessment of different light sources [15,16].

Within such a concept, the simplest approach to a colour rendition engine is a tetrachromatic solid-state lamp, composed of red (R), amber (A), green (G) and blue (B) LEDs. For a particular set of four primary LEDs, the three colour mixing equations [5] show that the metameric SPDs of the RAGB lamp can be controlled by a single degree of freedom, such as the ratio of spectral power of the red and amber LEDs. By varying this ratio, the RAGB lamp can generate white light within an infinite number of metameric SPDs, each having different colour rendition properties.

An appropriate set of LEDs can be selected from a range of standard commercial devices, such as offered by the Philips Lumileds Lighting Luxeon® Rebel family. These are, for instance, direct-emission royal-blue (peak wavelength 452 nm) and green (523 nm) InGaN LEDs, InGaN-based phosphor converted amber LED (589 nm), and direct-emission red AlGaInP LED (637 nm). Figure 2.2 shows the CIE 1931 chromaticity diagram with the colour points of the four LEDs and white sources with different CCTs displayed.

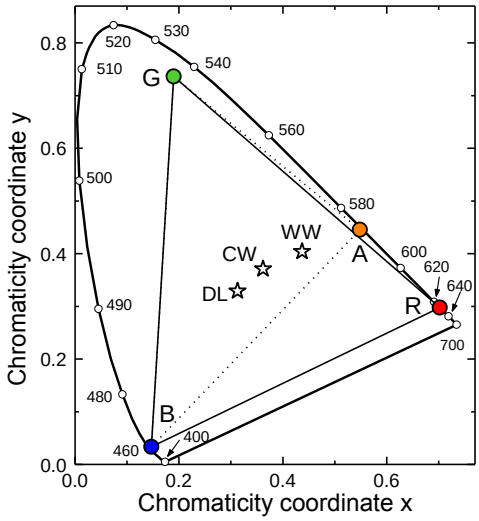

Fig. 2.2. CIE 1931 chromaticity diagram. Coloured circles, chromaticities of the four LEDs used in the RAGB lamp with tunable color rendition properties; white stars, chromaticities of blackbody at 3000 K (WW) and 4500 K (CW) and of daylight illuminant at 6500 K (DL) [P5].

The white chromaticities fall within the AGB and RGB triangles, whereas the other two possible triangles (RAB and RAG) contain no white chromaticity points. This means that metameric SPDs of white light can be generated as an RGB blend or AGB blend or a linear combination of those with the controlled red-to-amber ratio (degree of freedom). For instance, the SPDs of the AGB and RGB blends, $S_{\mathrm{AGB}}(\lambda)$ and $S_{\mathrm{RGB}}(\lambda)$, respectively, can be combined into any tetrachromatic SPD as a weighted sum

$$S_{\mathrm{RAGB}}(\lambda)=\sigma S_{\mathrm{AGB}}(\lambda)+(1-\sigma)S_{\mathrm{RGB}}(\lambda), \qquad (2.1)$$

where σ is the weight parameter ($0 \le \sigma \le 1$). Provided that the two end-point trichromatic sources have the same CCT and generate the same luminous flux, these two quantities will remain constant, while varying the weight parameter.

The relative partial radiant fluxes of the four components, c_i^{RAGB} (i = R, A, G, B), are derived from the chromaticity coordinates (CIE 1931 x,y) and weight parameter σ in two steps. First, the relative partial radiant fluxes c_i^{RGB} and c_i^{AGB} (i = R, A, G, B) for two metameric trichromatic sets of primary LEDs, RGB and AGB, respectively, are calculated (by default, $c_A^{RGB} = c_R^{AGB} = 0$). These calculations is based on the solution of two respective systems of colour mixing equations, which follow form the principle of additive colour mixing [5,32].

$$\begin{cases} \sum_{i=R,G,B} c_i^{RGB} X_i = x \sum_{i=R,G,B} c_i^{RGB} \left(X_i + Y_i + Z_i \right), \\ \sum_{i=R,G,B} c_i^{RGB} Y_i = y \sum_{i=R,G,B} c_i^{RGB} \left(X_i + Y_i + Z_i \right), \\ \sum_{i=R,G,B}^{n} c_i^{RGB} = 1, \end{cases} \tag{2.2}$$

and

$$\begin{cases} \sum_{i=A,G,B} c_i^{AGB} X_i = x \sum_{i=A,G,B} c_i^{AGB} \left(X_i + Y_i + Z_i \right), \\ \sum_{i=A,G,B} c_i^{AGB} Y_i = y \sum_{i=A,G,B} c_i^{AGB} \left(X_i + Y_i + Z_i \right), \\ \sum_{i=A,G,B}^{n} c_i^{AGB} = 1, \end{cases} \tag{2.3}$$

where X_i, Y_i, and Z_i are the tristimulus values of each primary-colour component of unit radiant power.

Second, the six computed values of the relative partial radiant fluxes ($c_i^{RGB}, i = \mathrm{R, G, B}$ and $c_i^{AGB}, i = \mathrm{A, G, B}$) and two default values ($c_A^{RGB} = c_R^{AGB} = 0$) are used for the calculation of the four relative partial radiant fluxes of the tetrachromatic RAGB cluster using the weight parameter σ,

$$c_i^{RAGB} = \sigma c_i^{AGB} + (1 - \sigma) c_i^{RGB}, i = \mathrm{R, A, G, B}. \tag{2.4}$$

The prototype tuneable RAGB light source containing 4 groups of 7 identical coloured LEDs each has been developed. A 10-bit pulse-width modulation electronic circuit controlled by a computer varied partial fluxes generated by each group of the LEDs. The software also allowed for varying CCT and maintaining constant net luminous flux while tailoring the SPD. To avoid

chromatic adaptation problems, the SPDs were tailored to bring the chromaticity point as close as possible to the blackbody locus (for CCT below 5000 K) or to the CIE daylight locus (for CCT above 5000 K). The LEDs were mounted on a massive heat sink cooled by air. The spectra were calibrated using a CCD spectrometer with a fibre-optic probe (Hamamatsu model PMA-11) under the conditions of the preheated heat sink. During the experiments described below, the chromaticity point of the LED cluster was maintained within 3 MacAdam ellipses (~0.006 *xy* distance from the required chromaticity point). The source was mounted on top of an experimental cabinet (Fig. 2.3) over a colour-mixing ceiling made of Plexiglas and provided an illuminance of about 700 lx at the bottom surface of the cabinet with unevenness better than 4%.

Fig. 2.3. Experimental cabinet with the tuneable RAGB source mounted on top and illuminated objects placed inside [P5].

Figure 2.4(a), (b), and (c) depict the variation of the radiant fluxes generated by each of the four LED groups with the weight parameter σ for CCTs of 3000 K, 4500 K, and 6500 K, respectively. In accordance with Eqs. (2.1), the flux of the red component linearly decreases from the peak value to zero and the flux of the amber component increases from zero to the peak value as the weight increases from 0 to 1. The flux of the green component linearly decreases with weight between the end-point values, whereas the flux of the blue component stays at

an almost constant value. With increasing CCT, the fluxes of the red and amber components decrease, whereas those of the green and blue components increase.

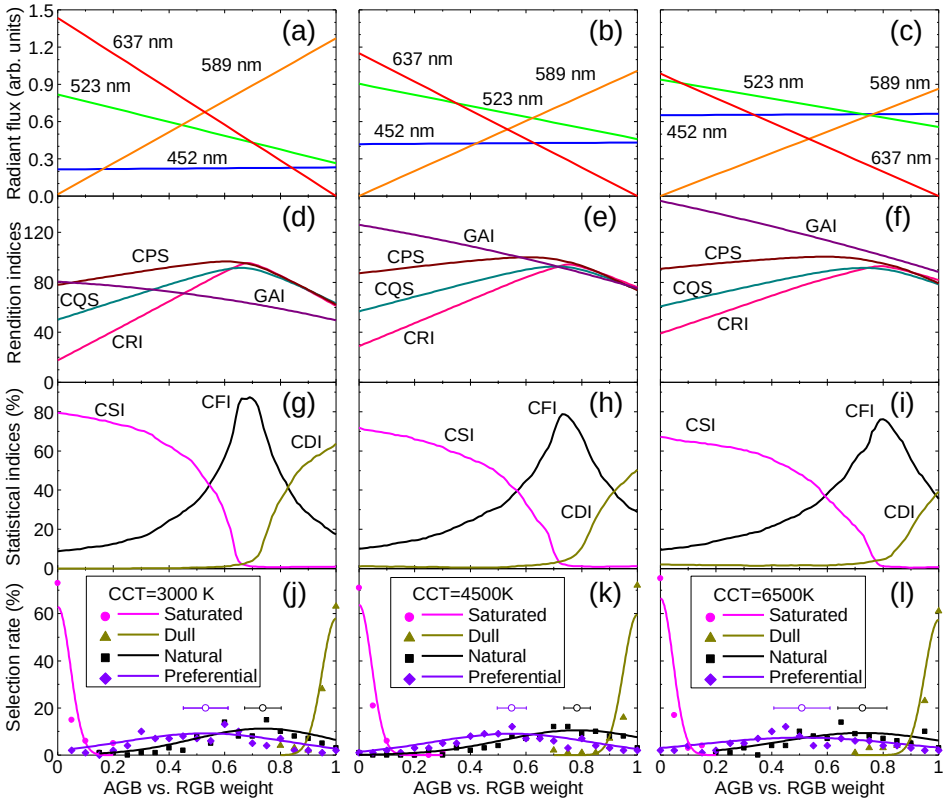

Fig. 2.4. (a), (b), and (c) Variation of the radiant fluxes of the four LED groups within the tuneable RAGB source with RGB vs. AGB weight. (d), (e), and (f) the general CRI (pink line), GAI (purple line), general CQS (cyan line), and CPS (brown line) as functions of weight. (g), (h), and (i) Statistical indices CSI (magenta line), CDI (olive line), and CFI (black line) as functions of weight. (j), (k), and (l) Percentage of the subjective selections of the weight parameter for illumination characterized as "most saturated" (magenta circles and line), "most dull" (olive triangles and line), "most natural" (black squares and line) and "preferential" (violet diamonds and line) (points, experiment; lines, Gaussian fit); open points with horizontal bars show the mean values and their 95% confidence intervals for the weight selected for "most natural" and "preferential" lighting. The first, second, and third columns show the data for CCTs of 3000 K, 4500 K, and 6500 K, respectively [P5].

Figure 2.4(d), (e), and (f) show the variation of the general CRI, GAI, the general CQS, and CQS colour preference scale Q_p (here designated as CPS) with the weight parameter for the three values of CCT. With the variation of AGB vs. RGB weight from 0 to 1, the gamut area (GAI) gradually decreases, whereas the general CRI, general CQS, and CPS vary none monotonously, i.e. they increase, pass through maximal values, and then decrease. These lamp properties clearly indicate that neither the general CRI nor general CQS can be used as single figures of merit, since they have values that correspond to different gamut areas.

The use of the two-metric (CRI/GAI) system [17] resolves this problem. Similarly, two distinct scales are to be used in the CQS metric (colour fidelity scale and gamut area scale [27]) instead of the integration of the two colour rendition characteristics within the general CQS.

Figure 2.4(g), (h), and (i) show the statistical colour quality indices CFI, CSI, and CDI as functions of weight for the same three values of CCT. The CFI (percentage of colour test samples rendered with high fidelity) has peak values of 87%, 79%, and 76% at weights of 0.69, 0.73, and 0.80 for CCT of 3000 K, 4500 K, and 6500 K, respectively. Interestingly, these peak values are very close to the peaks of the general CRI, which also measures the fidelity of colour rendition. However, the variation of CFI is much more pronounced due to the distinct discrimination of the colour-shift vectors. (In the statistical metric, colour-shift vectors that show perceivable colour distortions do not score to the fidelity index.) The highest values of CSI and CDI (percentages of test colour samples rendered with increased and decreased chroma, respectively) are attained at the end-points of $\sigma = 0$ and $\sigma = 1$, respectively. At $\sigma = 0$, CSI equals 80%, 72%, and 67% for CCT of 3000 K, 4500 K, and 6500 K, respectively. At $\sigma = 1$, CDI equals 64%, 51%, and 39%, respectively. As the weight parameter deviates from the corresponding end-point values, both indices rapidly decrease and drop to marginal values of 1 to 5%, when the highest values of CFI are attained. At the opposite end-points, the CSI and CDI nearly completely vanish (dropping below 2%). Again, these two statistical indices show much more pronounced behaviour than their gamut-area counterpart (GAI) due to the threshold-like discrimination of the colour-shift vectors, which avoids scoring unless the vector contributes to a perceptually perceived alteration of chroma.

2.4. Psychophysical validation of statistical metric

A psychophysical experiment was carried out to demonstrate the use of the tuneable RAGB source for the validation of colour rendition metrics and for the optimization of the tetrachromatic SPDs to meet subjective preferences to colour quality of illumination. In our experiment, the subjects continuously tuned the

colour rendition properties of the source to select a spectrum that, to their opinion, met particular colour rendition characteristics. This is different from previous studies [2,15,19-21,23,24], where the subjects ranked light sources within an unsystematic set.

During the experiment, subjects viewed a set of familiar objects [11,21,24], such as vegetables and fruits (lettuce, tomato, banana, lemon, light-green grapes, nectarine, and orange) and soft-drink aluminum cans of common brands: Coca-Cola® (red), Sprite® (yellow/green/blue), and Pepsi-Cola® (blue/red) (see Fig. 2.3). The objects were placed within a cabinet made of neutral grey matted plastic with dimensions of 46 cm by 46 cm by 46 cm and viewed from a distance of 60 to 70 cm. The cabinet was installed in a dark room. A laptop computer was used for the continuous control of the weight parameter of the SPD by incrementing it in steps of 0.05. Repetitive clicking the mouse pointer on either of two icons displayed on the monitor resulted in the cyclical incrementing of weight (from 0 toward 1, then back from 1 toward 0, and so on). Clicking the pointer on the other icon resulted in a reverse variation of the weight parameter. This allowed for precisely controlling the source by forward-backward tuning, without latching onto any of the end-points.

100 subjects (not acquainted with the details of colour rendition problem) took part in the experiments. Of those 41 were females and 59 were males; the age ranged from 14 to 78 (with the average age of 27). All subjects were Caucasians with Lithuanian cultural background. Prior to the experiment they were screened against colour vision deficiencies using Stilling's pseudo isochromatic plate tests. Each subject was verbally instructed for about 3 minutes and had about 5 minutes to adapt to the scene and to perform a trial tuning of the source. Afterward, the subjects were asked to select four options of lighting, which were verbally characterized as "most saturated," "most dull," "most natural," and "preferential." Each subject performed the selection of the four options in the above sequence from 21 circularly varied ones at three CCTs of 3000 K, 4500 K, and 6500 K (for each subject, the CCT was changed in a random sequence). The time allocated for a selection was not limited; however

selections of “most saturated” and “most dull” lighting were accomplished, on average, in about half a minute. The “most natural” and “preferential” selections took somewhat longer, typically about one minute, on average. As soon as the option was selected, the experimenter recorded the weight parameter, which the subject did not see. Since the experiment lasted for several weeks, fruits and vegetables were being replaced by those having similar appearance each 2-3 days.

The points in Fig. 2.4(j), (k), and (l) display the percentage of 21 weights corresponding to the four subjectively selected options of colour quality. The lines show the distributions of the data approximated by Gaussian functions. The open circles with the horizontal bars show the mean values with their 95% confidence intervals for the weight for “most natural” and “preferential” selections. The obtained distributions of selection rate exhibit the following trends:

- the subjective identification of lighting with the highest distortions of chroma (“most saturated” and “most dull”) are highly correlated with the highest CSI and CDI at the RGB and AGB end-points, respectively (the end-points were exactly identified in 61-75% trials);
- the identification of “most natural” and “preferential” lighting resulted in considerably wider distributions;
- the average AGB vs. RGB weights subjectively attributed to “natural” lighting (0.74 ± 0.07, 0.78 ± 0.05, and 0.73 ± 0.09 at CCTs of 3000 K, 4500 K, and 6500 K, respectively) agree with those estimated for the highest CFI (0.69, 0.73, 0.80, respectively) within the 95% confidence intervals;
- the average AGB vs. RGB weights subjectively attributed to “preferential” lighting (0.53 ± 0.08, 0.55 ± 0.05, and 0.51 ± 0.1 at CCTs of 3000 K, 4500 K, and 6500 K, respectively) are noticeably shifted (by about 0.22) toward higher saturation in respect of those attributed to “most natural” lighting (in over 70% of the trials, the preference was shifted to higher saturation, whereas a shift to lower saturation was made only in about 20% of the trials).

The experiment on continuous traversing metameric SPDs of the RAGB source provides the extended data on the psychophysical validation of the colour rendition metrics.

Figure 2.5 shows the SPDs of the four RAGB blends for the CCT of 4500 K corresponding to the highest subjective selection rate for the colour appearance characterized as “most saturated” (a), “preferred” (c), “most natural” (e), and “most dull” (g), respectively. Figure 2.5(b), (d), (f), and (h) show the corresponding distributions of the colour-shift vectors in respect of a blackbody radiator estimated for 218 Munsell samples of value /6, respectively. These distributions are presented within the a*-b* chromaticity plane of the CIELAB colour space; arrows schematically show the vectors that are estimated to have perceptual noticeable chromaticity distortions; circles correspond to the colour samples rendered with high fidelity. For 3000 K and 6500 K, the SPDs and colour-shift vector distributions have similar properties.

The experimental data (Fig. 2.4(j), (k) and (l)) show that the subjective tuning of the RAGB source for matching the most noticeable colour saturating and colour dulling conditions was the easiest and least ambiguous task to accomplish. Out of all metameric SPDs, the end-point RGB (σ = 0, Fig. 2.5(a)) and AGB (σ = 1, Fig. 2.5(c)) blends were almost exactly identified with the “most saturated” and “most dull” appearance of familiar objects. These two blends render the highest statistical percentage of a large number of colours with increased and decreased chroma (the largest CFI and CDI), respectively.

The colour-saturating RGB blend, which features a low spectral power in the 540-610 nm range (Fig. 2.5(a)), results in numerous colour-shift vectors with a perceptually noticeable component directed toward increased chroma (Fig. 2.5(b)). Alternatively, the colour dulling AGB blend (Fig. 2.5(g)), which features low spectral power beyond 610 nm, results in numerous vectors exhibiting perceptually noticeable reduction of chroma (Fig. 2.5(h)). With a typical consistency of subjective colour quality assessment of about 70% [21], the obtained rate of recognizing the end-point colour distortion patterns (while continuous tuning the SPDs) indicates that the subjective feeling of colour

saturation is highly correlated with the number of colours that have distorted the chroma. The high-saturating RGB end-point is well recognized despite a large number of colours with perceptually noticeable distortions of hue (typically, over 60% [29]).

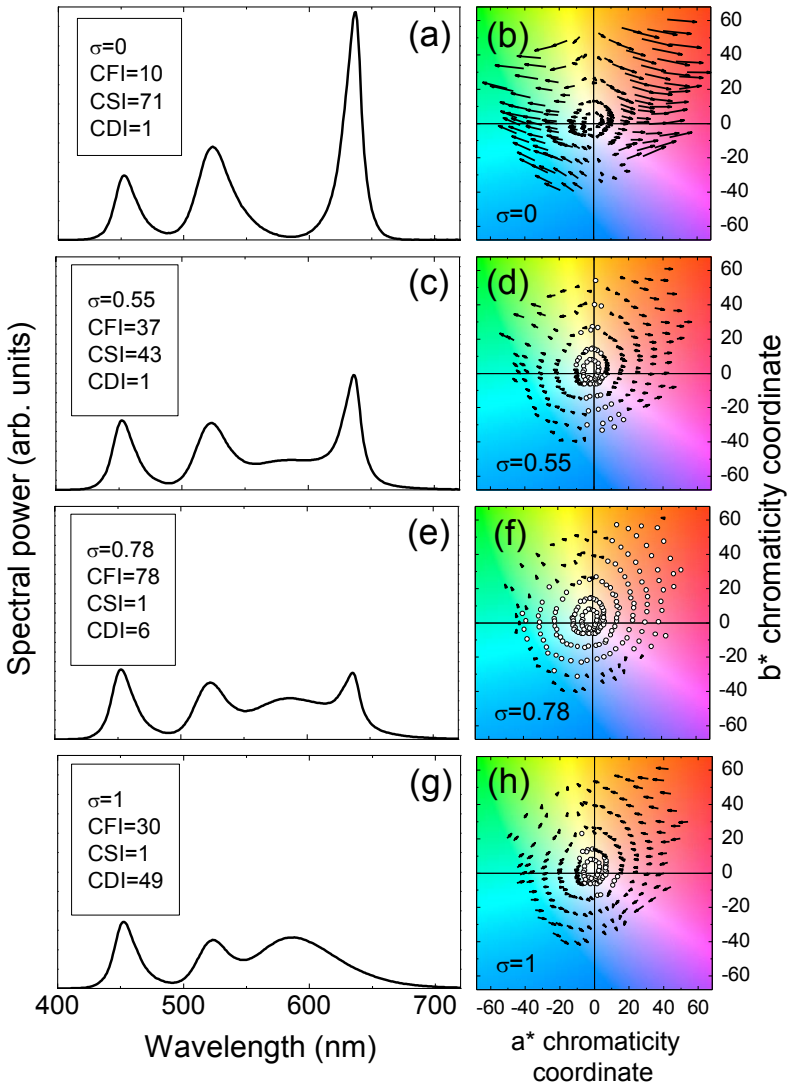

Fig. 2.5. Properties of the RAGB LED cluster for several values of the AGB vs. RGB weight parameter σ at a CCT of 4500 K. (a), (c), (e), and (g) SPDs that in average have been subjectively identified as providing the "most saturated" (σ = 0), "preferential" (σ = 0.55), "most natural" (σ = 0.78), and "most dulling" (σ = 1) appearance of familiar objects. (b), (d), (f), and (h), corresponding distributions of the colour-shift vectors for 218 Munsell samples of value /6 in the a^*–b^* chromaticity plane of the CIELAB colour space. Open points, samples that have colours rendered with high fidelity; arrows, schematic chromaticity shifts of samples that have colour distortions, such as increased or decreased saturation as well as distorted hue or luminance (the magnitude of each vector is normalized to the size of the individual MacAdam ellipse as in [27]) [P5].

The measure of gamut area for a small number of test colour samples (GAI) is also in line with the selection rates for “most saturated” and “most dull” lighting. For a particular set of continuously varied blends, such as generated by the RAGB colour rendition engine, GAI reasonably follows the variation colour-shift vector distributions, despite the limited accuracy of the *U*V*W** colour space used. However, GAI lacks global correlation with the statistical metric, which is more comprehensive. The ranking of light sources using GAI might be different from that based on CSI and CDI [29].

The data presented in Fig. 2.4(j), (k) and (l) shows a remarkable agreement of the subjective selection rates for the “most natural” appearance of familiar objects with the highest values of statistical CFI ($p < 0.05$). Such an agreement is clearly revealed, despite a rather wide distribution of the selections. The wide distribution is probably due to fact that when judging on the “most natural” appearance of the objects, the subjects relied on their memory rather than on direct visual impression as in the cases of “most saturated” and “most dull” specifications. Figure 2.5(e) shows the tetrachromatic SPD corresponding to the highest selection rate for “most natural” illumination ($\sigma = 0.78$). The blend has a balanced spectral power within the spectral ranges of 540-610 nm and beyond 610 nm. The distribution of the colour-shift vectors (Fig. 2.5(f)) shows that most test colour samples have no perceptually noticeable distortions of chroma (open circles) and those that do have very small distortions compared to the RGB and AGB end-points. These data prove that subjective feeling of colour rendition “naturalness” can be associated with a low number of chromatic distortions perceived while comparing the observed appearance of objects with memorized colours.

The subjective perception of colour “naturalness” represented by the distributions shown in Fig. 2.4(j), (k), and (l) agrees with the variation of the general CRI (Fig. 2.4(d), (e), and (f), respectively), which also measures the colour fidelity of illumination. Such an agreement of the selection rate vs. weight dependence with the peak of the general CRI occurs despite the limited accuracy of the *U*V*W** colour space. The reason is that when colour shifts shrink, any

figure of merit measuring colour fidelity in terms of reduced shifts arrives at its highest value, irrespectively of the colour space used (the general CRI attains values in the range of 93 to 95 in our case). However, the general CRI may miss many distorted colours, in particular of red hues, because of a small number of test colour samples used. The enhanced colour fidelity determined by using a large number of test colour samples requires the SPDs with the red components shifted to longer wavelengths [36] in respect of those in the SPDs obtained through maximizing the general CRI [37].

Figure 2.5(c) shows the SPD of the blend corresponding to the highest selection rate for "preferred" appearance of familiar objects (σ = 0.55). It differs from that selected for "most natural" lighting (Fig. 2.5(e)) by a larger red-to-amber spectral power ratio. The distribution of the colour-shift vectors for the "preferred" blend indicates a reduced number of the test colour samples rendered with high fidelity and an increased number of the test colour samples having increased chroma. However, the characteristics of "preferred" illumination are very far from those of highly saturating RGB end-point. This means that neither statistical CSI nor gamut-area or chroma-increase based indices, such as GAI and CQS gamut-area index, can serve as the indicators of the colour quality preference. The reason is that, in contrast to fluorescent lamps used in early experiments [11], the colour saturating ability of an RGB cluster can be so high that the colours of illuminated objects become oversaturated and lose their subjective attractiveness. Another reason for the observed shift of the "preferred" selections from highly saturating RGB blend to that providing higher fidelity might be the aforementioned large number of colours with perceptually noticeable hue distortions [3,29]. The CQS colour-preference scale has a maximum almost coinciding with the highest selection rate for "preferred" illumination. However, Fig. 2.4(e) shows that CQS Q_p is very insensitive to the increase of the colour-saturating ability of the RAGB source and does not distinguish distinctively between sources that render colours with high fidelity, increased saturation and subjective preference.

2.5. Conclusions of the second chapter

The colour rendition engine, based on an RAGB LED cluster has been developed basing on weighting the contributions of the colour saturating RGB subcluster and colour-dulling AGB subcluster, respectively. The ability to continuously tune various colour rendition indices by varying the weight parameter of the SPD of the engine has been demonstrated.

The psychophysicalological investigation revealed that while tuning the colour rendition engine, subjects confidently identify the "most saturated," "most dull," "most natural" lighting conditions with the highest values of statistical CSI, CDI, and CFI indexes, respectively.

The "preferential" colour quality of lighting has, on average, been matched to RAGB blends that provide colour rendition with fidelity somewhat reduced in favour of a higher saturation.

3. Artwork visualisation using a colour rendition engine

Artwork-specific illumination must satisfy adequate visual impression and meet the conservation requirements. Common lighting installations used in museums and art galleries are based on light sources with fixed SPD. They are optimized basing on the trade-off between luminance level and photochemical effect on the illuminated surfaces, but have limited possibilities to select and control colour rendition properties, however. In this chapter the main requirements for artwork illumination are overviewed and the application of the intelligently controlled colour rendition engine in artwork illumination is investigated in two aspects: a) the establishment of subjective needs in colour quality of illumination as a function of the contents of artworks and the observers' cultural background and b) the effect of the control of photochemical damage irradiance on the visual impression from artworks, while adjusting colour rendition properties [P4,P7-P11,P14-P16,P18,C8,C10,C12, C15-C17,C23,C25].

3.1. Cultural preferences to colour quality of illumination for artworks

3.1.1. Literature survey

The emergence and commercialization of illumination-grade LEDs has led to the development of solid-state sources of light with the SPDs meeting various needs in the colour quality of lighting [31,38]. Such sources can have very different ability to saturate and desaturate the colours of illuminated objects [33,35,39,40]. As described in Chapter 2, intelligently controlled polychromatic LED clusters can generate metamers of white light with continuously tuneable colour rendition properties [P5]. Such "colour rendition engines" can find many important applications in general lighting and in photo- and visual imaging, including improving visual impression of artistic paintings [22,41,42] and chromatic correcting for aged artwork [P4]. They can meet specific colour-quality requirements of people with different subjective needs, including those depending on cultural background, age, or gender.

Cross-culture studies indicate that different cultural groups show different responses and preferences to lighting conditions [43], colours [44], and colour combinations [45,46]. The subjective perception of colourfulness is also influenced by the content of the illuminated scene and is known to benefit from the image saturation level, especially for familiar objects, since familiarity contributes to colour adaptation [47]. The subjective need in colour rendition depends on the character of the illuminated object and its familiarity to the observer. However, little is known about cultural differences in assessing colour rendition quality of illumination. Until recently, such preferences were difficult to examine because of the lack of light sources with controllable colour rendition properties.

In this section, by using a tetrachromatic solid-state source of light with tuneable colour-rendition properties (colour rendition engine) described in the Chapter 2, the preferences to the colour quality of illumination for subjects from two different cultural groups was investigated.

3.1.2. Experimental method

The cluster of engine described in Chapter 2 was modified by replacing the LEDs with the following Philips Lumileds Lighting Luxeon® Rebel series LEDs: red (624 nm peak wavelength), green (523 nm), and blue (450 nm) direct-emission LEDs and phosphor-conversion amber (591 nm) LED. The control of the colour rendition properties are implemented in the same a way as described in Section 2.3. The colour rendition properties are tuned by varying the weight parameter of the SPD, which is a weighted sum of the red-green-blue (RGB) and amber-green blue (AGB) blends (see Eq (2.1)). The RGB and AGB blends have high ability to saturate and dull colours, respectively.

The psychophysical experiment was conducted using the procedure described in Section 2.4.

While tuning the AGB vs. RGB subjects were asked to find conditions of the highest subjective preference. Before the experiments, subjects were briefly introduced (in words) to the concepts of colour rendition quality (natural,

saturated, and dull colours). Colours rendered in the "most natural" way were explained as those having minimal distortions in comparison with natural lighting conditions, i.e. rendered with high fidelity and having "everyday-life" and "common" appearance. Colours rendered in the preferential way were defined as the "most appealing" and "most attractive." It was stressed that this means that they can appear not necessarily as "most natural" ones. After the vocal introduction, the concept of colour rendition and the operation of engine were demonstrated using an illuminated familiar object (orange).

205 subjects with normal colour vision were selected by Stilling's pseudo isochromatic plate tests and invited to take part in the experiment (see Table 3.1). 101 individuals were originated from People's Republic of China (they studied and lived in the US for less than a few years) and 104 individuals were locals of the United States. Of total number of subjects, 49 were females and 156 were males with the age ranging from 18 to 33 (the average age of 22). Most of the observers were students or staff and faculty members at Rensselaer Polytechnic Institute. None of subjects initially possessed detailed knowledge or understanding of the research. The pre-experimental introduction and demonstration was given in Chinese language for the Chinese observers and in English for the US subjects.

Table 3.1. Characteristics and number of observers [P10].

Cultural background	Males	Females	Sum	Age range (average)
American	79	25	104	18-32 (23)
Chinese	77	24	101	19-33 (22)
Total	156	49	205	18-33 (22)

Two experiments were carried out. In the first experiment, the cultural differences in the selection of colour quality of illumination were tested using familiar objects similarly to the experiment described in Chapter 2. Natural fruits and vegetables with different dominant colours were used, including a red apple, a tomato, an orange, two bananas, a lemon, a greenish cucumber and an onion with purple peel.

In the second experiment three paintings with the content of different familiarity were illuminated (Fig. 3.1).

Fig. 3.1. Images of three examined paintings that are assumed to have different level of familiarity to investigated subjects: Fire theme (I), Saint George fighting a dragon (II), and Vilnius downtown (III) [P10].

The first painting (Fig. 3.1(I); unknown author) was painted by acryl on canvas. It depicted a colourful fire theme that was assumed to be equally familiar to subjects with different cultural backgrounds. The second artwork (Fig. 3.1(II); unknown author) was painted on a cardboard. It depicted Saint George fighting a dragon in somewhat faded colours. This topic was assumed to be more familiar to subjects with Christian or multicultural background such as Americans rather than to Chinese. The third artwork used in the experiment (Fig. 3.2(III); by E. Kuokštis) was a post-impressionistic watercolour painting displaying a medieval downtown scene in Vilnius, Lithuania. The theme of the painting was assumed to be unfamiliar to all subjects, since none of them have been to Vilnius nor were acquainted with the style of the artist.

In this experiment, the CCT was also allowed to change from 2500 K to 7500 K and back from 7500 K to 2500 K with an increment of 500 K by pressing particular keys on the computer keyboard.

3.1.3. Results and discussion

The solid and dashed lines in Fig. 3.2(a) show the variation of the statistical colour rendition indices and general CRI of the engine with AGB versus RGB weight at CCTs of 3000 K and 6500 K, respectively. Similarly to the experiment described in Secion 2, in the first experiment (on very familiar objects, i.e., fruits and vegetables) subjects were asked to establish SPDs that rendered colours in

the “most natural” way (with high fidelity) and with the highest subjective preference under a constant CCT of 3000 K (such CCT corresponds to halogen incandescent lamps that are common in residential lighting). In this case, only the AGB versus RGB weight was allowed to tune.

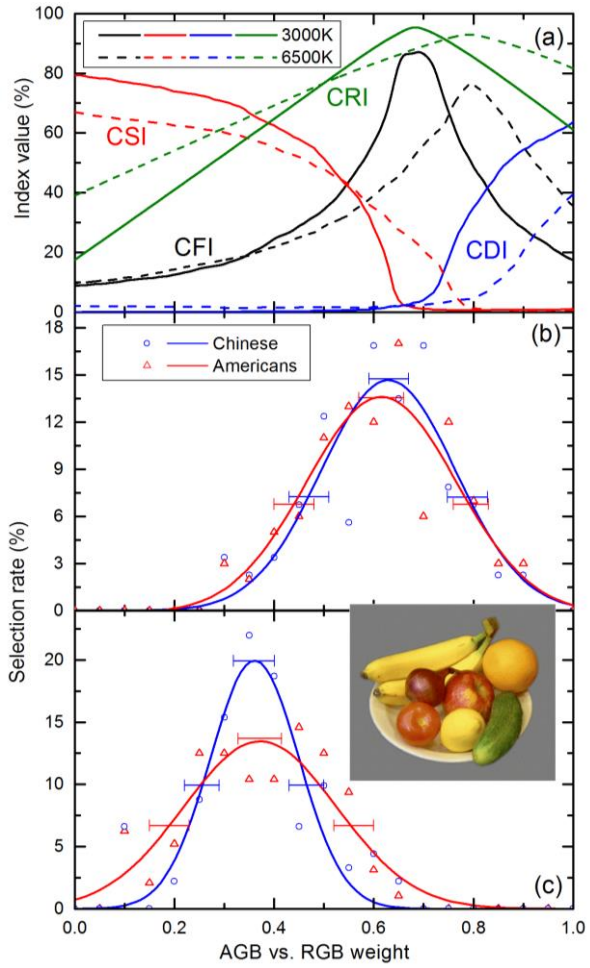

Fig. 3.2. (a) Statistical colour rendition indices and general CRI of the engine as functions of AGB vs. RGB weight for CCTs of 3000 K (solid lines) and 6500 K (dashed lines). (b) and (c) Points, percentage of the “most natural” and preferred subjective selections of the weight parameter σ, respectively, for the illumination of very familiar objects. Blue circles and red triangles, data obtained from Chinese and American subjects, respectively. Lines, the Gaussian distributions obtained by least-squares fitting. Horizontal bars, the 95% confidence intervals for the peak weights and FWHMs of the distributions [P10].

Figure 3.2(b) displays the selection rate for high fidelity blends as a function of the weight parameter. The blue circles and red triangles show the experimental results for Chinese and American subjects, respectively. The experimental results are well fit to Gaussian distributions by the method of least squares (solid lines in Fig. 3.2(b)). The horizontal bars show the 95% confidence intervals for the peak position and width of the distributions derived from the

fitting procedure. The distributions peak at $\sigma_p = 0.63 \pm 0.04$ and $\sigma_p = 0.64 \pm 0.04$ for the American and Chinese groups of subjects, respectively, i.e., no cultural differences in finding the "most natural" conditions of illumination for familiar objects, such as fruits and vegetables, were observed. Moreover, the FWHMs of the measured selection rate distributions are identical for the both groups of subjects (0.35 ± 0.07 and 0.33 ± 0.07, respectively). It is to be noted that the peak selection rates for the both groups of subjects match the highest value of the calculated CFI at $\sigma = 0.67$ within the experimental uncertainty and also agree with the highest general CRI ($\sigma = 0.67$).

Figure 3.2(c) displays the corresponding results for the selection rate for preferential blends. The peak positions of the distributions of the blends that render the colours of familiar objects with subjective preference are seen to be independent of subjects' cultural background ($\sigma_p = 0.37 \pm 0.04$ and $\sigma_p = 0.36 \pm 0.04$ for the Americans and Chinese, respectively). Similarly to the results presented in Chapter 2, these distributions, which are also well fit to Gaussian ones, are clearly shifted to lower values of the AGB versus RGB weight that correspond to the blends that render colours with somewhat increased saturation rather than to high fidelity blends. An important feature of the selection of preferential blends is that the FWHM of the distributions is significantly different for the two groups of subjects. It amounts 0.37 ± 0.07 and 0.21 ± 0.07 for the American and Chinese groups of subjects, respectively.

Figure 3.3 shows the experimental results on finding the preferential lighting for the paintings shown in Fig. 3.1. Figure 3.3(a), (c), and (e) and Fig. 3.3(b), (d), and (f) demonstrate the selection rates as functions of the AGB vs. RGB weight and CCT, respectively. The experimental data shown by points in Fig. 3.3 was fitted to Gaussian distributions. The blue and red lines in Fig. 3.3 correspond to the Gaussian fits for the two respective groups of subjects. The horizontal bars indicate the 95% confidence intervals of the distribution peaks and FWHMs.

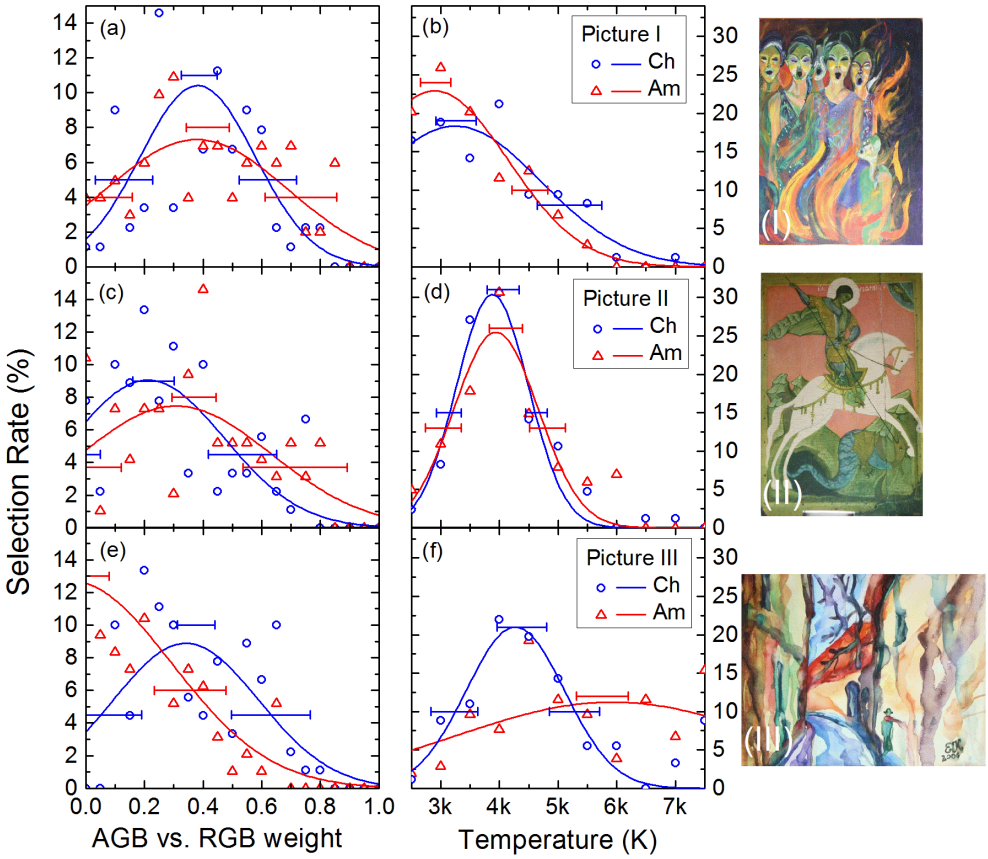

Fig. 3.3. Points, percentage of the subjective selections of the weight parameter σ (a, c, and e) and CCT (b, d, and f) for the most preferred illumination of paintings with various level of familiarity. Blue circles and red triangles, data obtained from Chinese and American subjects, respectively. Lines, Gaussian distributions obtained by least-squares fitting. Horizontal bars, the 95% confidence intervals for the peak weights and FWHMs of the distributions [P10].

For painting I, which is assumed to have the most familiar and culturally neutral content, no significant difference in the average selection rate of AGB vs. RGB weight was observed (Fig. 3.3(a)). However the American group of subjects showed a noticeably wider distribution of the selection rates than Chinese subjects. For painting II, which is assumed to be less familiar to subjects with the Chinese cultural background, the distributions of AGB vs. RGB weight differ in both the width and peak position (Fig. 3.3(c)). For these two paintings, the distributions of the CCT selection rate show almost no cultural differences within the experimental uncertainty (Fig. 3.3(b) and (d)). However, the average selected CCT is seen to depend on painting content: the fire topic required considerably lower CCT than the Saint George topic.

For painting III, which is assumed to be unfamiliar to both cultural groups, the selection rate distributions show cultural differences for both AGB vs. RGB weight and CCT (Fig. 3.3(e) and (f), respectively). As compared to Americans, the Chinese group of subjects selected less saturated colours and lower CCT on average. For both σ and CCT, the American group of subjects showed wider distributions.

The parameters of the distributions of preferential colour quality selection rate for the two cultural groups are summarized in Table 3.2.

Table 3.2. Peak positions and FWHMs of the Gaussian distributions of preferential colour quality selection rate [P10].

Objects, tasks	American subjects			Chinese subjects		
	CCT (K)	AGB vs. RGB weight		CCT (K)	AGB vs. RGB weight	
		σ_p	FWHM		σ_p	FWHM
Fruits, "natural"	3000	0.63±0.04	0.35±0.07	3000	0.64±0.04	0.33±0.07
Fruits, preference	3000	0.37±0.04	0.37±0.07	3000	0.36±0.04	0.21±0.07
Painting I, preference	2900±260	0.38±0.07	0.78±0.14	3250±370	0.39±0.06	0.46±0.08
Painting II, preference	3920±280	0.31±0.07	0.85±0.23	3900±280	0.21±0.08	0.47±0.15
Painting III, preference	5950±460	0.00±0.07	1.29±1.09	4260±430	0.35±0.07	0.59±0.11

The above results obtained by using the continuously tuneable colour rendition engine reveal both similarities and differences in the selection of colour quality of illumination by the groups of subjects with different cultural background.

The first important observation is that when selecting "most natural" colour rendition properties of illumination for very familiar objects, such as fruits and vegetables, the two groups of subjects exhibited almost identical distributions of selection rates that peak in the vicinity of the high-fidelity pole of the engine (σ = 0.67; Fig. 3.2(a)) and have very similar FWHMs of about 0.34. The reason is probably in that when judging on the "most natural" appearance of the familiar objects, the subjects rely on their memory [P5], which is a mental capacity that depends on physiological similarity of human brain rather than on cultural differences. These identical distributions of the selection rates also can be considered is a proof for the validation of the experimental approach based on the use of the colour rendition engine, described in Chapter 2. Also, this shows

no significant racial differences in the physiology of perceiving and recalling the appearance of coloured objects.

It is to be noted that our data on selecting the “most natural” appearance of familiar objects show no “colour memory” effect, which manifests itself in the selection of somewhat more saturated colours [24]. This can be attributed to the way of colour matching [48], which is the continuous tuning of SPD of our light source rather than the side-by-side comparison of lamps with different SPDs used in other investigations.

When the task was changed from finding the “most natural” conditions to those characterized as preferred, the average selection rate exhibited a known mismatch with the highest colour fidelity or highest general CRI [P5,11,19]. Similar result was observed in [49,50], where more saturated colours or illuminants with larger gamut area are preferred by observers. In this case, the selections relied on the individual way of judging rather than on memory and the cultural differences in the selection of the colour quality of illumination emerged.

For very familiar objects, such as fruits and vegetables, and even for an artwork with familiar contents (painting I), the average preference selection rate is shifted to more saturated colours but shows no dependence on cultural background (Fig. 3.3(a)). The distribution of the CCT selection rate (Fig. 3.3(b)) that was obtained for the illumination of familiar artwork also showed no significant cultural differences. These observations are in line with the cross-cultural comparison of colour emotion for two-colour combinations on the like/dislike scale [39]. However, the striking result of this experiments is that despite the similarity in the average judgements on illumination of familiar objects, different cultural groups exhibited statistically significant difference in the width of the distributions for the colour saturating ability of illumination. The American group of subjects showed almost twice as wide distributions over AGB vs. RGB weight than the Chinese group for the painting I (FWHM of 0.78 ± 0.14 vs. 0.46 ± 0.0). When switching to a less familiar paintings, a higher diversification of the judgements occurred within both cultural groups.

Assuming that the racial factor in perceiving colours is to be excluded, the observed difference in the width of the preference selection rate distributions is to be attributed entirely to the difference in the cultural background of the two groups of subjects. The multidimensionality and complexity of the cultural background aggravates finding the exact reasons of this phenomenon. Tentatively, the problem can be considered in terms of some simplified models. One of such models is G. Hofstede's approach to national cultural dimensions [51]. In particular, we can trace the correlation of results with the Hofstede's Individualism/Collectivism dimension (IDV), which can be understood as a measure of the integration of individuals into primary groups. The US population scores an IDV of 91, which shows a preference for a loosely-knit social framework, in which individuals are expected to take care of themselves, and implies highly individual decision making. In contrast, the Chinese score an IDV of 20, which infers that Chinese people act more as a group rather than individuals and their decision making might be influenced by group norms (intended behaviour of other group members).

Differentiation of the level of similarity of an object among different cultural groups of subjects results in more differences of the distribution of colour quality preferences. This is illustrated by the results for painting II, which content is assumed to be more familiar to Americans rather than to Chinese (Fig. 3.3(c)). In this case, not only a smaller FWHM but also a noticeable shift of the peak of the distribution toward more colour saturating conditions was observed for the Chinese subjects compared to the American subjects. One can speculate that faded colours of sacral artworks are more acceptable for the subjects connected to the Christian culture, while Chinese are more tending for the compensation of the faded colours by selecting a more saturating blend [52]. Note that the distribution of the selection rates for CCT is still almost independent of cultural background (Fig. 3.3(d)).

The largest cultural differences in the selection of the colour quality of illumination were found for painting III, which was assumed to be very unfamiliar for both groups of subjects. Differently from painting II, a reverse

shift of the peak of the distribution toward more colour dulling conditions was observed for the Chinese in respect of Americans. Meanwhile the Chinese group of subjects exhibited a need for lower cool-white CCTs (~4300 K) in respect of daylight (~6000 K) that the American group selected on average. Compared with the selections for the previous two paintings, the need for higher CCT lighting for this painting can be interpreted as the result of the domination of cool colours in the outdoor scene depicted. Such an effect has also been observed in [53]. The width of the distributions for both AGB vs. RGB weight and CCT was larger for the American group of subjects, probably due to the reasons discussed above. We can imply that these large cultural differences in the selection of the preferences to the colour appearance of the unfamiliar artwork are almost entirely determined by aesthetic judgement, which is strongly influenced by geographic, climatic, landscape, architectural, etc. characteristics of environment responsible for the formation of a particular cultural background.

3.2. Artwork visualization with controlled damage irradiance

3.2.1. Literature survey

The illumination of artworks is a complex problem, which necessitates not only pursuing adequate visual impression as described in the previous section, but also meeting conservation requirements [54,55]. There exists a non-zero probability that any photon absorbed by a pigment, binder, varnish, or substrate of an artwork will invoke an irreversible photochemical reaction on the molecular level, which eventually contributes to the alteration of the colour (typically, this probability increases with photon energy). Also, the radiant heating effect, which is less wavelength dependent, may contribute to artwork damage. Therefore from the standpoint of conservation, artworks must undergo as short as possible duration of exposure to as dim as possible light having as low as possible short-wavelength spectral content and non-visible spectral components removed. On the other hand, the colour discrimination of the human eye decreases with reducing luminance [56] and white light with low short-

wavelength spectral content (i.e. generally having low correlated colour temperature, CCT) renders colours differently from daylight, which the most of artworks have been created at, due to the shrunk chromatic gamut area [57]. Moreover, visual reconstruction of an aged artwork might require the use of short-wavelength enriched light [58], which is photochemically harmful. The aforementioned considerations imply that the approaches to the conservation and visualization of artworks might be within a conflict that is to be resolved by a reasonable compromise.

Early work on conserving illumination of artworks [59-62] has brought to the establishment of recommended illuminance of 50 lx, below which the colour discrimination ability dramatically drops, for materials with high and medium responsivity (e.g., textiles, water-colours, silk, low-grade paper) and illuminance of 200 lx, above which the colour discrimination ability increases slowly, for materials with low photo-responsivity (e.g., oil and tempera paintings, frescos, bone, and wood). Also, appropriate optical filters were recommended to use with light sources that generate violet-UV radiant flux (for wavelengths below 400 nm) per unit luminous flux in excess of 75 μW/lm, which is a characteristic of a common incandescent lamp. These recommendations were initially adopted by the lighting industry [63] and further the requirement for the violet-UV radiant flux was tightened to the limit of 10 μW/lm [64]. Also a common practice is to minimize infrared radiation by using, e.g. dichroic mirrors for tungsten radiators [64,65].

A straightforward approach to increasing photochemical safety is the use of light with the highest luminous efficacy of radiation (LER), which is the ratio of luminous flux to radiant flux [65]. However within an improved approach, the spectral responsivity in respect of light-induced colour shifts for various artwork materials is to be taken into account. The spectral responsivity can be approximated by a "damage" function, which exponentially decreases with increasing wavelength [66]. Krochmann et al. [67] investigated the damage functions and effective radiant exposures causing just noticeable colour shifts for several groups of artwork materials (low-grade paper, rag paper, oil paints

on canvas, textiles, and water colours on rag paper). With some limitations due to more peculiar spectral behaviour of actual responsivities of individual pigments [68], the exponential damage functions can be used for the estimation of the photochemical damage index of light, which is the ratio of the radiant power weighted by a damage function (damage flux) to luminous flux [64,69,70]. Minimizing the damage index is more meaningful in terms of artwork conservation than maximizing LER, which does not distinguish between light of different wavelengths posing different photochemical hazard.

Research on finding the optimal light sources for the visualization of artworks was focussed on the selection of the most appropriate CCT and colour rendition and colour discrimination properties of light. The optimal CCT was searched using subjective preferences to visual impression under tungsten radiators [53,71], monitor simulations based on hyperspectral images [72,73], and Xe lamp based digital light processor [74]. Typically, the most preferred CCTs (3600 to 5700 K) were below that of daylight (6500 K) at illuminances within the recommended "safe" range of 50-200 lx. This partially validates the Kruithof hypothesis [75,76], which claims that lower CCTs are required to make illumination appear "pleasing" at reduced illuminances. However, the above experiments on finding the optimal CCT were carried out without regarding the conservation issues to full extent, since the variation of CCT results in the variation of the photochemical damage potential of light [64,69].

Selecting the most appropriate colour rendition and colour discrimination properties of light for artwork illumination is a more complex issue. A common requirement is to use light sources with high colour rendering ability, which is usually understood as a degree of fidelity how colours are rendered in respect of a blackbody or daylight-phase illuminant, e.g. sources with the CIE general colour rendering index R_a [4] of at least 85 are recommended [63,64]. However, colour fidelity can be partially sacrificed for the sake of photochemical safety [77]. An approach to the reduction of photochemical damage potential while maintaining colour fidelity of light sources has been demonstrated using optical filters [78]. On the other hand, increased colour saturation (gamut area) at an

expense of colour fidelity might be desirable in order to compensate the reduced colour discrimination of the human eye at lower and thus photochemically safer illuminances [41,79]. Meanwhile, reduced colour saturation might be useful to simulate the appearance of artworks originally located in low-light conditions such as churches and caves [41]. Narrow-band (450 nm-540 nm-610 nm) "prime-colour" fluorescent lamps having both sufficiently high colour fidelity and increased gamut area have been proposed years ago [57,79]. Cuttle have demonstrated an application of a narrowband red-green-blue (RGB) illuminant for artwork illumination with reduced colour fidelity and increased colour discrimination [65]. A computational comparison of a large number of daylight metamers against colour discrimination ability for hyperspectral images of artworks has shown that more colours can be resolved with illuminants having structured spectra [80]. However despite the above findings, no versatile approach to the control of photochemical damage while varying the colour rendition and colour discrimination properties of light has been developed so far. In addition, the progress in this direction is hindered by the lack of a consensus on colour rendition metrics to be used [78].

With the appearance of solid-state lighting technology based on direct-emission and phosphor-converted light-emitting diodes (LEDs) [31], the flexibility of the selection of the optimal light spectrum for artwork illumination considerably increased. In comparison with common incandescent, fluorescent, and discharge light sources, LEDs feature important advantages, such as high efficacy, very low spectral power in the unwanted regions of the spectrum, the ease of assembling into polychromatic clusters with independent control of the output for each primary-colour component, and instantaneous switching and low-voltage power supply that facilitate intelligent control using computers and smart devices. These advantages and the maturity of solid-state lighting technology allows for the development of LED based painting-specific lighting, which can meet both conservation and visualization needs of an individual artwork [41,78].

Of particular interest for advanced illumination of artworks are polychromatic clusters of coloured LEDs with the peak wavelengths and relative radiant fluxes optimized for attaining pursued properties of composite light. The computational optimization of the cluster SPDs can be performed by searching within a multi-parameter space [81,82] and using objective functions with trade-offs between certain figures of merit [33,81,83] and/or constraints on some properties [32,39]. Using such approaches, the SPDs of high-fidelity [36,41], colour-saturating [33,41,82], and colour-desaturating (dulling) [39,41] LED clusters have been optimized. Typically, colour saturating LED sources are trichromatic red-green-blue (RGB) clusters and colour dulling sources are either dichromatic yellow-blue (YB) or trichromatic red-yellow-blue (RYB) or amber-green-blue (AGB) clusters. High-fidelity LED sources (with the general colour rendering index in excess of 90) typically feature a tetrachromatic red-yellow-green-blue (RYGB) or red-amber-green-blue (RAGB) design [29,36]. Important examples of the applications of polychromatic LED clusters in artwork illumination to mention are the matching of non-white LED blends to halogen and fluorescent lighting [22], enhancing the faded colours of museum artefacts [52], and finding cultural preferences to colour quality (CCT and chromatic saturation) of illumination of artwork objects [P10]. An example of an attempt to find a trade-off between the colour contrast and damage index for cave painting is presented in [83]. However usually, adjusting the SPD of polychromatic LED clusters for meeting the required colour quality of artwork visualization was being performed without taking into account the variation of photochemical damage index of light.

In this research, a technological approach to the use of tuneable LED clusters in artwork illumination with the control of photochemical safety has been presented. The approach is based on the above described intelligently controlled tetrachromatic (RAGB) colour rendition engine [P5], which has been appended with a built-in dimming functionality for instantaneously maintaining a constant damage irradiance with the variation of CCT and colour rendition properties. We also demonstrate the operation of the engine in artwork-specific lighting in

the three modes as follows: selecting CCT, tuning chromatic saturation, and shifting chromaticity outside the white locus.

3.2.2. Principle of damage irradiance control

Our concept of a solid-state lighting engine for artwork illumination is based on an intelligent tetrachromatic RAGB LED engine described in Chapter 2. The software of the engine has been improved in order to independently control three essential properties of the generated light as follows: i) chromaticity; ii) colour rendition, and iii) photochemical action. The radiant fluxes of each of four primary-colour components are set in such proportions that the composite light has desired painting-specific spectral properties, such as chromaticity and colour saturation ability. Meanwhile, the generated radiant flux is instantaneously adjusted in such a way that the net photochemical damage irradiance provided by the actual composite light equals that of a reference light for a particular type of photosensitive material.

For this investigation, the weight parameter σ (Eq. (2.1)) is replaced by the saturation factor Γ, which is related to σ by simple equation $\Gamma = 1 - \sigma$. Such approach is more easily interpreted by subjects, which are not familiar with previous research described in this thesis.

$$c_i^{\mathrm{RAGB}} = (1-\Gamma)c_i^{\mathrm{AGB}} + \Gamma c_i^{\mathrm{RGB}}, i = R, A, G, B \tag{3.1}$$

At the RGB endpoint ($\Gamma = 1$), the generated light has the highest ability to saturate the colours of illuminated objects, whereas at the AGB endpoint ($\Gamma = 0$), the highest degree of colour dulling is attained. In between the endpoints, the RAGB blends with the highest colour fidelity, as well as with subjective preferences to the colour quality of visualized objects and with the highest colour discrimination can be arrived to. It is to be noted that the peak magnitudes of different colour fidelity indices, such as R_a [4], statistical CFI [3], and Q_f of the CQS [27] are obtained at very similar values of the saturation factor [P5,P10]. However at reduced magnitudes, different colour fidelity indices have different meaning and cannot rate colour rendition when used solely. Therefore, our

approach relies on interactive finding subjective preferences to colour quality of light through continuously tuning the saturation factor [P5,P10] rather than on setting magnitudes of certain colour rendition indices. Such an approach is an alternative to resolving the ambiguities of colour rendition metrics.

The four values of the relative partial radiant fluxes of the RAGB cluster are used for the calculation of the actual partial radiant fluxes of each of the four primary-colour components,

$$\Phi_i = F c_i^{\mathrm{RAGB}} \times 1\,\mathrm{W}, i = R, A, G, B, \tag{3.2}$$

where F is the actual dimming coefficient, which ensures that the photochemical damage irradiance provided by the actual light is kept equal to that of the reference light. The calculation of the actual dimming coefficient F is based on the reference relative partial radiant fluxes ($\mathrm{c}_{i,\mathrm{ref}}^{\mathrm{RAGB}}, i = R, A, G, B$), the type of the photosensitive material, and the value of the reference dimming coefficient, F_{ref}. The latter defines the partial radiant fluxes of the reference light

$$\Phi_{i,\mathrm{ref}} = F_{\mathrm{ref}} c_{i,\mathrm{ref}}^{\mathrm{RAGB}} \times 1\,\mathrm{W},\ i = R, A, G, B. \tag{3.3}$$

The value of the actual dimming coefficient is obtained from equating the relative damage fluxes of the actual and reference lights, which are

$$D = \int_{300}^{780} D_b(\lambda) S(\lambda) d\lambda \tag{3.4}$$

and

$$D_{\mathrm{ref}} = \int_{300}^{780} D_b(\lambda) S_{\mathrm{ref}}(\lambda) d\lambda \tag{3.5}$$

respectively. Here, $D_b(\lambda)$ is the damage function [66,69]

$$D_b(\lambda) = \exp\left[-b(\lambda - 300\,\mathrm{nm})\right], \tag{3.6}$$

where the value of the coefficient b depends on the type of photosensitive material [64]. It equals 0.038, 0.0125, 0.0115, and 0.010 for low-grade paper,

rag paper, oil paints on canvas and water colours on rag paper, and textiles, respectively.

The SPDs of the actual and reference lights are

$$S(\lambda) = \sum_{i=R,A,G,B} c_i^{\mathrm{RAGB}} S_i(\lambda) \tag{3.7}$$

and

$$S_{\mathrm{ref}}(\lambda) = \sum_{i=R,A,G,B} c_{i,\mathrm{ref}}^{\mathrm{RAGB}} S_i(\lambda) \tag{3.8}$$

respectively, where $S_i(\lambda)$ are the SPDs of the primary-colour LED components normalized to unit power.

Eventually, the actual dimming coefficient is calculated form the condition $FD = F_{\mathrm{ref}} D_{\mathrm{ref}}$ with a glance to Eqs. (3.4)–(3.8) equals

$$F = F_{\mathrm{ref}} \sum_{i=R,A,G,B} c_{i,\mathrm{ref}}^{\mathrm{RAGB}} d_{bi}(b) \Big/ \sum_{i=R,A,G,B} c_i^{\mathrm{RAGB}} d_{bi}(b), \tag{3.9}$$

where d_{bi} is the damage index of the i-th component for a particular photosensitive material per unit radiant flux

$$d_{bi} = \int_{300}^{780} D_b(\lambda) S_i(\lambda) d\lambda, i = R, A, G, B. \tag{3.10}$$

The actual dimming coefficient found form Eq. (3.9) is used for setting the four values of the actual partial radiant fluxes defined by Eq. (3.2).

3.2.3. Colour rendition engine with the control of damage irradiance

Practical light engine comprises two basic modules: an external smart device (e.g., tablet computer or mobile phone) with uploaded software and a tetrachromatic LED luminaire containing a microcontroller-based four-channel current source with firmware. The two modules are connected by a wireless link based on the Bluetooth standard. Figure 3.4 shows the block diagram of the engine and Fig. 3.5 displays the screenshot of the graphic interface.

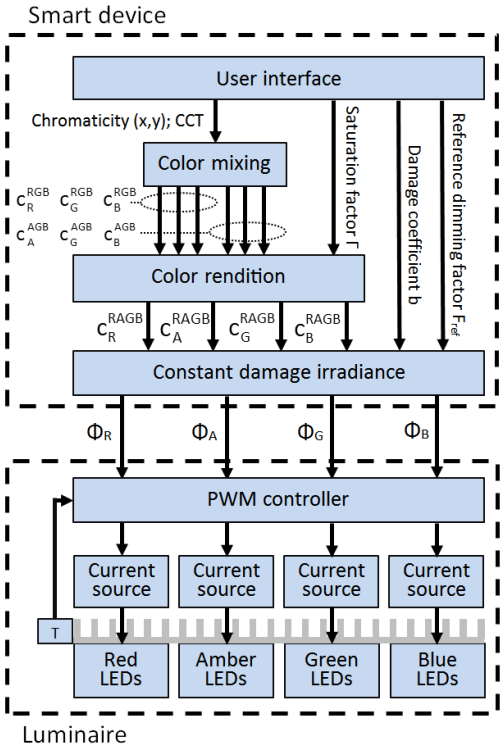

Fig. 3.4. Block diagram of the light engine [P15].

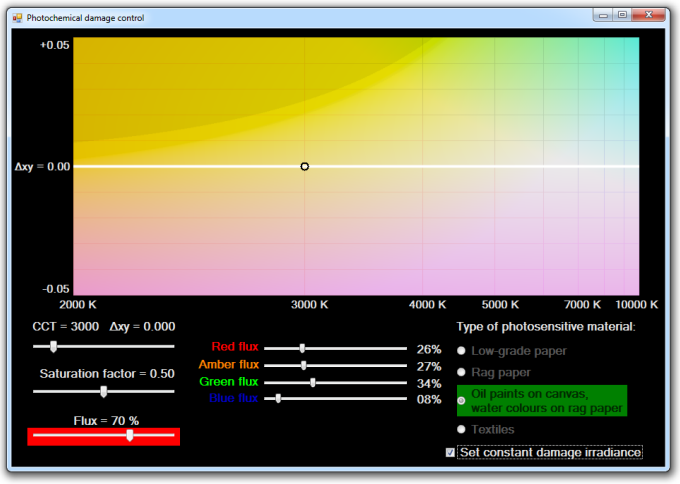

Fig. 3.5. Snapshot of the graphic interface of the smart device that is used for the control of light engine [P15].

The graphical user interface of the software allows the user to input painting-specific data (chromaticity and/or CCT, saturation factor, type of photosensitive material) and to fixate the spectral composition and dimming coefficient of a light selected as providing a reference damage iraadiance. The software also contains a calculation script and a database of LED parameters (normalized SPDs, tristimulus values, and damage indices for different photosensitive

materials). Upon inputting the chromaticity coordinates of desired light (CIE 1931 *x, y* or those derived form CCT) and the saturation factor, the software computes the four relative partial radiant fluxes of the tetrachromatic RAGB cluster.

Upon setting the spectral properties of a reference light (e.g., CCT = 3000 K, saturation factor $\Gamma = 0.5$) and the type of photosensitive material (e.g., oil paints on canvas) and adjusting the dimming level (e.g., 50 lx measured by an auxiliary light meter at the surface of the illuminated artwork), the reference relative partial radiant fluxes and the reference dimming coefficient are recorded using the fixation checkbox on the graphical interface. With further tuning the chromaticity and colour saturating factor, the software instantaneously recalculates the value of the dimming coefficient and the resulting values of the partial radiant fluxes of the actual light, using Eq. (3.9) and Eq. (3.2), respectively. The latter values are sent to the luminaire via the wireless connection.

Based on the input data, the microcontroller of the luminaire generates PWM signals for the four-channel current source, which drives the four groups of coloured LEDs. The output of each group of coloured LEDs is digitally regulated against the drift of LEDs junction temperature using feed forward compensation [84], which is based on the calibration data on LEDs output as a function of heat sink temperature (measured by a thermistor) and driving current. The calibration data is stored in the memory of the firmware of the microcontroller.

The primary-colour LEDs for the tetrachromatic RAGB cluster were selected from a range of standard commercial devices. The main criteria for the selection of particular types of LEDs were attaining as high as possible diversity in colour rendition properties [29] and high luminous efficacy of the cluster at CCTs of 3000-4000 K that fall within the range of most preferred ones [72-74] and may potentially determine a lower photochemical damage index. The selected LEDs were as follows: direct-emission red LED (Cree model XP-E2 XPEBRD, 639 nm peak wavelength), green LED (Cree model XP-E2 XPEBGR, 518 nm), and blue LED (Cree XP-E2 XPEBRY, 452 nm) and phosphor converted amber

LED (Philips Lumileds model LXM2-PL01, 597 nm). (These primary LEDs differ from those used in our previous versions of the engine [P10,52].) The calibration data on the SPDs of the LEDs were obtained using a Labsphere model Illumia® Pro system.

Table 3.3 displays the colour rendition indices and photochemical damage parameters for the selected set of primary-colour LEDs for three values of CCT (3000 K. 4500 K, and 6500 K). Each value of CCT is represented by three limiting blends, RGB ($\Gamma = 0$), AGB ($\Gamma = 0$), and high-fidelity tetrachromatic blend with the value of σ indicated. These blends have the highest colour-saturating, colour-dulling, and colour fidelity abilities, respectively. Also are shown the characteristics typical of tungsten radiators, CIE standard illuminant A (2856 K blackbody) and that with the SPD truncated below 400 nm, which mimics an incandescent lamp with a UV filter widely used in museum lighting.

The colour rendition indices in Table 3.3 are presented for three colour rendition approaches: R_a and GAI used in the two-metrics approach [17], CSI, CDI, and CFI used in the statistical approach [3], and Q_f and Colour Gamut Scale (Q_g) used the CQS approach [27]. The RGB blends have the highest ability to saturate the colours of illuminated objects, which is represented by the highest values of GAI, CSI and Q_g. Contrarily, the AGB blends have the highest desaturation ability, which is represented by the lowest values of GAI, CSI and Q_g and the highest value of CDI. The high-fidelity RAGB blends, which correspond to the peak values of CFI, also have high values of R_a and Q_f.

The photochemical damage indices in Table 3.3 are presented by LER, the UV radiant flux per unit luminous flux, and relative damage factor [70], which is the ratio of the damage indices of a source and the CIE standard illuminant A and can be defined as

$$\mathrm{RDF} = \frac{D/\mathrm{LER}}{D_\mathrm{A}/\mathrm{LER}_\mathrm{A}}, \tag{3.11}$$

where D and D_A are the relative damage fluxes for the RAGB blend under consideration and CIE standard illuminant A, respectively, defined by Eq. (3.4)

and LER and LER_A are the respective luminous efficacies of radiation. Table 3.3 shows the RDF values for two photosensitive materials: low-grade paper (b = 0.038) and oil paint on canvas (b = 0.0115).

The LED cluster is seen to have LERs of up to twice as higher as those of tungsten illuminants and the UV radiant flux per unit luminous flux is more than twice as lower that of the unfiltered tungsten illuminant. However within a more consistent approach based on damage functions, the RDF of light generated by the LED cluster at 3000 K is comparable with that of the filtered tungsten illuminant. The RDF increases with CCT showing the necessity of reducing illuminance in order to maintain the damage flux at a constant value. Also, the variation of illuminance is seen to be reasonable while the variation of colour rendering properties, since the RDF has a general tendency to increase with decreasing the colour saturation ability of light (i.e. while tuning from the colour-saturating RGB endpoint to the colour dulling AGB endpoint).

Table 3.3. Colour rendition indices and photochemical damage parameters of the RAGB LED cluster and tungsten illuminants [P15].

CCT (K)	Light source	Colour rendition metrics							LER (lm/W)	Irradiance below 400 nm per unit luminous flux (μW/lm)	RDF	
		Two-metric		Statistical			CQS					
		Colour rendition indices									low-grade paper	oil paint on canvas
		R_a	GAI	CSI (%)	CFI (%)	CDI (%)	Q_f	Q_g				
3000	AGB (Γ = 0)	79	55	0	39	46	80	90	343	38	0.28	0.77
	RAGB (Γ = 0.47)	96	62	1	93	1	91	102	296	36	0.27	0.80
	RGB (Γ = 1)	16	79	78	7	0	35	132	231	27	0.23	0.89
4500	AGB (Γ = 0)	89	84	0	64	20	87	97	301	38	0.37	1.03
	RAGB (Γ = 0.28)	95	90	1	89	2	92	105	290	36	0.36	1.04
	RGB (Γ = 1)	30	125	70	9	1	41	138	236	28	0.33	1.12
6500	AGB (Γ = 0)	92	100	1	74	8	87	100	281	38	0.46	1.27
	RAGB (Γ = 0.15)	93	104	1	84	2	89	104	276	38	0.46	1.28
	RGB (Γ = 1	38	147	67	9	2	44	138	231	30	0.43	1.35
2856	CIE A	100	56	0	100	0	98	98	156	82	1.00	1.00
2848	CIE A filtered	100	56	0	100	0	98	98	157	0	0.17	0.85

3.2.4. Demonstration of artwork visualization with controlled photochemical safety

Below the examples of application of our light engine in three different operation modes for adjusting the visual appearance of artworks and museum exhibits under a constant damage irradiance are presented. The purpose of the demonstration is to prove the effect of the alteration of visual impression due to the control of photochemical safety rather than to psychophysically assess or find subjective preferences to colour quality of artwork illumination, which are artwork-specific and even depend on the cultural background of an observer [P10].

The first example refers to the control of CCT, which is a well-known approach to advanced artwork illumination [P10,53,71-74]; here in addition, the highest colour fidelity is maintained while tuning CCT. In the second example, we demonstrate the control of colour rendition by continuously tuning the saturation factor under metameric conditions. Such tuning is required for the compensation of reduced colour discrimination under dim light, enhancing faded colours or meeting artwork-specific needs in chromatic representation [P10,41,52,65,83]. The third example shows shifting the chromaticity out of the white light locus along an isotemperature line (assuming that the CCT and colour saturation factor have been already established). Such shifting might be helpful for visual reconstruction of aged artworks and/or for visualization using non-white light [22,58].

Each example is presented for an individual artwork or museum exhibit that is selected on the basis of its relevance to a particular mode of operation of the engine. For revealing the effect of photochemical damage control on artwork visualization, two series of photoimages are displayed in each case: one series at a constant illuminance of 50 lx and another series at a constant damage irradiance that equals that under reference light with an illuminance of 50 lx. The visual differences between the series of images are to be traced with the limited colour accuracy of the photoimages borne in mind.

3.2.4.1. Colour temperature selection

For the demonstration of the selection of CCT with controlled photochemical safety, a post-impressionistic water-colour painting by E. Kuokštis was selected. The artwork displays a medieval downtown scene in Vilnius, Lithuania and has been painted in 2004 under daylight. According to the author, the colours of the artwork underwent minor changes since the date of creation. Therefore at first tending, the optimization of the conditions of illumination can be restricted to the selection of CCT at the conditions of the highest colour fidelity, i.e. without visual correction of the hue and chroma of the colours.

Figure 3.6(a)-(e) show the SPDs of the light engine for different CCTs in the range of 2500-6500 K with the saturation factor set for the highest colour fidelity (for specificity, here we use R_a as a scale for colour fidelity, although the statistical CFI and CQS Q_f attain the peak values at almost the same value of Γ). The SPDs are seen to continuously cover the visible spectrum and differ in the proportions between the components: with increasing CCT, the relative parts of the blue and green components increase, whereas those of the red amber components decrease.

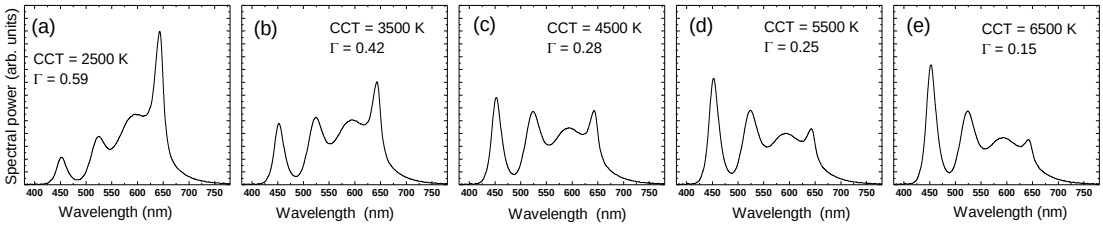

Fig. 3.6. SPDs of the light engine for CCTs of 2500 K (a), 3500 K (b), 4500 K (c), 5500 K (d) and 6500 K (e) with the saturation factor (indicated) tuned to the highest values of the general colour rendering index R_a [P15].

Table 3.4 shows the RDFs and colour rendition indices for the used high-fidelity tetrachromatic blends with different CCTs in the range of 2500-6500 K. The RDFs are estimated for different materials having spectral damage functions specified in Ref. [64] and their values are seen to increase with CCT by a factor of 2 for low-grade paper, which has the steepest damage function (highest value of the coefficient *b*) and by a factor of 1.67 for textiles, which have the flattest damage function (lowest value of the coefficient *b*). The colour rendition indices

are displayed for the three metrics discussed above (two-metrics, statistical, and CQS). The colour fidelity indices (R_a, CFI, and Q_f) are seen to have very high values. The GAI, which shows the gamut area in respect that of the CIE standard illuminant E, increases with CCT and attains a value of about 100 at daylight chromaticity. The CQS Q_g shows the gamut area similar to that for reference illuminants with the same CCT. The statistical indices CSI and CDI, which show the percentage of test colour samples with distorted chroma, are low.

Table 3.4. Relative damage factors for different materials and colour rendition indices of different metrics as functions of CCT for the light engine operating in the high-fidelity regime [P15].

Correlated colour temperature (K)		2500	3500	4500	5500	6500
RDF for different materials	Low-grade paper	0.23	0.31	0.36	0.41	0.46
	Rag paper	0.69	0.92	1.04	1.18	1.29
	Oil paint on canvas, water colours on rag paper	0.71	0.92	1.04	1.16	1.28
	Textiles	0.73	0.91	1.01	1.12	1.22
Two-metric indices	General colour rendering index R_a	96	95	95	93	93
	Gamut area index GAI	48	75	90	98	104
Statistical indices	Colour saturation index CSI (%)	0	1	1	1	1
	Colour fidelity index CFI (%)	95	93	89	86	84
	Colour dulling index CDI (%)	1	2	2	2	2
CQS indices	Colour fidelity scale Q_f	90	93	92	90	89
	Colour gamut scale Q_g	103	106	105	105	104

Figure 3.7(a)-(e) show the images of the painting for different CCTs under a constant illuminance of 50 lx. On top of each image, the applied light is characterized by CCT and RDF estimated for water colours (b = 0.0115). Most observers would notice that with increasing CCT, the colour palette of the painting enhances. At a CCT typical of daylight (6500 K; Fig. 3.7(e)), the conditions most close to those when the artwork has been created are reproduced. While increasing CCT from 2500 K to 6500 K, the RDF is seen to increase by a factor of 1.8, which indicates a substantial variation of damage irradiance.

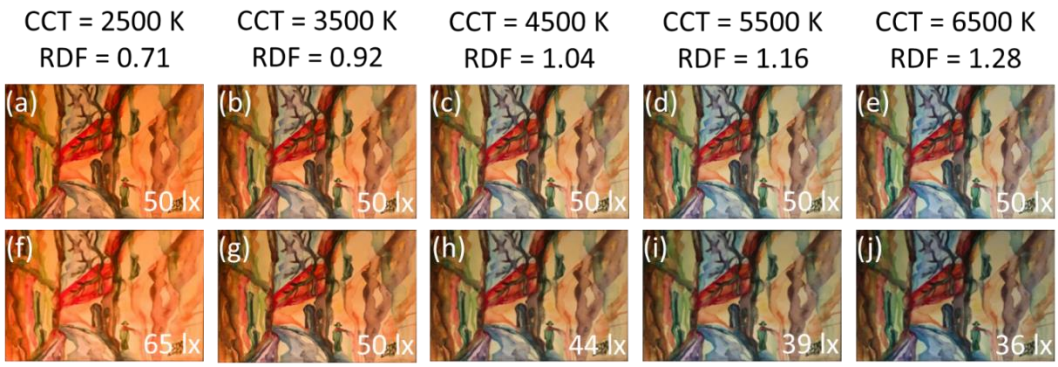

Fig. 3.7. (a)-(e) Images of a water-colour painting "Downtown Vilnius" (E. Kuokštis, 2004) for different CCTs at a constant illuminance of 50 lx. (f)-(j) Images of the same painting for different CCTs with the damage irradiance kept constant at a value equal to that at a CCT of 3500 K. The illuminance is indicated in the bottom-right corner of the images [P15].

In order to avoid the effect of increasing damage irradiance with increasing CCT, the product of illuminance and RDF is to be kept constant. Fig. 3.7(f)-(j) show the images for respective CCTs with illuminance varied in such a way that the damage irradiance is maintained at a constant value equal to that for 50 lx illuminance at a CCT of 3500 K. Now with increasing CCT, an observer would notice a substantial dimming effect, which converts to an illuminance of only 36 lx at a CCT of 6500 K. Contrarily with reducing CCT to 2500 K, the illuminance is increased to 65 lx. Such noticeable variation in illuminance might influence the selection of preferential lighting conditions in favour of CCTs that are lower than that of daylight.

3.2.4.2. Colour saturation tuning

In order to demonstrate colour rendition tuning with controlled photochemical safety, we selected a folk-art exhibit, a Lithuanian national ribbon. The ribbon has been woven in 1977 and since that time exposed to daylight (for 37 years). Due to aging, the colours have partially lost vividness; in particular, the dominating red colour of the woollen threads that were dyed using a natural pigment has darkened. In order to visually compensate the darkening, the optimization of illumination can be performed by selecting an appropriate saturation factor. While varying the saturation factor, the CCT was kept constant at a value of 3000 K, which is typical of halogen lamps widely used in museum lighting.

Figure 3.8(a)-(d) show the metameric SPDs of the light engine for different values of the saturation factor at a CCT of 3000 K.

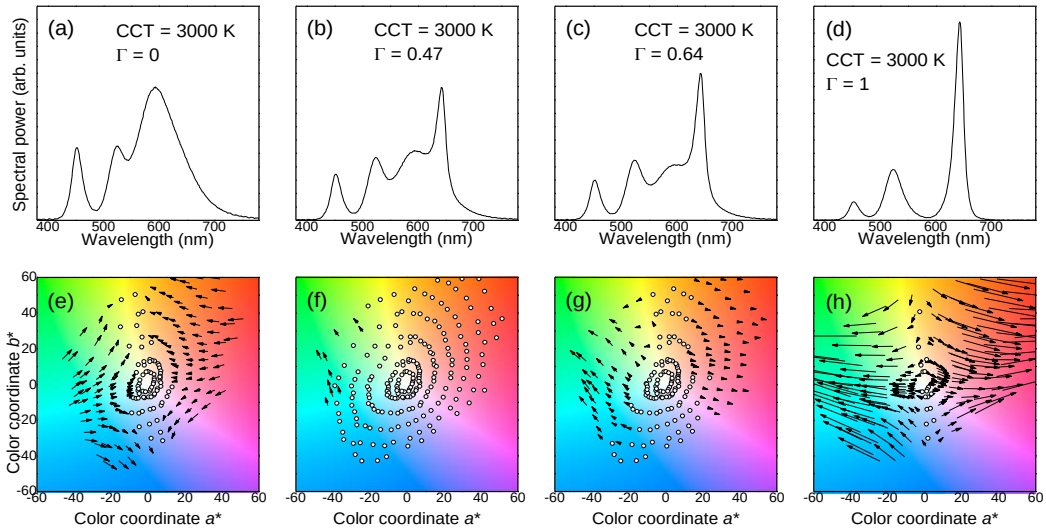

Fig. 3.8. SPDs of the light engine for the values of the saturation factor of 0 (a), 0.47 (b), 0.64 (c), and 1 (d) at a constant CCT of 3000 K. (e)-(f) Corresponding distributions of the colour-shift vectors for 218 Munsell samples of value /6 in the a*−b* chromaticity plane of the CIELAB colour space. Open circles, chromaticites of the colour test samples rendered with high fidelity; arrows, schematic representation of the vectors of the samples that are rendered with perceptually noticeable colour distortion [P15].

With increasing the saturation factor, the amber component is seen to be gradually replaced by the red one; also the green component increases. Figure 3.8(e)-(h) depict the corresponding distributions of the colour-shift vectors in respect of the metameric reference light (blackbody) for 218 Munsell samples of value /6 in the a^*-b^* chromaticity plane of the CIELAB colour space. The open circles in Fig. 3.8(e)-(h) denote chromaticites of the colour test samples that have the colour-shift vectors residing within the three-step MacAdam ellipses, i.e. rendered with high fidelity. The arrows schematically represent the vectors of the samples that stretch out of the three-step MacAdam ellipses. Figure 3.8(e), (f), (g), and (h) show the distribution of the colour shift vectors for the colour dulling AGB end-point (Γ = 0), high-fidelity RAGB blend (Γ = 0.47), "colour-preference" RAGB blend (Γ = 0.64) [P5], and colour saturating RGB end-point (Γ = 1) that correspond to SPDs shown in Fig. 3.8(a), (b), (c), and (d), respectively. At Γ = 0, a substantial portion of the vectors is seen to be directed inwards, i.e. many colours have reduced chroma. At Γ = 0.47,

a maximal number of colours rendered with high fidelity is attained. With further increase of Γ, the number of vectors directed outward, i.e. showing increased chroma of the samples, starts increasing at an expense of samples rendered with high fidelity. At Γ = 0.64, preferential colour rendition with a still high number of high-fidelity colours can be established. At Γ = 1, the number of samples having increased chroma attains a maximum (also for this blend, many colour test samples have perceptually noticeable distortions of hue [3]).

Table 3.5. Relative damage factors for different materials and colour rendition indices of different metrics as functions of the saturation factor for the light engine at a CCT of 3000 K [P15].

Saturation factor Γ		0	0.47	0.64	1
RDF for different materials	Low-grade paper	0.28	0.27	0.27	0.23
	Rag paper	0.75	0.79	0.80	0.91
	Oil paint on canvas, water colours on rag paper	0.77	0.80	0.81	0.89
	Textiles	0.76	0.80	0.82	0.95
Two-metric indices	General colour rendering index R_a	78	96	89	16
	Gamut area index GAI	55	62	66	79
Statistical indices	Colour saturation index CSI (%)	0	1	27	78
	Colour fidelity index CFI (%)	39	93	60	7
	Colour dulling index CDI (%)	46	1	0	0
CQS indices	Colour fidelity scale Q_f	80	91	87	35
	Colour gamut scale Q_g	90	102	108	132

Table 3.5 shows the RDFs and colour rendition indices for the used tetrachromatic blends with different saturation factors at a CCT of 3000 K. The RDF decreases with the saturation factor for low-grade paper (by a factor of 0.82). For the rest materials, it increases by factors from 1.16 to 1.25 depending on the material. The colour fidelity indices (R_a, CFI, and Q_f) are seen to be reduced with moving from the high-fidelity value of Γ in both directions. With increasing the saturation factor, the GAI, CQS Q_g, and statistical CSI increase, whereas the statistical CDI decreases.

Figure 3.9(a)-(d) display the images of the ribbon for the corresponding saturation factor under a constant illuminance of 50 lx. The saturation factor and RDF estimated for textiles (b = 0.010) are indicated on top of each image. It can be noticed that with increasing Γ above the high fidelity value of 0.47, the colours of the ribbon, especially the red one, become more vivid, which indicate on the compensation of the darkening effect. Meanwhile at Γ = 0, the colours

appear even more dull than under high-fidelity conditions. Within the entire range of the variation of the saturation index from 0 to 1, the RDF is seen to increase by a factor of about 1.25. At a constant illuminance, this corresponds to an increase of damage irradiance by the same factor.

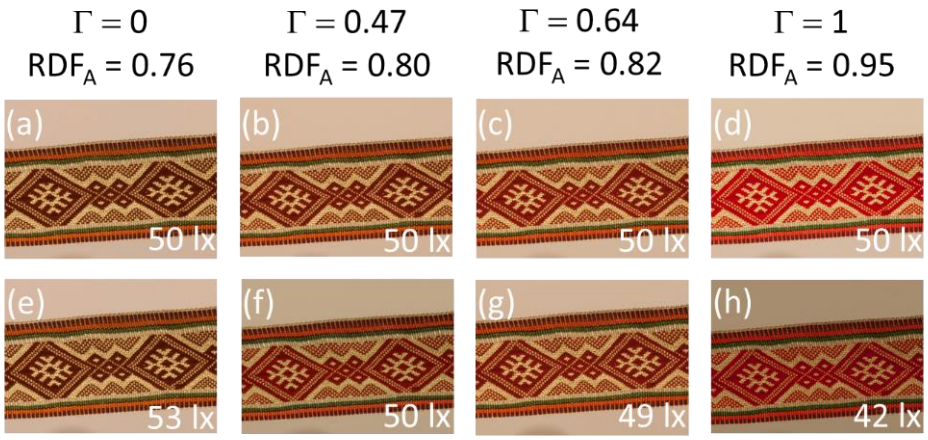

Fig. 3.9. (a)-(d) Images of a Lithuanian national ribbon for different saturation factor at a CCT of 3000 K and at a constant illuminance of 50 lx. (e)-(h) Images of the same ribbon for different saturation factor at a constant damage radiance. The illuminance is indicated in the bottom-right corner of the images [P15].

The effect of the variation of damage irradiance with increasing Γ can be avoided through the corresponding control of illuminance. Figure 3.9(e)-(h) show the images for respective values of the saturation factor with the illuminance varied in such a way that the damage flux is maintained at a constant value equal to that for 50 lx illuminance at Γ = 0.47. This results in an illuminance increase to 53 lx at Γ = 0, which corresponds to the highest colour-dulling effect, and in a drop of illuminance to 42 lx at Γ = 1, which corresponds to the highest colour-saturating effect. Again, such a variation of illuminance is seen to noticeably affect the variation of visual impression provided by the ribbon. This means that while varying the colour saturation ability of illumination, subjective preferences to colour rendition at a constant illuminance and at a constant damage irradiance might be different.

3.2.4.3. Shifting chromaticity along an isotemperature line

The photochemically safe shifting of the chromaticity out of the white light locus is demonstrated on a painting by Lithuanian artist ant mystic M. K. Čiurlionis (1875–1911). The artwork “Funeral symphony” has been

painted in 1909 with pastel on paper. After exhibiting for more than one hundred year, the colours of this painting partly faded and some brownishing of the substrate appeared. The latter effect resulted in the overall shift of the chromaticity gamut, which can be partially compensated by shifting the chromaticity of the light source out of white light locus. Prior to such a shifting, the most appropriate CCT and saturation factor are to be selected. To maintain a constant value of CCT, we performed shifting along the isotemperature line within the colour space.

Figure 3.10 shows a segment of the CIE 1931 chromaticity diagram with the blackbody locus (solid line) and an isotemperature line (dashed line). The CCT was selected to equal that of standard illuminant B (4870 K).

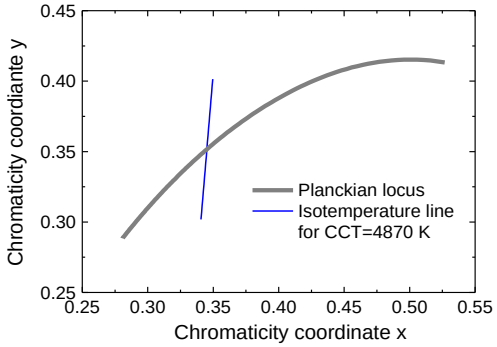

Fig. 3.10. Segment of the CIE 1931 chromaticity diagram with the Planckian (blackbody) locus (solid line) and an isotemperature line for a CCT of 4870 K (dashed line) shown. The isotemperature line stretches out of the Planckian locus by Δxy = 0.05 in both directions [P15].

Figure 3.11 shows the SPDs of the light engine for three chromaticities of the selected isotempertaure line: (a) below the Plancian locus ($\Delta xy = -0.05$), (b) right on the locus ($\Delta xy = 0$), and (c) above the locus ($\Delta xy = +0.05$). All SPDs have a value of the saturation factor of 0.5 that was selected in order to partially compensate the fading of colours by increased saturation rather than to provide high fidelity blend ($\Gamma = 0.28$). While moving upward along the isotemperature line (i.e. from purple region to white point and further to yellow-green region), the red and blue components are seen to decrease, whereas the amber and green components increase.

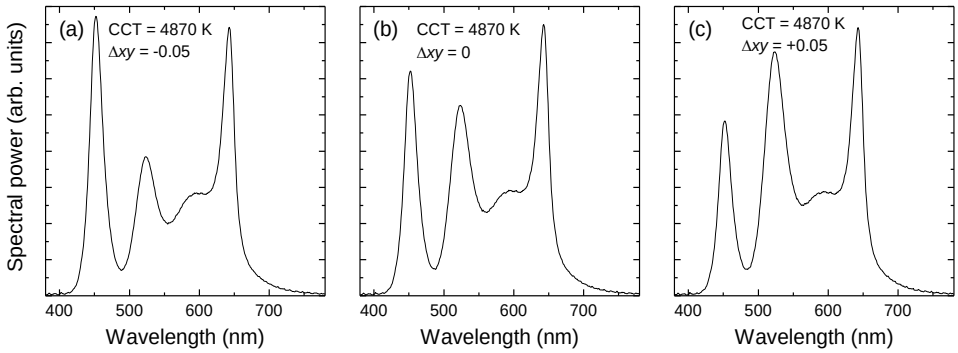

Fig. 3.11. SPDs of tetrachromatic light engine tuned along an isotemperature line (CCT = 4870 K, Γ = 0.5). The deviation from the Planckian locus Δxy is −0.05 (a), 0 (b), and +0.05 (c), respectively [P15].

Table 3.6 shows the RDFs and colour rendition indices for the used tetrachromatic blends with different chromaticity shifts along the isotemperature line of CCT = 4870 K and at Γ = 0.5. With the variation of the chromaticity shift from –0.05 to +0.05, the RDF is seen to decrease by a factor of 0.67 to 0.76 depending on the material. The colour rendition indices (shown for the white chromaticity at $\Delta xy = 0$) indicate on an increase of the colour saturating effect at an expense of colour fidelity.

Table 3.6. Relative damage factor for different materials and colour rendition indices as functions of the chromaticity shift along the isotemperature line for CCT = 4870 K at a saturation factor of 0.5 [P15].

Chromaticity shift Δxy		−0.05	0	+0.05
Chromaticity coordinate x		0.341	0.348	0.35
Chromaticity coordinate y		0.302	0.352	0.401
RDF for different materials	Low-grade paper	0.42	0.37	0.28
	Rag paper	1.34	1.13	0.98
	Oil paint on canvas, water colours on rag paper	1.31	1.12	0.98
	Textiles	1.27	1.09	0.96
Two-metric indices	General colour rendering index R_a	–	84	–
	Gamut area index GAI	–	103	–
Statistical indices	Colour saturation index CSI (%)	–	34	–
	Colour fidelity index CFI (%)	–	44	–
	Colour dulling index CDI (%)	–	1	–
CQS indices	Colour fidelity scale Q_f	–	84	–
	Colour gamut scale Q_g	–	113	–

Figure 3.12(a)-(c) display the images of the painting for different chromaticity shifts under a constant illuminance of 50 lx. The chromaticity shift and RDF estimated for $b = 0.010$ (equal to that of oil paint on canvas or water

colours on rag paper) are indicated on top of each image. For the chromaticity shift of $\Delta xy = -0.05$, the brownishing effect on the colours of the painting is seen to become even more pronounced in respect of white light ($\Delta xy = 0$) due to the emerging of purplish hues. Meanwhile For the chromaticity shift of $\Delta xy = +0.05$, the brownishing effect is noticeably compensated. With the variation of the chromaticity shift from –0.05 to +0.05, the RDF is seen to decrease by a factor of about 0.75, i.e. with the damage irradiance decreases correspondingly.

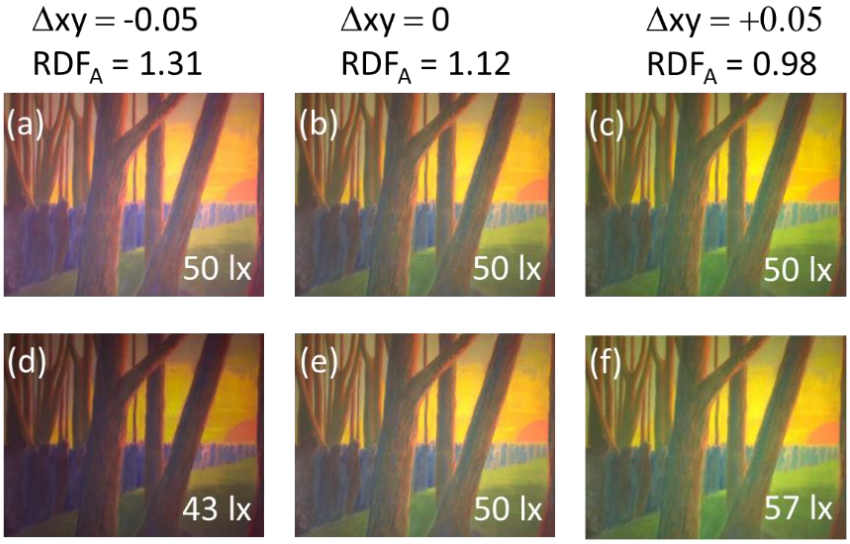

Fig. 3.12. (a)-(c) Images of a pastel painting "Funeral symphony" (M. K. Čiurlionis, 1909) for the different shifts of the chromaticity of incident light along an isotemperature line of 4870 K CCT at a constant illuminance of 50 lx. (d)-(f) Images of the same painting for different CCTs with the damage irradiance kept constant at a value equal to that at $\Delta xy = 0$. The illuminance is indicated in the bottom-right corner of the images [P15].

The effect of the decrease of RDF with the favoured shift of the chromaticity of light in the upward direction can be exploited for increasing the illuminance without increasing damage irradiance. Figure 3.12(d)-(f) show the images for respective values of the chromaticity shift with the illuminance varied in such a way that the damage flux is maintained at a constant value equal to that for 50 lx illuminance at $\Delta xy = 0$. This results in an illuminance decrease to 43 lx at $\Delta xy = -0.05$, which corresponds to the enhancement of the undesirable brownishing effect, and in an increase of illuminance to 57 lx at $\Delta xy = +0.05$, which corresponds to the partial compensation of the brownishing effect. Such a variation of illuminance with the shift of the chromaticity of incident light might affect the selection of subjective preferences to colour rendition. Note that once

the Δxy = +0.05 option is selected for the painting under consideration, the illuminance can be reduced in order to reduce the damage irradiance in respect of that of white light.

For the particular set of four primary LEDs used in the RAGB illuminant of our engine, the most noticeable visual effect due to maintaining constant damage irradiance was dimming by a factor of up to 1.8 when increasing CCT in the range of 2500-6500 K. Tuning colour saturation in between colour-dulling (AGB) and colour-saturating (RGB) endpoints of the RAGB illuminant requires the variation of illuminance by up to 25% depending on the CCT and type of photosensitive material. Also, the sign of the illuminance variation was found to depend on the material (e.g., for low-grade paper, increased colour saturation results in an increase of illuminance at a constant damage irradiance, whereas for other materials, the effect is reverse). Shifting the chromaticity along the isotemperature line at a CCT of 4870 K resulted in an increasing of illuminance by up to 15% per positive chromaticity increment of Δxy = 0.01.

3.3. Conclusions of the third chapter

The concept artwork- and observer- specific illumination was developed based in the tetrachromatic solid-state lighting engine with tuneable CCT and colour rendition properties.

The preferences to colour quality of illumination for two representative groups of subjects with different cultural background (Chinese and American) were investigated using the solid-state lighting engine with the continuously tuneable quadrichromatic blends. For very familiar objects, cultural differences did not affect the average of the selected blends. For paintings, which are less familiar objects, cultural differences in the average selected blends depended on the level of the familiarity of the painting content. An unfamiliar painting also showed preferences to CCT being dependent on the cultural background. In all cases, the American subjects exhibited noticeably wider distributions of selection rates.

By using an instantaneous dimming functionality, the photochemical influence into illuminated surfaces can be controlled. The effect of constant damage irradiance on the visual impression from artworks while operating the lighting engine in three different modes, such as selecting colour temperature, tuning colour saturation, and shifting chromaticity outside white light locus, respectively. These control modes can be used for attaining the most appropriate visual appearance of an artwork, visual reconstruction of the colours altered due to aging, and meeting specific visual needs of observers (e.g., colour deficient or elderly people).

4. Optimization of luminance distribution for intelligent outdoor lighting

The main scope of outdoor lighting is the extension of an acceptable human life quality for the dark period of the day. Life quality comprises the accessibility of social activities, crime prevention, traffic safety, aesthetic impact, and human behaviour. On the other hand, outdoor lighting is connected to energy saving and related environmental issues. In particular, street and road lighting consumes about ~2 % of global electric power and is responsible for the annual exhaust of more than 300 million tons of carbon dioxide (CO_2) in the European Union and USA. This chapter is focused on the application of solid-state technology for outdoor lighting. Here, the results on the optimization of the luminance distribution within an intelligent lighting installation for pedestrian areas using the identification of subjective impressions by Likert scale and SDS are presented [P3,P6,P13,P17,C4,C6,C18].

4.1. Literature survey

In recent years, the interest in LED based outdoor illumination is increasing due to the energy saving potential and versatility in spectral power distribution provided by solid-state lighting technology [85-87]. In particular, intelligently dimmed LED-based outdoor lighting installations that track pedestrians and vehicles in real time offer substantial economical benefits [P3,88,89-91]. Such dynamical tracking can be implemented using different dimming scenarios and luminance distributions (lighting patterns) around a traffic participant [P3,89,91]. However, the approaches to the selecting of dynamically controlled lighting patterns that are advantageous in terms of subjectively evaluated lighting quality have not been established so far.

The assessment of outdoor lighting quality is based on the measurement of physical parameters, evaluation of human visual perception aspects and influence of lighting on the environment [92-94]. Commonly, two types of criteria are used to evaluate outdoor lighting quality. The objective criteria are based on statistical data of accidents, and the subjective criteria are based on

psychophysical data from laboratory or real-situation conditions. The objective criteria are the crime rate and traffic accident rate. In fact, historically, road and street lighting was introduced in order to combat the crime rate [95]. Although this is still one of the major considerations in justifying the installations of road lighting, presently the chief criterion is the reduction of the night-time traffic accident rate [96,97]. Researchers have investigated discrete parameters that might be affected by lighting characteristics such as perceived brightness [98], preference [99], visual acuity [100], feeling of safety [89,100], reaction time [93,101-103], visual field [104], colour identification [105,106] and recognition threshold and small target visibility [107]. In practice, the application of such a large number of parameters to the subjective evaluation of the lighting quality of intelligently controlled installations poses a difficult problem [108-111].

The goal of this investigation was to establish the main subjective factors and criteria for the assessment of lighting quality relevant to pedestrians subjected to different lighting patterns within an intelligently controlled LED-based installation. A psychophysical method based on questionnaires was applied. The subjective impressions were identified using the SDS [112,113] and Likert scale [114]. The factor analysis of the data was used in order to reveal a structure in the relationship between the scaling items and to reduce the number of variables for the establishing of lighting quality.

4.2. Methods

4.2.1. Experimental lighting installation

The experiment was carried out within an intelligent LED-based outdoor lighting installation [P3]. Six lamp posts (luminaires mounted on 10 m high posts) were illuminating a section of a street passing through a moderately urbanized pinewood area of the Vilnius University campus (Fig. 4.1). The distance between the posts was 30 meters.

Fig. 4.1. Photograph of the lighting installation at Vilnius University campus [P13].

Each lamp (Zhejiang Howell Illuminating Technology Co. Ltd model HL-A00101) consisting of 66 high-power white phosphor-conversion LEDs (Cree model XR-E) with a correlated colour temperature of 3060 K and with the general colour rendering index of 82 were used. The spectral power distribution of these LEDs contains a narrow band peaking at about 450 nm and a broad band peaking at about 600 nm (Fig. 4.2). The rated photopic luminous flux of each lamp was 7180 lm. A luxmeter (Konica-Minolta model T10) was used to measure horizontal illuminance at ground level. Without dimming, the illuminance was 23 lx and 13 lx under a post and in the middle of two posts, respectively. The luminance of road surface and luminance uniformity were measured according to the EN 13201-3 standard using an imaging photometer (System Instruments model Lumicam 1300 Color). The average luminance of road surface was 1.7 cd/m^2 with the maximal and minimal values of 3.2 cd/m^2 and 1.0 cd/m^2, respectively. The longitudinal luminance uniformity along the road centre line was about 0.8.

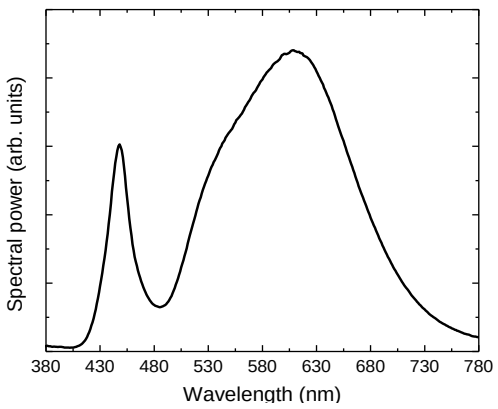

Fig. 4.2. Spectral power distribution of LEDs used in the lamps [P13].

Using a microcontroller based control system operated by PLC, the lamps were individually dimmed in order to simulate different lighting patterns. Each lamp was operated either at the full rated flux (100%), or dimmed to 50%, 10%, or 0% (switched-off) of the rated flux. Bi-directional PLC was provided by individual adapters (TP-Link model TL-PA201) operating at a data transfer rate of 200 Mbps. The station and pole electronics was connected to individual Ethernet mini-modules (Propox model MMnet01) comprising an Ethernet controller and microcontroller. An external computer was used to set the lighting patterns.

The preliminary experiment was run with 7 female subjects who ranged in age from 21 to 28 years. These girls were presented with different lighting modes and filled the SDS and Likert scale. Also, while varying number of the street lights posts (from 1 to 6 lamps), we were looking for a point where the subject stated that switching on an additional lamp doesn't make street lighting better, but switching off an additional lamp deteriorates street lighting. After this preliminary experiment, the procedure of the research was discussed in detail and was updated according to the observations of subjects. Also Cronbach alpha was calculated for the SDS and for each test group of statements of Likert scales.

The preliminary experiment suggested that the output level of the lamp in the fourth post has already no noticeable influence on the results of evaluation. Thus in the main experiment only the patterns with the variable output level of the lamps in the first, second, and third posts was used. Also, the lighting patterns evaluated negatively by all participants of the preliminary experiment were withdrawn. Eventually, seven lighting patterns pertinent to the location of a subject were selected for the examination. Below, the patterns are marked by 3-number notations. For example, a notation "0.1/0.5/1" corresponds to a pattern with the output level of the lamp in the first, second, and third posts of 10%, 50%, and 100%, respectively. Figure 4.3(a)-(g) display the distribution of horizontal illuminance along the central line of the street and Fig. 4.3(h) shows the two-dimensional distribution of horizontal illuminance for pattern 7 (1/1/1).

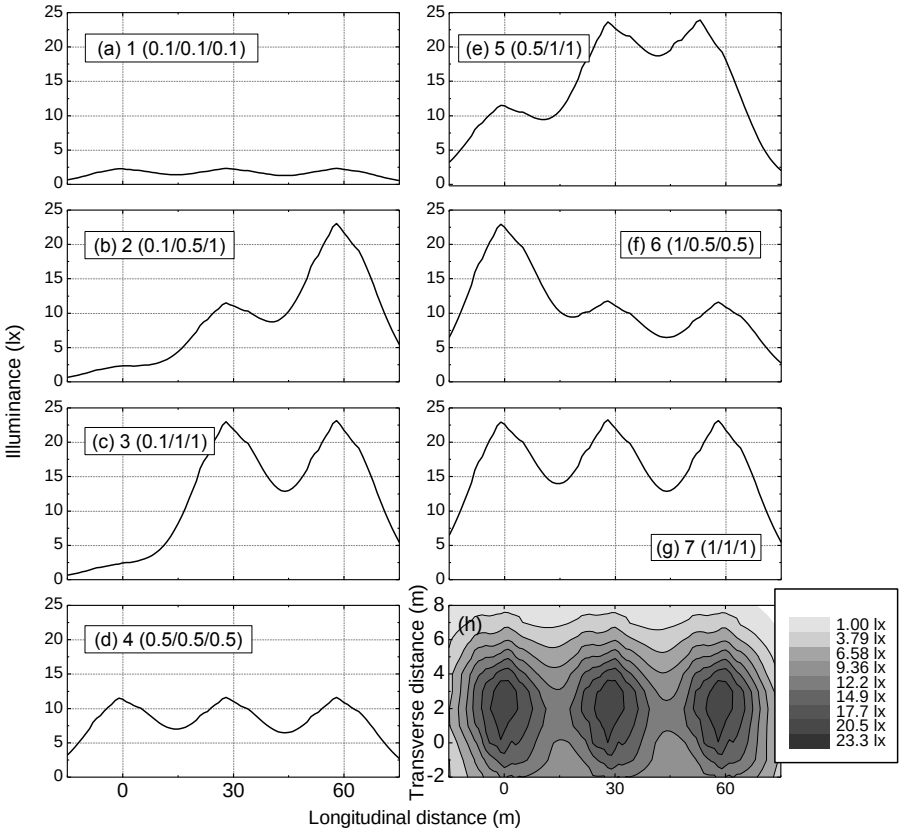

Fig. 4.3. (a)-(g) Distribution of horizontal illuminance along the central line of the street for the seven lighting patterns used in experiment; (h) two-dimensional distribution of horizontal illuminance for pattern 7 [P13].

The experiment was carried out in the dark period of the day and during the experiment the street section was kept empty. A subject was standing under the first post and was viewing along the street in the direction of other posts. The subjects were not acquainted with geographical environment.

To avoid a sequence effect, the presentation order of the light patterns for each subject was randomized. Each subject participated in the research only once. The subjects were not able to communicate with each other.

The lighting patterns were subjectively assessed using the two scales (SDS and Likert). These scales are common for similar research, for example, for the assessment of subjective response to interior lighting [108,115,116] and for the prediction of the preferences for urban open spaces [117]. As suggested by Fotios and Atli [118] and previously by Houser and Tiller [108], also by Tiller and Rea [113], we took a lot of efforts to define the nature of the rating items to

subjects. All subjects were carefully instructed on the precise meaning of the items of the scales and the way to respond to them.

4.2.2. Semantic-differential scaling

At first, 211 bipolar adjectives (in Lithuanian) were preliminarily selected from Lithuanian antonym dictionary for the evaluation of lighting quality. The expert group (32 students of psychology) was presented a slide with the view of the same street of Vilnius University campus and was asked to evaluate the relevance of each antonym pair for describing the street view in scale from -2 to 2. Then 65 adjectives that exhibited positive score means were selected.

After this selection, we determined the locations of the different SDS in the identified (4-D) factor space and separated compact clusters of SDS having almost equal projections on one of the factor axes. In other words, each cluster of the SDS determined the same scores of the identified factor and the Cronbach alpha of these cluster scores were high: the Cronbach alpha of the cluster forming the first, second and third factors were between 0.8–0.9. Finally, 12 bipolar adjectives with the highest scores were selected for SDS.

The set of SDS items (polar opposite adjectives) translated to English in the most appropriate way is as follows: a) Pleasant/unpleasant; b) Far/near; c) Dim/bright; d) Stimulating/suppressing; e) Valuable/cheep; f) Uneven/even; g) Calming /scary; h) Frightening/encouraging; i) Ugly/nice; j) Dangerous/safe; k) Wide/narrow; l) Exposing /hiding.

During the experiment, each polar opposite adjective was rated within a seven-point scale (from −3 to 3) established between the extremes. Such scaling allowed for the characterization of the quality and intensity of attributes along the range of responses for different items. For an item with the first adjective that is positive to a subject, such as “not dangerous/dangerous,” the responses were 3, 2, 1, 0, −1, −2, and −3, whereas for an item with the first adjective that is negative, the responses were −3, −2, −1, 0, 1, 2, and 3. Thus higher values of the responses indicated more preferred conditions.

21 subjects (students of psychology, 20–25 year old, all females) participated in the SDS experiment. Each of the seven lighting patterns was assessed using the set of the SDS items. The scaling was run in 21 sessions with one subject per session. Each subject received SDS printed in a random, spatially and temporally balanced order. Within a session, all lighting patterns were presented and the subject responded to each of 12 SDS items for each pattern.

4.2.3. Likert scaling

The Likert scale was used for the verification of the results of the SDS and was carried out within a smaller program with only three lighting patterns out of seven assessed by SDS. Also, a twice as smaller number of subjects (11) participated in this experiment. The subjects were randomly chosen out of 21 ones that participated in the SDS experiment.

The Likert scaling items and their groups are presented in Table 4.1. The items were partially clarified by means of the Appleton's prospect-refuge theory declarations [119]. Prospect-refuge theory expands on Lorenz's phrase "to see without being seen" [120] as a primitive human behaviour. According to the author, prospect and refuge provide the spatial and geographical mechanisms by which humans maximize their security and seek places that allow them to see their surroundings clearly, without being seen [119]. Although it is a theory developed mainly by reference to rural and natural landscapes, it can also be applied to complex urban spaces created by buildings, topography and vegetation.

Five groups of statements (refuge, prospect, safety, escape, and mask) were used and each group consisted of three statements. The mean score from the preliminary experiment (across 7 experimental conditions) of these three items was used in the analysis and Cronbach's alpha was calculated for each test group of statements (its values were between 0.6 and 0.9). The statements of the mask group served as a validity check on the experimental design in order to detect no difference of lighting patterns when no difference was expected.

Table 4.1. The Likert scaling items and their groups [P13].

Item	Group
1. There are plenty of places where criminals can lurk on this	Refuge
2. To see stars is the most important to me when walking on	Mask
3. It is easy to see even the smallest objects on this street	Prospect
4. I feel that even after playing tricks on this street I would not	Escape
5. I wouldn't choose to go home alone throughout this street	Safety
6. Streets lightened in this way will only increase the number	Escape
7. I feel safe on this street	Safety
8. Street lighting will never be the same as in pictures	Mask
9. I wouldn't like to drive a car on the street lightened in this	Prospect
10. I could easily escape from an attacker on this street	Escape
11. Such an unusual street lighting annoys me	Prospect
12. If needed I could easily romp throughout this street	Refuge
13. In fact, I never pay attention to the street lighting	Mask
14. I love that this street is surrounded by the darkness of the	Refuge
15. I think one could be easily assaulted on this street	Safety

The five-point agree-disagree scale for each statement was used, namely: strongly disagree, disagree, neither agree nor disagree, agree, strongly agree. For the statements that are positive to subject, the responses were 2, 1, 0, –1, and –2, whereas for the statements that are negative, the responses were –2, –1, 0, 1, and 2. Thus higher positive values of the responses indicated more preferred conditions.

Each of the three lighting patterns was assessed using the set of the Likert scale items. The scaling was run in 11 sessions with one subject per session. Within a session, all lighting patterns were presented and the subject responded to each of 15 Likert items for each pattern.

4.2.4. Procedure of evaluation

The procedures of the assessment of the outdoor lighting installation were the same for SDS and Likert scaling and were sequenced as follows:

1. Data on the responses of subjects to the items of the questionnaires was acquired for lighting patterns in question.
2. The items with scores that showed statistically significant differences between lighting patterns were selected.

3. The factor analysis of the selected items was used for the reduction of the number of variables (items) and to reveal the main factors that characterise lighting patterns.
4. The established main factors were applied for the assessment of the lighting patterns.

4.3. Results of evaluation and assessment

4.3.1. Results of SDS

The results of the SDS experiment are shown in Table 4.2. Lines 1 to 12 in Table 4.2 shows the means of the item responses averaged over all subjects for each lighting pattern. The bottom row shows the total scores averaged over the means of the item responses. The total scores bring to a conclusion that the positive evaluations of lighting patterns increase with increasing the flux of the lamp in the first post. For a constant flux of the lamp in the first post, the positive evaluations of lighting patterns increase with increasing the flux of the lamp in the second post.

The sensitivity of the SDS items to lighting pattern was verified by the Kruskal-Wallis test [121], which checked whether for a particular item a lighting pattern is statistically significantly different from at least one of the other patterns. The test has shown that the lighting patterns differed significantly ($p < 0.05$) in respect to all SDS items except item 2 ($H = 6.1$, $N = 142$, $p = 0.41$). Since item 2 was ineffective for comparing the lighting patterns, it was excluded from the further analysis of the data.

In order to reduce the number of variables (SDS items) and to reveal a structure in the relationship between variables, the factor analysis of the responses to the items was performed. The principal components method of factor analysis and Varimax rotation [122] was used. According to the Kaiser criterion [123] two factors with an eigenvalue larger than 1 were established. These two factors accounted for 72% of the total information about the responses to items: 63% and 9% by the first (major) and second (minor) factors,

respectively. Each of the remaining factors accounted for less than 6% of the total variance. The item factor loadings, which quantify the correlation between the factors and the items, are shown in Table 4.2. The factor loadings that exceed 0.7 are marked in bold. (In practice, the factor loadings below the threshold 0.7 are not accepted [124].) One can learn from Table 4.2 that the first factor mostly depends on items 1, 7, 8, and 9 that are related to the feelings of pleasantness, calmness, encouraging and nicety in respect of the illuminated environment. The second factor mostly depends on items 6, 11, and 12 that are related to the feelings of evenness, wideness and exposure. The first factor can be attributed to subjective "well-being" and the second one refers to the physical properties of the lightened environment, respectively.

Table 4.2. Results of SDS. The mean response values and factor loadings for each item and the total scores for each lighting pattern averaged over all items are presented. The factor loadings in excess of 0.7 are marked in bold [P13].

Item	Lighting patterns							Factor 1	Factor 2
	1	2	3	4	5	6	7		
	0.1/0.1/0.1	0.1/0.5/1	0.1/1/1	0.5/0.5/0.5	0.5/1/1	1/0.5/0.5	1/1/1		
1	–1.48	–1.38	–0.90	–0.40	0.95	0.76	1.38	**0.87**	0.20
2	0.29	0.48	0.14	–0.25	–0.24	–0.67	–0.25	–	–
3	–1.76	–1.52	–1.05	–0.35	0.52	1.14	2.38	0.58	0.69
4	–0.81	–0.86	–0.71	–0.65	–0.14	0.57	1.00	0.39	0.34
5	–1.81	–1.33	–1.48	–0.95	0.00	0.38	1.63	0.60	0.58
6	–0.76	–0.57	–0.57	0.15	0.52	0.43	1.50	0.04	**0.80**
7	–1.57	–1.10	–0.67	–0.15	0.67	0.43	1.31	**0.84**	0.26
8	–1.57	–1.05	–0.76	–0.25	0.67	0.67	1.44	**0.77**	0.51
9	–0.95	–0.43	–0.48	0.20	0.33	0.67	1.00	**0.75**	0.32
10	–1.95	–1.38	–1.19	–0.35	0.71	0.67	1.75	0.63	0.68
11	–1.86	–1.14	–1.14	–0.60	0.76	0.05	1.25	0.33	**0.82**
12	–2.10	–1.43	–1.05	–0.60	0.48	0.57	1.81	0.46	**0.78**
Score	–1.36	–0.98	–0.82	–0.35	0.44	0.47	1.35		

The established factors were used to assess the lighting patterns. Using the item scores and factor loadings, the first and second factor scores were calculated for each of 21 participants and for each of seven lighting patterns. A comparison of the seven lighting patterns by means of the factor scores is shown in Fig. 4.4.

As shown in Fig. 4.4, the mean of the first factor scores increases as the flux of the lamp in the first and second posts increases. This is the same tendency as for the mean of item responses mentioned above.

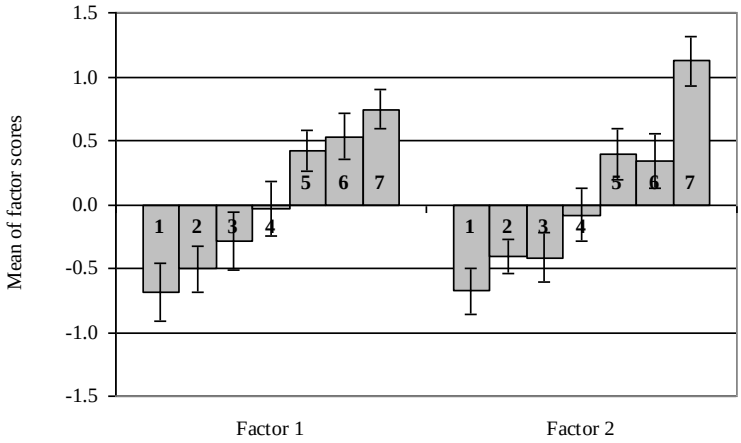

Fig. 4.4. Comparison of the seven lighting patterns by means of the factor scores established from SDS. The error bars show standard errors of the means. The lighting patterns are labelled by numbers in the bars [P13].

The Wilcoxon matched pairs test [121] was used to establish statistically significant difference ($p < 0.05$) between the pairs of lighting patterns. The results of the test are presented in Table 4.3. The comparison of lighting patterns by the first (major) factor shows a statistically significant difference between the lighting patterns having different fluxes of the first post lamp and equal fluxes of second post lamp (between lighting patterns 3, 5, and 7 and between lighting patterns 2, 4, and 6). However, the same factor shows no significant differences between the lighting patterns with equal fluxes of the first post lamp and different fluxes of the second post lamp (between lighting patterns 1, 2, and 3, between lighting patterns 4 and 5, and between lighting patterns 6 and 7). One can conclude from these results that the assessed lighting patterns differ significantly only by the flux of the first post.

The comparison of lighting patterns by the second (minor) factor shows similar results with except that the differences between some pairs of the lighting patterns lack significance.

Table 4.3. Comparison between the pairs of lighting patterns by the first and second factors established from SDS (the upper and lower tables, respectively). The differences are quantified by the value Z and significance level p of the Wilcoxon matched pairs test. The results for the pairs of lighting patterns that differ significantly ($p < 0.05$) are presented in bold [P13].

Lighting patterns		1	2	3	4	5	6	7	1	2	3	4	5	6	7
		Factor 1							Factor 2						
1. 0.1/0.1/0.1	*Z*		0.96	0.78	**2.59**	**3.77**	**3.25**	**2.74**		1.30	0.89	**2.35**	**3.77**	**2.90**	**3.52**
	p		0.34	0.43	**0.01**	**< 0.01**	**< 0.01**	**0.01**		0.19	0.38	**0.02**	**< 0.01**	**< 0.01**	**< 0.01**
2. 0.1/0.5/1	*Z*	0.96		0.85	**1.93**	**3.35**	**2.87**	**2.74**	1.30		0.02	1.72	**2.83**	**2.24**	**3.15**
	p	0.34		0.39	**0.04**	**< 0.01**	**< 0.01**	**0.01**	0.19		0.99	0.09	**< 0.01**	**0.02**	**< 0.01**
3. 0.1/1/1	*Z*	0.78	0.85		1.03	**2.28**	**2.31**	**2.33**	0.89	0.02		1.37	**3.01**	1.96	**3.15**
	p	0.43	0.39		0.31	**0.02**	**0.02**	**0.02**	0.38	0.99		0.17	**< 0.01**	0.05	**< 0.01**
4. 0.5/0.5/0.5	*Z*	**2.59**	**1.93**	1.03		1.65	**2.31**	**2.22**	**2.35**	1.72	1.37		1.76	0.96	**3.00**
	p	**0.01**	**0.04**	0.31		0.10	**0.02**	**0.03**	**0.02**	0.09	0.17		0.08	0.34	**< 0.01**
5. 0.5/1/1	*Z*	**3.77**	**3.35**	**2.28**	1.65		0.02	**2.01**	**3.77**	**2.83**	**3.01**	1.76		0.26	**2.43**
	p	**< 0.01**	**< 0.01**	**0.02**	0.10		0.99	**0.04**	**< 0.01**	**< 0.01**	**< 0.01**	0.08		0.79	**0.02**
6. 1/0.5/0.5	*Z*	**3.25**	**2.87**	**2.31**	**2.31**	0.02		0.98	**2.90**	**2.24**	1.96	0.96	0.26		1.65
	p	**< 0.01**	**< 0.01**	**0.02**	**0.02**	0.99		0.33	**< 0.01**	**0.02**	0.05	0.34	0.79		0.10
7. 1/1/1	*Z*	**2.74**	**2.74**	**2.33**	**2.22**	**2.01**	0.98		**3.52**	**3.15**	**3.15**	**3.00**	**2.43**	1.65	
	p	**0.01**	**0.01**	**0.02**	**0.03**	**0.04**	0.33		**< 0.01**	**< 0.01**	**< 0.01**	**< 0.01**	**0.02**	0.10	

4.3.2. Results of Likert scaling

The results of Likert scaling are shown in Table 4.4. Lines 1 to 15 in Table 4.4 show the means of the item responses averaged over all subjects for each lighting pattern. The bottom row shows the total scores of the items for the three lighting patterns. The total scores are seen to increase with increasing the flux of the lamp of the first post. This conclusion is similar to that following from the results of SDS (Table 4.2).

Table 4.4. Results of the Likert scaling. The mean response values and factor loadings for each item and the total scores for each lighting pattern averaged over all items are presented. The factor loadings in excess of 0.7 are marked in bold [P13].

Item	Lighting patterns			Factor 1	Factor
	2	5	6		
	0.1/0.5/1	0.5/1/1	1/0.5/0.5		
1	-0.64	-0.4	0.42	-	-
2	-0.18	0	0.08	-	-
3	-1.27	-0.6	1	**0.79**	0.39
4	0.18	0	-0.75	-	-
5	-0.18	-0.3	0.75	-	-
6	-0.55	0.2	1.25	0.53	0.59
7	-0.73	-0.5	0.92	**0.76**	0.52
8	0.18	-0.3	-0.08	-	-
9	0.09	0.8	1.5	0.18	**0.9**
10	-0.36	-0.5	-0.33	-	-
11	-0.64	0.2	1.25	0.44	**0.74**
12	0.27	-0.3	-1.25	-	-
13	-1.09	-1	-1.17	-	-
14	-1	-0.4	-0.83	-	-
15	-1.18	-0.6	-0.08	**0.89**	0.13
Score	-0.5	-0.2	0.32		

The sensitivity of the Likert questionnaire items to lighting patterns was tested by the Kruskal-Wallis test. The results of the test showed that the evaluations of lighting patterns differ significantly ($p < 0.05$) for all items of the prospect group (3, 9, and 11), for two items of the safety group (7, 15), and for one item of the escape group (6). The scores of the items of the mask group (2, 8, and 13) showed no significant difference ($p > 0.5$) between the evaluations of lighting patterns. Same ($p > 0.05$) applies to the scores of the items of the refuge group (1, 12, and 14).

Using the results of the Kruskal-Wallis test, the items that showed no significant difference between evaluations of lighting patterns were excluded form the further factor analysis and only items 3, 6, 7, 9, 11, and 15 with significant difference ($p < 0.05$) between lighting patterns were used. The principal components method of factor extraction and Varimax rotation revealed two factors that account for 77% of the total information about the responses to items (66% and 11% for the first and second factors, respectively). Each of the remaining factors accounted for less than 7% of the total variance. The item factor loadings are shown in Table 4.4. The factor loadings exceeding 0.7 are presented in bold. What can be learned from Table 4.4 is that the first factor mostly depends on the prospect (item 3) and the feeling of safety (items 7 and 15), whereas the second factor depends only on the prospect (items 9 and 11) of lighted environment. Similarly to the case of the SDS, the first factor may be interpreted as subjective "well-being", whereas the second factor is probably related to the physical properties of the lightened environment.

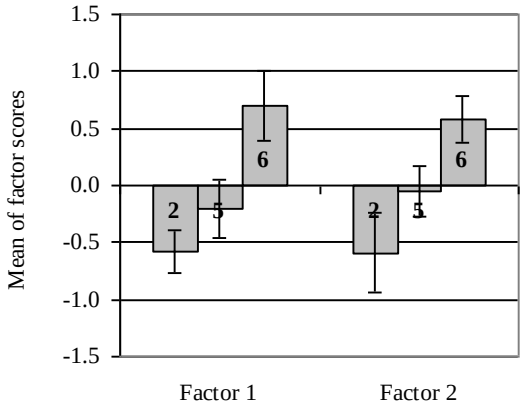

Fig. 4.5. Comparison of three lighting patterns by means of the factor scores established from Likert scaling. The error bars show standard errors of the means. The lighting patterns are labelled by numbers in the bars [P13].

The established factors were used to assess the lighting patterns. A comparison of the three lighting patterns by means of the factor scores is shown in Fig. 4.5.

As shown in Fig. 4.5, the means of the both factor scores increase as the flux of the lamp of the first post increases. This tendency is similar to that for the means of the factor scores established from the results of SDS. This is in line

with the study of Haans and de Kort [125], where the first experiment showed that stationary pedestrians prefer having light in their own immediate surroundings over light on the more distant parts of the road and the second experiment revealed that participants valued least the lighting distribution in which their immediate surroundings were poorly lit (i.e. the dark spot condition).

The Wilcoxon matched pairs test was used to establish the statistically significant difference ($p < 0.05$) between the pairs of lighting patterns. The results of the test are presented in Table 4.5. The comparison of lighting patterns by both factors shows a statistically significant difference between the lighting patterns having different fluxes of the first post lamp and equal fluxes of second post lamp (between lighting patterns 2 and 6).

Table 4.5. Comparison between the pairs of lighting patterns by the by the first and second factors established from Likert scaling (left and right tables, respectively). The differences are quantified by the value Z and significance level p of the Wilcoxon matched pairs test. The results for the pairs of lighting patterns that differ significantly ($p < 0.05$) are presented in bold [P13].

Lighting patterns		2	5	6	2	5	6
		Factor 1			Factor 2		
2. 0.1/0.5/1	*Z*		1.27	**2.13**		1.58	**2.04**
	p		0.2	**0.03**		0.11	**0.04**
5. 0.5/1/1	*Z*	1.27		**2.19**	1.58		1.48
	p	0.2		**0.03**	0.11		0.14
6. 1/0.5/0.5	*Z*	**2.13**	**2.19**		**2.04**	1.48	
	p	**0.03**	**0.03**		**0.04**	0.14	

The above analysis shows that the major factor of SDS and Likert scaling accounts for 63% and 66% of the total information about the responses to items, respectively. For both scales this factor may be interpreted as the "well-being" factor. The minor factor of the two scales accounts for only 9% and 11% of the total information, respectively. This factor can be attributed to as the evaluation of the physical characteristic of environment.

For a particular intelligent street lighting installation within a moderately urbanized woody area, the assessment of seven lighting patterns by SDS showed that the mean of the first factor scores primarily depends on the flux of lamp of the first post, whereas for equal fluxes of the first post, the fluxes of the remote posts are less important. The results of the assessment of three lighting patterns

by Likert scaling showed the same tendency. However, differently lit areas, such as wasteland, park, industrial, highly urbanized and socially or architecturally significant (city centre) areas, might need modified items of the questionnaires and might show different preferences to lighting patterns.

4.4. Conclusions of the fourth chapter

The main subjective factors for the assessment of different lighting patterns within an intelligently controlled LED-based installation were established using a psychophysical method based on the response of subjects to the items of SDS and Likert questionnaires and on the analysis of the both sets of response data in the same way.

The two methods showed similar results and revealed two factors that need to be considered when assessing intelligent outdoor lighting installations: a major factor that is related to the subjective feeling of well-being and a minor factor that is related to the physical properties of the environment.

For our particular intelligent street lighting installation, the assessment of seven lighting patterns by the two scales showed that the mean of the first factor scores primarily depends on the flux of lamp of the first post, whereas for equal fluxes of the first post, the fluxes of the remote posts are less important.

5. Low-circadian action LED source for outdoor lighting

The energy efficiency and reliability offered by solid state-lighting technology brought to a massive replacement of HPS lamps by LEDs in outdoor illumination. However, common LEDs emit blue-enriched light, which is claimed to disrupt circadian rhythms and to pose aesthetic issues at low luminances. In this chapter the results of the assessment of visual and non-visual performance characteristics of a practical firelight (blue–amber) LED cluster metameric to a HPS lamp was presented. In particular, the SPD of the firelight cluster has been assessed in the mesopic range of luminances typical of outdoor lighting by quality indices relevant to different lighting issues (efficacy, colour rendition, melatonin suppression, skyglow, and eye lens yellowing) and compared to those of common white LEDs and sodium-based light sources. Also, psychophysical performance characteristics relevant to driving (time of reaction to achromatic stimulus, detection threshold of luminance contrasts for achromatic targets, and colour discrimination) have been measured against the HPS counterpart in laboratory under mesopic vision conditions [P12,P19,C2, C11,C14,C19,C20,C22,C24].

5.1. Literature survey

LEDs are efficacious, longevous, have improved directionality, and are easy to intelligently control [P3,85,86]. In addition, the needs in colour rendition and colour discrimination can be better met, since the SPD of LED-based sources can be versatilely tailored through the conversion of short-wavelength electroluminescence in semiconductor chips to photoluminescence in different phosphors or through assembling clusters of LEDs having different colours [18,126].

Common white pc LEDs have short-wavelength rich SPDs and their luminous efficacy increases with reducing adaptation luminance (L) due to the Purkinje effect, which is the short-wavelength shift of the spectral sensitivity of the human eye. This has been claimed as an additional advantage of LEDs for outdoor lighting in respect of common HPS lamps, which have blue-deficient

SPD and reduced luminous efficacy at low luminances [86]. However, switching from blue-deficient light sources (typically, HPS lamps) to blue-enriched ones (metal-halide lamps and, presently, LEDs) in outdoor lighting created numerous concerns and issues that are being actively debated [127]. In particular, with the discovery of ipRGCs, which contain blue-light absorbing melanopsin photopigment [128-130], the application of blue-enriched light in night-time environments was recognized to be harmful due to the unwanted non-visual photobiological effect (suppressing pineal melatonin production and shifting melatonin phase), which disrupts circadian rhythms and poses serious health issues even at low illuminances [131-138]. Also, light pollution due to molecular (Rayleigh) and aerosol (Mie) scattering causes increased urban skyglow in the vicinity of blue-enriched light sources. Such skyglow has a detrimental effect on astronomical research [127,138,139] and ecological processes [140]. One more important issue is the aggravation of night-time driving conditions for elderly people due to the yellowing of the lenses of the eye with age [138,141]. For equal conditions of ambient luminance, such a yellowing results in a reduction of retinal illuminance under blue-enriched light in addition to that due to the age-related decrease of the overall optical transmission of the lenses. Finally, some outdoor lighting environments can lose aesthetic attractiveness when switching from HPS lamps to common white LEDs, which have a higher CCT. This unwanted effect may occur according to the Kruithof hypothesis [75], which suggests that for illuminances typical of outdoor lighting, the lighting is considered “pleasing” when the light source has a CCTs below 2500 K. Although this hypothesis has been the subject of controversy for years [142,143], recently it has been partially validated in that the of impressions of comfort, pleasantness and relaxation increase, when CCT decreases [76].

The above concerns and issues indicate on the necessity of the adaptation of solid-state lighting technology to the specific needs of outdoor lighting with a balanced approach to improving efficacy and colour quality on the one hand and avoiding photobiological hazards, light pollution, discrimination of elderly

drivers, aesthetic inconvenience, and other issues related to the use of blue-enriched light at night time on the other hand.

Recently, the SPDs of LED-based sources of light have been numerically optimized for low-luminance photobiologically-friendly lighting applications [87]. The optimal SPDs have extra low CCTs and are composed of two components, a narrow-band blue one peaked in the range around 440 nm and a wider-band complementary one peaked in the yellow-orange range of the spectrum. Such dichromatic light sources, which are the solid-state counterparts of HPS lamps, have been designated in [87] as "firelight" solid-state lamps. The firelight lamps have the lowest partial power in the short-wavelength region of the visible spectrum out of all solid-state sources of light with the chromaticity close to that of the blackbody. They can be composed of either clusters of blue and amber coloured LEDs or implemented as single-package LEDs with the partial conversion of blue electroluminescence to amber photoluminescence in phosphors [144]. (One more approach to the development of low-CCT LEDs is based on the reduction of short-wavelength spectral power of common white LEDs using optical filters [145]; however, such an approach lacks reasoning from the standpoint of the inherent concept of solid-state lighting technology, which is based on the straightforward tailoring of SPD without introducing optical losses.)

5.2. Firelight LED cluster

An experimental firelight LED cluster was assembled of eight pc amber LEDs (Philips Lumileds model Luxeon Rebel LXM2-PL01) and one InGaN direct emission royal blue LED (LXML-PR02) with peak wavelengths of 594 nm and 452 nm, respectively. The peak wavelengths of the component LEDs were selected in such a way that the resulting chromaticity of the cluster was as close as possible to that of the reference HPS lamp (Philips model SON-T PIA PLUS 70W E E27 1SL with an electronic ballast) and the minimal ratio of the circadian action to mesopic luminous efficacy of radiation (MLER) was attained [87]. The LEDs were mounted on a metal-core printed-circuit board within an area of

13×16 mm^2 and the board was attached to a massive heat sink. The ratio of the amber and blue spectral components within the cluster was precisely adjusted using buck LED drivers (Diodes, Inc. model AL8805). The SPD was calibrated using a Labsphere model Illumia® Pro Light measurement system consisting of a 50 cm integrating sphere and a spectrometer SMS 500.

5.3. Assessment of SPDs

Figure 5.1(a) displays the SPDs of the firelight LED cluster and HPS lamp with equal integral radiant power. In comparison with the structured SPD of the HPS lamp, the LED cluster is seen to have a smooth SPD with increased spectral power in the red (around 630 nm) and yellow-green (540-580 nm) ranges of the spectrum and reduced spectral power at the peaks of the main lines of sodium emission. Also, a characteristic feature of the dichromatic firelight LED cluster is a very low spectral power in the cyan-green (480-520 nm) range due to a Eu^{2+} activated amber phosphor with a moderate width of the band used.

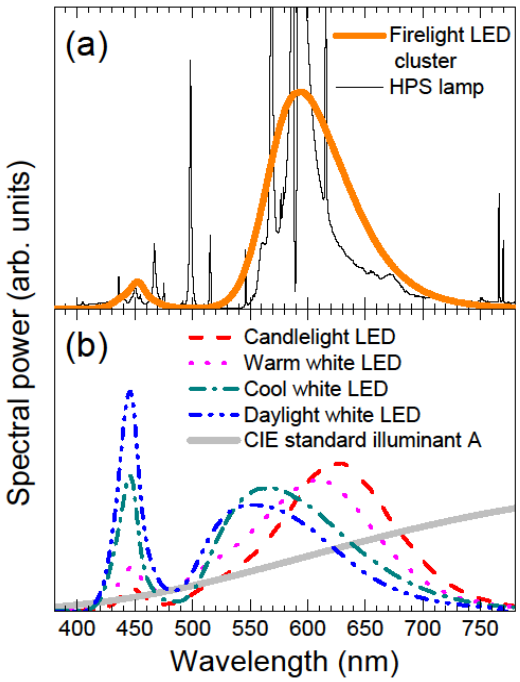

Fig. 5.1. Spectral power distributions of light sources: (a) firelight LED cluster (bold line) and HPS lamp (thin line; truncated top); (b) candlelight (dashed line), warm white (dotted line), cool white (dash-dotted line), and daylight (dash-dot-dotted line) phosphor converted LEDs and CIE standard illuminant A (bold grey line) [P12].

Figure 5.1(b) shows the SPDs of other light sources used for the comparative assessment of the firelight LED cluster: quasi-white "candlelight," warm white,

cool white, and daylight pc LEDs (Stanley model GTDW1656JTE-20Y and Philips Lumileds models Luxeon Rebel LXM8-PW27, LXML-PWN2, and LXML-PWC2, respectively), and the CIE standard illuminant A. Not shown is the SPD of LPS lamp (SOX), which contains a narrow duplet of 589.0 nm and 589.6 nm lines. In comparison with the firelight LED cluster, the SPDs of the common pc white LEDs, which are optimized for high colour rendering, have broader long-wavelength bands due to Ce^{3+} activated phosphors or diphosphor composition of the wavelength converter.

5.3.1. Photometric, colorimetric and colour rendition properties of the light sources

The most relevant photometric and colorimetric properties of the sources under assessment are presented in Table 4.6. The ratio of scotopic to photopic weighted lumen outputs (S/P ratio) for an SPD $S(\lambda)$ (λ is the wavelength) is defined as

$$\mathrm{S/P} = K_0' \int_{380}^{780} V'(\lambda) S(\lambda) d\lambda \Big/ K_0 \int_{380}^{780} V(\lambda) S(\lambda) d\lambda, \qquad (5.1)$$

where $V(\lambda)$ and $V'(\lambda)$ are the CIE scotopic and photopic spectral luminous efficiency functions, respectively, and K'_0 = 1700 lm/W and K_0 = 683 lm/W are the maximum values of spectral luminous efficacy for scotopic and photopic vision, respectively.

The MLER was estimated by weighting the SPDs by mesopic luminous efficiency function $V_{\mathrm{mes}}(\lambda)$ of the MES-2 visual-performance-based photometric system [146]:

$$\mathrm{MLER} = K_{\mathrm{mes0}} \int_{380}^{780} V_{\mathrm{mes}}(\lambda) S(\lambda) d\lambda \Big/ \int_{380}^{780} S(\lambda) d\lambda, \qquad (5.2)$$

where $K_{\mathrm{mes0}} = K_0/V_{\mathrm{mes}}(555\ \mathrm{nm})$ is the maximum value of spectral luminous efficacy for mesopic vision. Beyond the endpoints of the mesopic range of adaptation luminances (0.005 cd/m^2 and 5 cd/m^2), the mesopic luminous efficacy function and the maximum value of spectral luminous efficacy have the values that correspond to scotopic and photopic vision, respectively.

In Table 5.1, the values of MLER are presented for two values of mesopic luminance that delimit the upper part of the mesopic region relevant to outdoor lighting, 0.1 cd/m^2 (lowest-class pedestrian area, ~2 lx illuminance) and 2 cd/m^2 (highest-class road), respectively. Also, the photopic values of LER are presented.

Table 5.1. Photometric and colorimetric properties of the light sources. [P12]

Light source	CCT (K)	Chromaticity coordinates		S/P	(M)LER (lm/W)		
		x	*y*		0.1 cd/m^2	2 cd/m^2	photopic
LPS lamp	1814	0.5669	0.4324	0.23	380	493	517
HPS lamp	1886	0.5390	0.4104	0.54	325	376	387
Firelight LED cluster	**1859**	**0.5424**	**0.4101**	**0.49**	**295**	**347**	**358**
Candlelight pc LED	2001	0.5215	0.4067	0.85	249	260	263
Warm white pc LED	2725	0.4582	0.4114	1.19	331	314	311
Cool white pc LED	3991	0.3839	0.3893	1.39	388	350	342
Daylight white pc LED	6084	0.3207	0.3287	1.92	414	332	314
CIE standard illuminant A	2854	0.4475	0.4074	1.41	178*	160*	156*

In comparison with a reference HPS lamp, our firelight LED cluster has somewhat smaller mesopic LER, which can be increased to about 400 lm/W by selecting an amber phosphor with a narrower band [87], howerver. Potentially (under conditions of 100% radiant efficiency of the semiconductor blue emitter) similar firelight LEDs with partial conversion of blue radiation in phosphors can have radiant efficiency of about 75% [147], which converts to mesopic luminous efficacy of about 300 lm/W at a LER of 400 lm/W. Such a luminous efficacy is within the range of limiting efficacies of common white LEDs and is more than twice as higher as that of HPS lamp and 1.5 times higher than that of LPS lamp.

The S/P ratio and MLER of the firelight LED cluster is seen to be by 10% smaller than that of the HPS lamp. The S/P ratio of the LPS lamp is much smaller, whereas it is considerably larger for common LEDs. Despite this, owing to the optimized SPD the firelight LED cluster has MLER comparable to that of common cool white pc LED at an adaptation luminance of 2 cd/m^2 and exceeds the MLER of the candlelight LED by 18% at an adaptation luminance of 0.1 cd/m^2. However at the latter low adaptation luminance, blue-enriched SPDs

of warm white, cool white, and daylight pc LEDs have higher MLERs than the blue-deficient one of the fire light LED cluster.

The CIE 1931 chromaticity coordinates of the firelight LED cluster and HPS lamp are depicted by solid points in Fig. 5.2. The chromaticity coordinates of the two sources do not deviate from the Planckian locus (bold line in Fig. 5.2) by more than $\Delta xy \sim 0.0004$. The HPS lamp has a somewhat higher CCT of 1886 K than the LED cluster (1859 K). However, the two light sources are almost metameric with the chromaticity difference falling within a 3-step MacAdam ellipse (the fine lines in Fig. 5.2 show MacAdam ellipses of 1, 2, and 3 steps obtained by the geodesic interpolation method [3]).

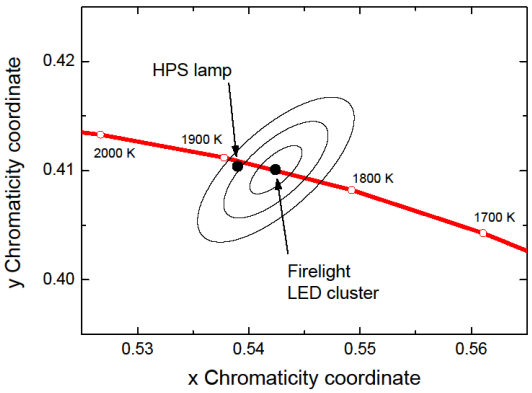

Fig. 5.2. Solid points, chromaticity coordinates of the firelight LED cluster and HPS lamp within a segment of the CIE 1931 diagram. The Planckian locus and MacAdam ellipses of 1, 2, and 3 steps centered at the chromaticity coordinates of the LED cluster are shown by bold and fine lines, respectively [P12].

Table 5.2 presents the colour rendition indices of the light sources under assessment. The values of the CIE R_a [4] are presented for standard photopic conditions, as well as for mesopic conditions with the rescaling of the colour shifts due to the reduced colour discrimination ability of human vision taken into account [87]:

$$R_{a,mes} = 100 - \gamma\left(L_{mes}\right)\left(100 - R_a\right). \tag{5.3}$$

Here $\gamma(L_{mes})$ is the colour shift rescaling factor, which is the ratio of the mean size of the MacAdam ellipses at photopic conditions to that at a particular mesopic luminance. The values of the rescaling factor deduced from the mean size of MacAdam ellipses at mesopic conditions [56,148] equal 0.16 and 0.51 for adaptation luminances of 0.1 cd/m^2 and 2 cd/m^2, respectively.

Also shown in Table 5.2 GAI [17] and the statistical colour rendition indices obtained from the statistical analysis of the colour-shift vectors for 1269 Munsell test colour samples in respect of 3-step MacAdam ellipses and 2% lightness toleration [3]: the CFI, CSI, CDI, HDI, and LDI, which are the percentages of colours rendered with high fidelity, increased chroma, decreased chroma, distorted hue, and distorted lightness, respectively.

Table 5.2. Colour rendition indices of the light sources [P12].

Light source	R_a equivalent			GAI	CFI	CSI	CDI	HDI	LDI
	0.1 cd/m^2	2 cd/m^2	photopic						
LPS lamp	76	25	−47	0.1	3	0	95	0	80
HPS lamp	86	55	12	17	9	0	84	38	69
Firelight LED cluster	**90**	**68**	**37**	**24**	**9**	**1**	**79**	**32**	**63**
Candlelight pc LED	97	92	84	36	51	0	39	**5**	18
Warm white pc LED	97	91	82	50	43	0	43	11	24
Cool white pc LED	95	83	66	67	18	5	57	48	47
Daylight white pc LED	96	86	72	89	19	5	51	50	45
CIE standard illuminant A	100	100	100	56	100	0	0	0	0

The LPS lamp is seen to have no colour fidelity (negative R_a and very low CFI) and highly shrunk gamut area (low GAI); it renders colours with almost lost chroma (the CDI is such high that hue distortions are not resolved at all) and high distortions of luminance. This makes this light source inappropriate for illumination of most environments, except for very low luminances when the colour discrimination ability of human vision is very low.

In the photopic limit, R_a and GAI of the firelight LED cluster is seen to be as 3 times and 1.4 times higher than that of HPS lamp, respectively, although these indices are much smaller than those of common candlelight and white pc LEDs. Meanwhile at mesopic conditions, the rescaled (equivalent) values of R_a show that the latter drawback of the firelight LED cluster is mitigated making this index comparable with that of common pc LEDs at photopic conditions. It is to be noted that for adaptation luminances typical of outdoor lighting, most common white pc LEDs with blue-enriched SPD have the equivalent values of R_a that can be considered as redundant [149].

A deeper insight into the colour rendition properties based on the statistical analysis of the colour shift vectors for a large number of test colour samples

shows that the reduced colour fidelity (reduced CFI values) of both solid-state and sodium-based sources considered is due mainly to a large number of colours rendered with reduced chroma (increased CDI values). All sources do almost not render colours with increased chroma (low CSI values) and many colours are rendered with distorted hue and chroma (high HDI and LDI values, respectively).

5.3.2. Circadian action

The quantification of circadian response to a light source is a complex problem that is not completely resolved for all conditions. So far, the scientific community reached a consensus only on that the circadian action increases with increasing retinal irradiance and shifting the light source spectrum to shorter wavelengths [150]. The simplest model of the spectral sensitivity of the human circadian system introduced by Gall [151] is based on a single spectral circadian efficiency function $C(\lambda)$, which approximates the experimental action spectra of melatonin suppression [128,129]. Within such an approach, the circadian action of light for adaptation luminances relevant to outdoor lighting can be quantified by a MMSI, which is defined as the melatonin suppression efficacy of radiation per unit mesopic luminous flux. For ease of scaling, here we normalized the value of MMSI for a light source under assessment to that for the CIE standard illuminant A per unit photopic luminous flux as follows

$$\mathrm{MMSI_A} = \frac{\int_{380}^{780} C(\lambda) S(\lambda) d\lambda}{K_{\mathrm{mes0}} \int_{380}^{780} V_{\mathrm{mes}}(\lambda) S(\lambda) d\lambda} \Bigg/ \frac{\int_{380}^{780} C(\lambda) S_{\mathrm{A}}(\lambda) d\lambda}{K_0 \int_{380}^{780} V(\lambda) S_{\mathrm{A}}(\lambda) d\lambda} \quad (5.4)$$

where $S_{\mathrm{A}}(\lambda)$ is the SPD of the CIE standard illuminant A.

The approach of Gall suffers from that it is based on melatonin suppression action spectra measured under narrow-band light. Rea et al. [152] introduced a non-linear approach, which accounts for the circadian action due a spectral opponent input to the ipRGC from the blue-yellow visual channel (S-cone excitation). This approach is claimed to be suitable for both wide-band (polychromatic) and narrow-band light, although it lacks independent validation.

With a glance to the mesopic sensitivity of the human eye, the photopic "circadian light" of a light source normalized to that of the CIE standard illuminant A (CL_A [152]) can be converted to a mesopic circadian light index $MCLI_A$ as follows

$$MCLI_A = \frac{CL_A}{1000} \times \frac{LER}{MLER}, \tag{5.5}$$

where LER and MLER are the photopic and mesopic LERs of the light source SPD defined by Eq. (5.2).

Further improving the model of circadian spectral sensitivity might require accounting for such conditions as the duration, periodicity, and time of day of exposure to light, as well as for non-linear response in respect of illuminance level and the long-wavelength enhancement of blue-light effect due to melanopsin bistability [153].

Despite some limitations, here we present the results of assessment of solid-state and sodium-based light sources using the above two models described by Eqs. (5.4) and (5.5), respectively. The estimated values of the circadian factors are shown in Table 5.3 for two mesopic luminances and in the photopic limit. Basically, both factors are seen to have very similar values for the sources with low CCTs; they increase with increasing CCT (the spectral opponent effect manifests itself in considerably lower values of $MCLI_A$ in respect of $MMSI_A$ for cool white and daylight LEDs).

Table 5.3. Melatonin suppression indices of the light sources [P12].

Light source	CCT (K)	(M)MSI$_A$			(M)CLI$_A$		
		0.1 cd/m^2	2 cd/m^2	photopic	0.1 cd/m^2	2 cd/m^2	photopic
LPS lamp	1814	0.06*	0.05*	0.05*	0.06	0.05	0.05
HPS lamp	1886	0.36	0.31	0.30	0.38	0.33	0.32
Firelight LED cluster	**1859**	**0.28**	**0.24**	**0.23**	**0.29**	**0.25**	**0.24**
Candlelight pc LED	2001	0.50	0.48	0.48	0.55	0.53	0.52
Warm white pc LED	2725	0.76	0.80	0.81	0.78	0.82	0.83
Cool white pc LED	3991	1.03	1.14	1.16	0.41	0.45	0.46
Daylight white pc LED	6084	1.53	1.91	2.02	0.94	1.18	1.24
CIE standard illuminant A	2854	0.87	0.97	1	0.87	0.97	1

* Since the Gall function is not defined for wavelengths longer than 580 nm, the (M)MSI$_A$ values for LPS lamp are equated to the corresponding (M)CLI$_A$ ones.

The LPS lamp, which has a limited applicability in outdoor lighting due to colour rendering issues, has the lowest values of the circadian action factors.

Due to the optimized SPD, the firelight LED cluster is seen to have by 22-25% lower values of the circadian factors in comparison with the metameric HPS lamp and about twice as lower values in comparison with the common candlelight pc LED. The effect is even higher when the firelight LED is compared to common warm white and daylight pc LEDs.

5.3.3. Light pollution

Nocturnal skyglow due to light reflected upward from illuminated outdoor surfaces is the most difficult to avoid light pollution provided by solid-state light sources. Generally, skyglow occurs due to molecular and aerosol scattering of light in the atmosphere. Molecular and aerosol scattering is described by the Rayleigh and Mie theories, respectively, with the scattering cross-section strongly dependent on the wavelength as λ^{-4} in the former case and with typically less wavelength-sensitive cross-section (scaled with λ^{-1}) in the latter case. Additionally in both cases, the observed luminance of skyglow depends on the distance from the light source [139,154].

Based on solely Rayleigh scattering, an approach that allows for quantitatively comparing light sources within the hypothetical limit of scatter by only sub-wavelength size particles at short distances can be introduced [138,155]. Here we assess the light sources by three different indices that quantify the limiting (Mie scattering free) effect of SPD on skyglow per unit mesopic luminous flux provided by a source. The indices relevant to three different observation conditions under Rayleigh skyglow are as follows: i) the $MGVI_A$ relevant to visually perceived skyglow in the entire visible spectrum; ii) the $MFVI_A$ relevant to visual observation trough an optical band-pass optical filter; and iii) the $MFII_A$ relevant to the detection of photons through the same optical band-pass filter. For the ease of scaling, all the three indices are

normalized to the corresponding values for the CIE standard illuminant A per unit photopic luminous flux.

The $MGVI_A$ is derived from the SPD of a light source weighted by the scotopic luminous efficacy function and Raleigh scattering factor λ^{-4} in the entire range of visible spectrum as follows

$$\mathrm{MGVI_A} = \frac{\int_{380}^{780} \lambda^{-4} V'(\lambda) S(\lambda) d\lambda}{K_{\mathrm{mes}0} \int_{380}^{780} V_{\mathrm{mes}}(\lambda) S(\lambda) d\lambda} \Bigg/ \frac{\int_{380}^{780} \lambda^{-4} V'(\lambda) S_{\mathrm{A}}(\lambda) d\lambda}{K_0 \int_{380}^{780} V(\lambda) S_{\mathrm{A}}(\lambda) d\lambda}. \quad (5.6)$$

The $MFVI_A$ differs from $MGVI_A$ in that the weighting is performed within the "protected" band of 440 nm to 540 nm, which can be isolated using an appropriate optical band-pass filter [138]:

$$\mathrm{MFVI_A} = \frac{\int_{440}^{540} \lambda^{-4} V'(\lambda) S(\lambda) d\lambda}{K_{\mathrm{mes}0} \int_{380}^{780} V_{\mathrm{mes}}(\lambda) S(\lambda) d\lambda} \Bigg/ \frac{\int_{440}^{540} \lambda^{-4} V'(\lambda) S_{\mathrm{A}}(\lambda) d\lambda}{K_0 \int_{380}^{780} V(\lambda) S_{\mathrm{A}}(\lambda) d\lambda}. \quad (5.7)$$

The $MFII_A$ differs from $MFVI_A$ in that the spectral power of the glow and the scotopic luminous efficiency function are replaced by the spectral photon flux, which is proportional to $\lambda S(\lambda)$, and a wavelength independent instrumental response function, respectively:

$$\mathrm{MFII_A} = \frac{\int_{440}^{540} \lambda^{-3} S(\lambda) d\lambda}{K_{\mathrm{mes}0} \int_{380}^{780} V_{\mathrm{mes}}(\lambda) S(\lambda) d\lambda} \Bigg/ \frac{\int_{440}^{540} \lambda^{-3} S_{\mathrm{A}}(\lambda) d\lambda}{K_0 \int_{380}^{780} V(\lambda) S_{\mathrm{A}}(\lambda) d\lambda} \quad (5.8)$$

Table 5.4 presents the results of the assessment of the solid-state and sodium-based light sources by the three limiting Raleigh skyglow indices. (Note that when two light sources are compared by the ratio of corresponding limiting indices, the actual ratio of the skyglow luminance is smaller due to Mie scattering.)

The general visual index $MGVI_A$ shows a tendency to increase with increasing CCT; also, with increasing luminance it increases for blue-enriched SPDs and decreases for blue-deficient sources. The lowest values of $MGVI_A$ are achieved for monochromatic LPS lamp. The firelight LED cluster has about as three times as higher values of $MGVI_A$ than those of the LPS lamp, but by 12-

15% lower values in comparison with the HPS lamp. When compared to common white pc LEDs, the short-distance Rayleigh scattering effect of the firelight LED cluster is smaller by a factor of 1.7 to 5.2 depending on the type of pc LED and adaptation luminance it provides with.

Table 5.4. Mesopic Rayleigh skyglow indices of the light sources [P12].

Light source	General visual index (M)GVI$_A$			Filtered visual index (M)FVI$_A$			Filtered instrumental index (M)FII$_A$		
	0.1 cd/m^2	2 cd/m^2	Pho-topic	0.1 cd/m^2	2 cd/m^2	Pho-topic	0.1 cd/m^2	2 cd/m^2	Pho-topic
LPS lamp	0.13	0.10	0.09	0.00	0.00	0.00	0.00	0.00	0.00
HPS lamp	0.40	0.35	0.34	0.29	0.25	0.24	0.29	0.25	0.24
Firelight LED cluster	**0.35**	**0.30**	**0.29**	**0.17**	**0.15**	**0.14**	**0.23**	**0.19**	**0.19**
Candlelight pc LED	0.58	0.55	0.55	0.50	0.48	0.48	0.53	0.51	0.51
Warm white pc LED	0.77	0.81	0.82	0.73	0.77	0.78	0.77	0.81	0.82
Cool white pc LED	0.89	0.98	1.01	0.79	0.87	0.90	0.96	1.06	1.09
Daylight white pc LED	1.16	1.44	1.52	1.13	1.41	1.49	1.39	1.73	1.83
CIE standard illuminant A	0.87	0.97	1	0.87	0.97	1	0.87	0.97	1

For MFVI$_A$, the effect of the LPS lamp can be completely eliminated, whereas the firelight LED cluster performs even better than in the general case. The reduction of MFVI$_A$ in respect of the HPS lamps is by about 40% and by a factor of 2.9 to 6.4 in respect of the common white pc LEDs. For filtered instrumental Raleigh skyglow (MFII$_A$), the reduction is by about 20% in respect of the HPS lamp and by a factor of 2.3 to 5.7 for the common white pc LEDs, respectively. For filtered skyglow, the impact of the firelight LED cluster can be reduced even more at an expense of observed luminance or detected radiance provided that an optical filter with a narrower band, e. g. 480-520 nm is used.

5.3.4. Eye lens yellowing

For outdoor lighting applications, the effect of reduced retinal illuminance due to the yellowing of the lens of the human eye with age can be quantified by the mesopic lens yellowing index MLYI, which is defined as follows

$$\mathrm{MLYI}_{\mathrm{age}} = \frac{\int_{380}^{780} V_{\mathrm{mes}}(\lambda) T_{\mathrm{age}}(\lambda) S(\lambda) d\lambda}{\int_{380}^{780} V_{\mathrm{mes}}(\lambda) T_{25}(\lambda) S(\lambda) d\lambda}, \tag{5.9}$$

where $T_{age}(\lambda)$ and $T_{25}(\lambda)$ are the transmission spectra of the lens of the human eye at a particular age and at an age of 25, respectively. Figure 5.3 shows the transmission spectra of the lens at ages of 50 and 75 normalized to that at an age of 25 [141,156].

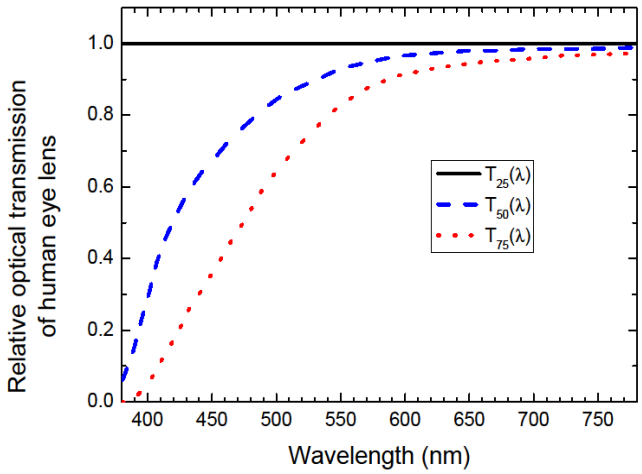

Fig. 5.3. Normalized transmission spectra of the lens of the human eye at ages of 25 (solid line), 55 (dashed line), and 75 (dotted line). After [141,156] [P12].

Table 5.5 presents the results of the assessment of light sources by MLYI for ages 50 and 75. Basically for all sources, some reduction in retinal illuminance is found with reducing the ambient luminance due to the shift of the luminous efficiency function to shorter wavelengths. This effect is seen to be higher for blue-enriched SPDs. The firelight LED cluster performs very similarly to sodium based sources showing a reduction of transmittivity due to the yellowing by factors of 0.94 and 0.87 at the lowest mesopic luminance of 0.1 cd/m^2 for ages of 50 and 75, respectively. For common pc white LEDs, the MLYI has smaller values depending on the CCT and age. For instance at a luminance of 0.1 cd/m^2, the MLYI of the firelight LED cluster is higher by 8% and 19% in respect of the daylight pc LED for ages of 50 and 75, respectively. Although these differences might appear small, they might be comparable to the differences between luminances specified for adjacent road lighting classes (form 33% to 67%).

Table 5.5. Mesopic eye lens yellowing indices of the light sources. Characteristics and number of observers [P12].

Light source	CCT(K)	$MLYI_{50}$			$MLYI_{75}$		
		0.1 cd/m^2	2 cd/m^2	photopic	0.1 cd/m^2	2 cd/m^2	photopic
LPS lamp	1814	0.96	0.96	0.96	0.90	0.90	0.90
HPS lamp	1886	0.94	0.95	0.96	0.86	0.89	0.89
Firelight LED cluster	**1859**	**0.94**	**0.95**	**0.96**	**0.87**	**0.89**	**0.89**
Candlelight pc LED	2001	0.93	0.94	0.95	0.83	0.87	0.87
Warm white pc LED	2725	0.91	0.93	0.94	0.80	0.85	0.86
Cool white pc LED	3991	0.90	0.93	0.93	0.77	0.83	0.84
Daylight white pc LED	6084	0.87	0.91	0.93	0.73	0.81	0.83
CIE standard illuminant A	2854	0.90	0.93	0.94	0.78	0.84	0.85

5.4. Psychophysical assessment

The psychophysical assessment of the firelight LED cluster was carried out by comparing it to the almost metameric HPS lamp, which is a well-established light source for outdoor lighting, within the visual performance based approach under mesopic visual conditions [157,158]. Three visual performance tasks that are the most relevant to night-time driving and pedestrian walking and are commonly applied for the comparative studies of different outdoor light sources were selected as follows: detection response to a visual stimulus [102,103,159,160], contrast discrimination [99,102,160,161], and colour discrimination [156,162,163]. In this work the three tasks were executed by the measurements of reaction time and correct detection rate, the detection threshold of achromatic contrast, and the error rate in the F-M 100-hue test, respectively.

The experiments were performed for four photopic adaptation luminance values of 0.1, 0.3, 1.0 and 3.0 cd/m^2 covering the upper part of the mesopic region, which is important for night-time driving and pedestrian walking. The corresponding mesopic luminances within the MES-2 photometric system [146] equalled 0.084, 0.275, 0.953 and 2.948 cd/m^2 for the HPS lamp and 0.081, 0.272, 0.947 and 2.942 cd/m^2 for the firelight LED cluster, respectively, i.e. differed by less than 4% and by 0.2% at the lowest and highest luminance used, respectively.

The two sources of light were mounted on top of two respective experimental cabinets (80 cm height by 70 cm width by 70 cm depth) with neutral grey matted interior and ceiling made of Plexiglas. The ceiling was used for uniformly

distributing luminance over the walls of the cabinets (with an unevenness of less than 5% at the bottom surface of a cabinet) and for colour mixing (the chromaticity point was maintained within a distance of xy~0.005 across the bottom surface of a cabinet). The luminance was controlled by a diaphragm and an additional frosted glass filter placed between a lamp and the ceiling and monitored by an imaging photometer-colorimeter (Instruments Systems model LumiCam 1300 Color).

A homogeneous group of four thoroughly instructed and well trained young subjects took part in the experiment. Of those one was female and three were males; the age ranged from 22 to 25 in order to avoid the effects related to the yellowing of the human eye lens. All subjects had normal or corrected to normal visual acuity and normal colour vision tested by the F-M 100-hue test under photopic conditions. Subjects sat next to the cabinet placed in a dark room with the head fully immersed into the cabinet in order to ensure 180 deg. adaptation to the visual field. For each subject, experiments were performed with the luminance level gradually incremented form the lowest one to the highest one within multiple sessions that were scheduled at different days. In each session the lamps were presented in a random sequence. Before starting the measurements observers adapted to the illuminance level of the background for a minimum of 10 min at a luminance of 0.1 cd/m^2 and then for a minimum of 5 min for each higher luminance level, which are typical times of adaptation to mesopic luminance conditions [164].

The results of the experiments on the three tasks were aggregated for all subjects and execution sessions and the mean values and 95% confidence intervals were calculated for each luminance/source condition as presented by data points and error bars in the figures below. The significance of the differences between each pair of data points for the two sources were analysed using a t-test.

5.4.1. Reaction time

For the measurement of reaction time, a rotating stimulus placed with 18 deg. right peripheral eccentricity within a cabinet was used. In order to maintain the eccentricity, the head of observer was mildly restrained within a chinrest and the view was positioned at a fixation point centred on the back wall of the cabinet at a distance of 60 cm. The stimulus comprised an achromatic circular patch with a luminance similar to that of the cabinet interior and with a centred darker rectangular bar (2 by 0.5 deg. of visual angle, which is relevant to driving tasks; see insert in Fig. 5.4). The Weber contrast $(L_b - L_p)/L_p$ of the bar to patch background, as calculated basing on the measurement results provided by the imaging photometer-colorimeter, equaled –0.3 (L_b and L_p are the bar and patch background luminances, respectively). The patch was mounted on a computer controlled stepper motor that moved clockwise or anticlockwise into two random positions tilted by 45 deg. in respect of the vertical (characterized as "right" and "left," respectively) within random intervals of 5 to 15 s. Once subject noticed the motion (120 ms long) he/she ought to execute a simple decision making task by pressing a respective button of a computer mouse and the reaction time in respect of the termination of the motion was recorded. A detection error was recorded if no correct response was received in 1500 ms on the first attempt. Each of four subjects executed seven sessions with 40 repeated measurements for each luminance level provided by each source.

Figure 5.4 displays the dependence of reaction time on photopic luminance for the achromatic off-axis stimulus under lighting conditions provided by the firelight LED cluster (rectangles) and HPS lamp (circles). Each point presents a mean of 280 attempts for each of four subjects (1120 attempts in total). The reaction time increases from about 380 ms to about 560 ms with decreasing adaptation luminance from 3 to 0.1 cd/m^2. The results for the two sources show no statistically significant differences at luminances of 0.1 and 1 cd/m^2 ($p > 0.15$) and small differences with a moderate significance at luminances of 0.3 and 3 cd/m^2 ($p = 0.036$ and $p = 0.044$, respectively) can be resolved. These measured values of reaction time are larger and exhibit a stronger dependence on

luminance than those measured for a HPS lamp for an off-axis stimulus without decision making (~240-270 ms [76]) and smaller than those measured using a driving simulator (~650-800 ms [160]).

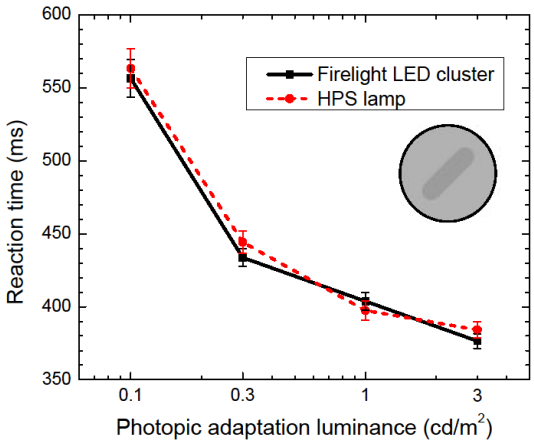

Fig. 5.4. Time of reaction to the achromatic off-axis rotating stimulus as a function of photopic adaptation luminance for the firelight LED cluster (rectangles) and HPS lamp (circles). The error bars show the 95% confidence intervals. The lines are a guide for the eye. The insert displays an image of the rotating stimulus [P12].

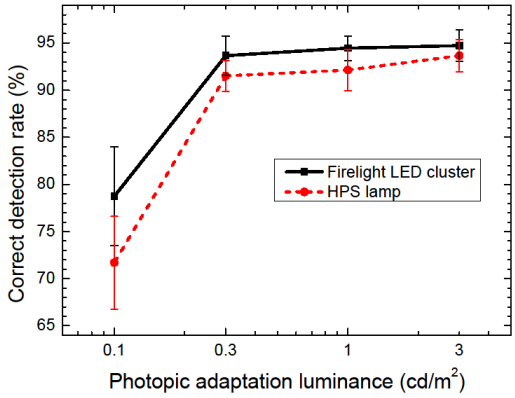

Fig. 5.5. Rate of the correct detection of the achromatic off-axis rotating stimulus as a function of photopic adaptation luminance for the firelight LED cluster (rectangles) and HPS lamp (circles). The error bars show the 95% confidence intervals. The lines are a guide for the eye [P12].

Figure 5.5 shows the corresponding dependence of the correct detection rate as a function of photopic adaptation luminance for the firelight LED cluster (rectangles) and HPS lamp (circles). Each point presents a mean of 28 sessions. These data are in line with similar measurements for an HPS lamp [160]. At adaptation luminances of 0.3-3 cd/m^2, the correct detection rate has values around 93% with no statistically significant difference ($p > 0.06$) between the two light sources. At a luminance of 0.1 cd/m^2 a drop of the correct detection rate is observed for both sources with a score of 79% vs. 72% in favor of the

firelight LED cluster, but the difference has a low statistical significance (p = 0.049).

Our results show that the two sources are almost identical in terms of response to the off-axis achromatic stimulus despite a difference of SPDs (less structured spectrum of the LED cluster as compared to the HPS lamp). This can be attributed to that the S/P ratio and CCT of the two sources are almost equal and provide with both similar involvement of the peripheral retinal receptors into generating a detection response to a visual stimulus and with similar colour appearance of achromatic background and target.

5.4.2. Detection thresholds of luminance contrast

The measurement of the detection thresholds of luminance contrast was performed in the same cabinets. The thresholds were estimated using four sets of 45 circular patches similar to that used in the reaction time measurement (see the insert in Fig. 5.4), each containing a bar (2 by 0.5 deg. of visual angle) with different Weber luminance contrasts. The patches were arranged into 5x9 tables with sequential increase of Weber contrast from about –0.3 to +0.3 with comparable increments of 0.014 on the average. The bars were tilted by ±45 deg. in a random sequence and each of four tables differed in the randomization of the tilting. The tables were printed on A5 format matted photo paper with 256 bit contrast resolution. The tables were placed on the bottom surface of the cabinets. After adaptation subjects had to choose two patches with the lowest detected opposite (positive and negative) luminance contrast and tell the orientation and number indicated below them. The detection threshold was estimated as an average of the moduli of the two contrasts. Each subject executed five sessions with each of four tables for each specific luminance/source condition without limiting the execution time. During a session the tables were presented in a random sequence.

The two light sources were found to have very similar properties in terms of achromatic contrast discrimination. Figure 5.6 shows the detection threshold of luminance contrast as a function of photopic adaptation luminance for our

targets. Each point presents a mean of 20 attempts for each of four subjects (80 attempts in total). The threshold contrast is seen to increase from about 0.025 to about 0.05 when the background luminance decreases from 3 to 0.1 cd/m^2 with no statistically significant difference between the values obtained for the two sources ($p \geq 0.07$). This variation is in line with the well-known results on contrast discrimination [165,166], although it has a much larger span than that obtained for a HPS lamp using large (10 by 13 deg.) grating targets [102]. Our data imply that contrast discrimination does not depend on SPD at least for metameric sources with almost equal S/P ratio.

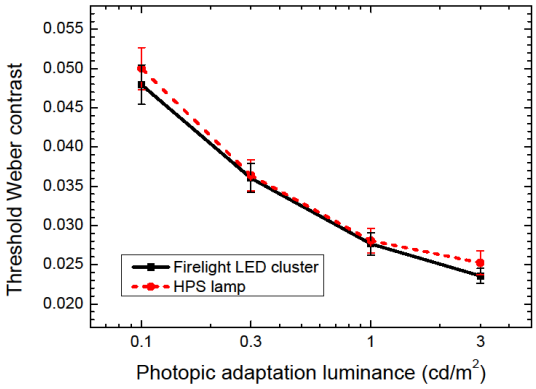

Fig. 5.6. Detection threshold of luminance contrast as a function of photopic adaptation luminance for the firelight LED cluster (rectangles) and HPS lamp (circles). The error bars show the 95% confidence intervals. The lines are a guide for the eye [P12].

5.4.3. Fransworth-Munsell 100-hue test

The F-M 100-hue test [167] was carried out within the above described cabinets. The test consists of 85 coloured caps, which are numbered in sequence and have colours that differ in small increments. The task of a subject is to arrange the caps in the correct hue sequence within four boxes that have two anchor caps at each end. The output of the test is the error score, which is a sum of the absolute differences between the numbers of the arranged caps and the numbers of the adjacent caps with 2 points deduced for each cap. Each subject repeated the test 6 times in different sessions for all specific luminance/source conditions. The execution time was not limited.

Differently from detection response and contrast discrimination, the firelight LED cluster exhibited a noticeable improvement in colour discrimination

against the HPS lamp. Figure 5.7 shows the F-M 100-hue test error score as a function of photopic adaptation luminance for the two light sources. Each point presents a mean of 6 trials for each of four subjects (24 trials in total). The results for the HPS lamp and firelight LED cluster show a gradual increase of the error score from about 205 to 310 and from about 165 to 300, respectively, when the adaptation luminance is reduced from 3 to 0.1 cd/m^2. At an adaptation luminance of 3 cd/m^2 the estimated error scores for both sources are much higher than those for typical fluorescent lamps (30-70) [17]. At a luminance of 0.1 cd/m^2 they exceed those obtained under high-quality daylight illuminant (~100 [168]) by a factor of about 3. However with exception of the lowest luminance of 0.1 cd/m^2, where the two sources show no significant difference (p = 0.3), the error score for the firelight LED cluster is lower than that for the HPS lamp in the rest part of the adaptation luminance range (0.3–3 cd/m^2) with a high statistical significance of the difference (p < 0.003).

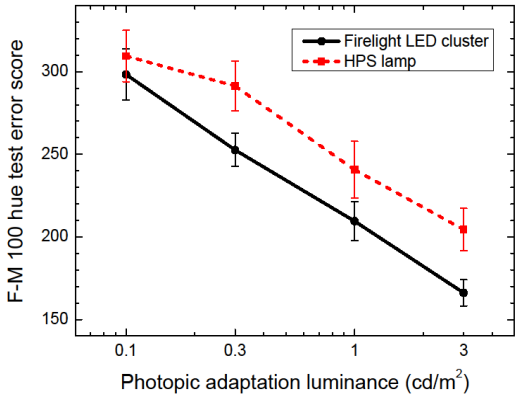

Fig. 5.7. Farnsworth-Munsell 100-hue test error score as a function of photopic adaptation luminance for the firelight LED cluster (rectangles) and HPS lamp (circles). The error bars show the 95% confidence intervals. The lines are a guide for the eye [P12].

It is to be noted that the reduction of colour discrimination of human vision in the mesopic region does not allow for comparing the error scores of the F-M 100-hue test estimated at different mesopic luminances on the absolute scale. (In fact, such comparing requires a refinement of the F-M 100-hue test by rarefying the set of coloured caps for particular luminances in such a way that the hue increments were matched with the altered colour discrimination ability.) Despite this limitation, the increase of the F-M 100-test error score with reducing

adaptation luminance can be understood in terms of the reduction of colour discrimination of human vision in the mesopic region [56]. At the same time the improved colour discrimination properties of the firelight LED cluster in respect of the HPS lamp can be attributed to the reduced colour shifts and less shrunk gamut represented by higher R_a and GAI values, respectively, as well as by somewhat smaller percentages of colours rendered with reduced chroma and distorted hue and lightness (see Table 5.2).

5.5. Conclusions of the fifth chapter

A balanced approach to the performance of solid-state lighting for outdoor environments has been demonstrated by introducing a practical blue–amber LED cluster optimized for mesopic conditions, which is a solid-state metamer of HPS lamp.

When compared with common white LEDs, the firelight LED cluster shows considerably reduced indexes of melatonin suppression and skyglow, increased retinal illuminance for elderly people, but a reduced performance of perceiving colours, which, however, can be tolerated at mesopic luminance.

In comparison with an almost metameric high-pressure sodium lamp, the cluster exhibits a potentially higher luminous efficacy, similar reaction time and detection threshold of luminance contrasts for achromatic targets, and noticeably improved colour discrimination characteristics.

Concluding summary

The tetrachromatic (RAGB) solid-state lighting engine with continuously tuneable colour rendition properties has been developed. The psychophysiological investigation revealed that by tuning colour rendition engine, subjects, confidently lighting with the highest values of the corresponding indexes of the statistical colour rendition metric. “Preferential” lighting conditions were identified as those in between “most saturated” and “most natural.”

The preferences to colour quality of illumination have been investigated for two representative groups of subjects with different cultural background using the colour rendition engine with the continuously tuneable colour saturation ability and CCT of quadrichromatic blends. Differently from very familiar objects, paintings exhibited cultural differences in the average selected blends depending on the level of the familiarity of the content. The most unfamiliar painting also showed preferences to CCT being dependent on the cultural background. In all cases, the width of the distribution of the selection rates was found to depend on the cultural background of a group of subjects.

The lighting engine with a controlled photochemical irradiance has been introduced. The effect of constant damage irradiance on the visual impression from artworks while operating the lighting engine in different modes (selection of chroamticity and colour-rendition properties), which can be used for attaining the most appropriate visual appearance of an artwork, was demonstrated.

For an intelligent street lighting installation, the assessment of seven lighting patterns by SDS and Likert scaling revealed two factors that need to be considered when assessing intelligent outdoor lighting installations: a major factor that is related to the subjective feeling of well-being and a minor factor that is related to the physical properties of the environment. The mean of the first factor scores primarily depends on the flux of lamp of the first post, whereas for equal fluxes of the first post, the fluxes of the remote posts are less important.

A blue-orange (“firelight) LED cluster with extra-low CCT (~1860 K) optimized for outdoor lighting under mesopic conditions has been introduced.

When compared with common white LEDs, the firelight LED cluster shows considerably reduced indexes of melatonin suppression and skyglow, increased retinal illuminance for elderly people, but a reduced performance of perceiving colours, which, however, can be tolerated at mesopic luminance. In comparison with an almost metameric high-pressure sodium lamp, the cluster exhibits a potentially higher luminous efficacy, similar reaction time and detection threshold of luminance contrasts for achromatic targets, and noticeably improved colour discrimination characteristics.

References

1. H. J. Round, "A note on carborundum," Electr. World **49**, 309 (1907).
2. Commission Internationale de l'Éclairage, "Colour rendering of white LED sources," Pub. CIE 177, 2007.
3. A. Žukauskas, R. Vaicekauskas, F. Ivanauskas, H. Vaitkevičius, P. Vitta, and M. S. Shur, "Statistical approach to color quality of solid-state lamps," IEEE J. Select. Topics Quantum Electron. **15**, 1753–1762 (2009).
4. Commission Internationale de l'Éclairage, "Method of measuring and specifying colour rendering properties of light sources," Pub. CIE 13.3, 1995.
5. G. Wyszecki and W. S. Stiles, *Color Science: Concepts and Methods, Quantitative Data and Formulae* (Wiley, 2000).
6. N. Sándor and J. Schanda, "Visual colour rendering based on colour difference evaluations," Lighting Res. Technol. **38**, 225–239 (2006).
7. M. R. Luo, G. Cui, and C. Li, "Uniform colour spaces based on CIECAM02 colour appearance model," Color Res. Appl. **31**, 320–330 (2006).
8. C. Li, M. R. Luo, G. Cui, and C. Li, "Evaluation of the CIE colour rendering index," Color. Technol. **127**, 129–135 (2011).
9. D. B. Judd, "A flattery index for artificial illuminants," Illuminating Engineering **62**, 593–598 (1967).
10. W. A. Thornton, "Color-discrimination Index," J. Opt. Soc. Am. **62**, 191–194 (1972).
11. W. A. Thornton, "A validation of the color-preference index," J. Illum. Eng. Soc. **4**, 48–52 (1974).
12. S. M. Aston and H. E. Bellchambers, "Illumination, color rendering, and visual clarity," Lighting Res. Technol. **1**, 259–261 (1969).
13. K. Hashimoto and Y. Nayatani, "Visual clarity and feeling of contrast," Color Res. Appl. **19**, 171–185 (1994).
14. H. Xu, "Color-rendering capacity of illumination," J. Opt. Soc. Am. **73**, 1709–1713 (1983).
15. Y. Nakano, H. Tahara, H. Suehara, J. Kohda, and T. Yano, "Application of multispectral camera to color rendering simulator," in *Proceedings of 10th Congress of the International Colour Association*, J. L. Nieves and J. Hernandez-Andres, eds., pp. 1625–1628 (2005).
16. K. Hashimoto, T. Yano, M. Shimizu, and Y. Nayatani, "New method for specifying color-rendering properties of light sources based on feeling of contrast," Color Res. Appl. **32**, 361–371 (2007).
17. M. S. Rea and J. P. Freyssinier-Nova, "Color rendering: A tale of two metrics," Color Res. Appl. **33**, 192–202 (2008).
18. M. S. Shur and A. Žukauskas, "Solid-state lighting: Toward superior illumination," Proc. IEEE **93**, 1691–1703 (2005).
19. N. Narendran and L. Deng, "Color rendering properties of LED light sources," Proc. SPIE **4776**, 61–67 (2002).
20. I. Shakir and N. Narendran, "Evaluating white LEDs for outdoor landscape lighting application," Proc. SPIE **4776**, 162–170 (2002).
21. S. Jost-Boissard, M. Fontoynont, and J. Blanc-Gonnet, "Perceived lighting quality of LED sources for the presentation of fruit and vegetables," J. Mod. Opt. **56**, 1420–1432 (2009).
22. S. Boissard and M. Fontoynont, "Optimization of LED-based light blendings for object presentation," Color Res. Appl. **34**, 310–320 (2009).
23. M. S. Rea and J. P. Freyssinier, "Color rendering: Beyond pride and prejudice," Color Res. Appl. **35**, 401–409 (2010).
24. K. A. G. Smet, W. R. Ryckaert, M. R. Pointer, G. Deconinck, and P. Hanselaer, "Memory colours and colour quality evaluation of conventional and solid-state lamps," Opt. Express **18**, 26229–26244 (2010).

25. W. Davis and Y. Ohno, “Toward an improved color rendering metric,” Proc. SPIE **5941**, 59411G (2005).
26. K. Smet, W. R. Ryckaert, M. R. Pointer, G. Deconinck, and P. Hanselaer, “Colour appearance rating of familiar real objects,” Color Res. Appl. **36**, 192–200 (2010).
27. W. Davis and Y. Ohno, “Color quality scale,” Opt. Eng. **49**, 033602 (2010).
28. P. van der Burgt and J. van Kemenade, “About color rendition of light sources: The balance between simplicity and accuracy,” Color Res. Appl. **35**, 85–93 (2010).
29. A. Žukauskas, R. Vaicekauskas, and M. S. Shur, “Colour-rendition properties of solid-state lamps,” J. Phys. D. Appl. Phys. **43**, 354006 (2010).
30. D. L. Macadam, “Visual sensitivities to color differences in daylight,” J. Opt. Soc. Am. **32**, 247-273 (1942).
31. A. Žukauskas, M. S. Shur, and R. Gaska, *Introduction to Solid-State Lighting* (Wiley, 2002).
32. R. Vaicekauskas and A. Žukauskas, “LEDs in lighting with tailored color quality,” Int. J. High Speed Electron. Systems **20**, 287–301 (2011).
33. A. Žukauskas, R. Vaicekauskas, and M. Shur, “Solid-state lamps with optimized color saturation ability,” Opt. Express **18**, 2287–2295 (2010).
34. Y. Ohno, “Spectral design considerations for white LED color rendering,” Opt. Eng. **44**, 111302 (2005).
35. V. Viliūnas, H. Vaitkevičius, R. Stanikūnas, A. Švegžda, and Z. Bliznikas, “LED-based metameric light sources: Rendering the colours of objects and other colour quality criteria,” Lighting Res. Technol. **43**, 321–330 (2011).
36. A. Žukauskas, R. Vaicekauskas, F. Ivanauskas, H. Vaitkevičius, and M. S. Shur, “Rendering a color palette by light-emitting diodes,” Appl. Phys. Lett. **93**, 021109 (2008).
37. W. A. Thornton, “Luminosity and color-rendering capability of white light,” J. Opt. Soc. Am. **61**, 1155–1163 (1971).
38. E. F. Schubert, *Light-Emitting Diodes* (Cambridge University Press, 2003).
39. A. Žukauskas, R. Vaicekauskas, and M. Shur, “Color-dulling solid-state sources of light,” Opt. Express **20**, 9755–9762 (2012).
40. E. Mahler, J.-J. Ezrati, and F. Viénot, “Testing LED lighting for colour discrimination and colour rendering,” Color Res. Appl. **34**, 8–17 (2009).
41. R. S. Berns, “Designing white-light LED lighting for the display of art: A feasibility study,” Color Res. Appl. **36**, 324–334 (2011).
42. P. D. Pinto, P. E. R. Felgueiras, J. M. M. Linhares, and S. M. C. Nascimento, “Chromatic effects of metamers of D65 on art paintings,” Ophthalmic Physiol. Opt. **30**, 632–637 (2010).
43. R. Küller, S. Ballal, T. Laike, B. Mikellides, and G. Tonello, “The impact of light and colour on psychological mood: a cross-cultural study of indoor work environments,” Ergonomics **49**, 1496–1507 (2006).
44. R. B. Hupka, Z. Zaleski, J. Otto, L. Reidl, and N. V. Tarabrina, “The colors of anger, envy, fear, and jealousy: A cross-cultural study,” J. Cross Cult. Psychol. **28**, 156–171 (1997).
45. X.-P. Gao, J. H. Xin, T. Sato, A. Hansuebsai, M. Scalzo, K. Kajiwara, S.-S. Guan, J. Valldeperas, M. J. Lis, and M. Billger, “Analysis of cross-cultural color emotion,” Color Res. Appl. **32**, 223–229 (2007).
46. L.-C. Ou, M. Ronnier Luo, P.-L. Sun, N.-C. Hu, H.-S. Chen, S.-S. Guan, A. Woodcock, J. L. Caivano, R. Huertas, A. Treméau, M. Billger, H. Izadan, and K. Richter, “A cross-cultural comparison of colour emotion for two-colour combinations,” Color Res. Appl. **37**, 23–43 (2012).
47. Y. Mizokami, C. Kamesaki, N. Ito, S. Sakaibara, and H. Yaguchi, “Effect of spatial structure on colorfulness adaptation for natural images,” J. Opt. Soc. Am. A **29**, A118–A127 (2012).

48. S. M. Newhall, R. W. Burnham, and J. R. Clark, “Comparison of Successive with Simultaneous Color Matching,” J. Opt. Soc. Am. **47**, 43–54 (1957).
49. O. Masuda and S. M. Nascimento, “Best lighting for naturalness and preference,” J. Vis. **13**, 4 (2013).
50. S. M. C. Nascimento and O. Masuda, “Psychophysical optimization of lighting spectra for naturalness, preference, and chromatic diversity,” J. Opt. Soc. Am. A **29**, A144–A151 (2012).
51. G. Hofstede, G. J. Hofstede, and M. Minkov, *Cultures and Organizations: Software of the Mind, Third Edition* (McGraw-Hill, 2010).
52. F. Viénot, G. Coron, and B. Lavédrine, “LEDs as a tool to enhance faded colours of museums artefacts,” J. Cult. Herit. **12**, 431–440 (2011).
53. M. Scuello, I. Abramov, J. Gordon, and S. Weintraub, “Museum lighting: Optimizing the illuminant,” Color Res. Appl. **29**, 121–127 (2004).
54. G. Thomson, *The Museum Environment* (Butterworth-Heinemann, 1986).
55. C. Cuttle, *Light for Art's Sake: Lighting for Artworks and Museum Displays* (Routledge, 2007).
56. W. R. J. Brown, “The influence of luminance level on visual sensitivity to color differences,” J. Opt. Soc. Am. **41**, 684–688 (1951).
57. W. A. Thornton, “Fluorescent lamps with high color-discrimination capability,” J. Illum. Eng. Soc. **3**, 61–64 (1973).
58. R. H. Lafontaine, “Seeing through a yellow varnish: a compensating illumination system,” Stud. Conserv. **31**, 97–102 (1986).
59. G. Thomson, “A new look at colour rendering, level of illumination, and protection from ultraviolet radiation in museum lighting,” Stud. Conserv. **6**, 49–70 (1961).
60. G. Thomson, “Annual exposure to light within museums,” Stud. Conserv. **12**, 26–36 (1967).
61. B. H. Crawford, “Just perceptible colour differences in relation to level of illumination,” Stud. Conserv. **18**, 159–166 (1973).
62. D. L. Loe, E. Rowlands, and N. F. Watson, “Preferred lighting conditions for the display of oil and watercolour paintings,” Lighting Res. Technol. **14**, 173–192 (1982).
63. Illuminating Engineering Society of North America, *Museum and Art Gallery Lighting: A Recommended Practice* (IESNA, 1996).
64. Commission Internationale de l’Éclairage, “Control of damage to museum objects by optical radiation,” Pub. CIE 157, 2004.
65. C. Cuttle, “A proposal to reduce the exposure to light of museum objects without reducing illuminance or the level of visual satisfaction of museum visitors,” J. Amer. Inst. Conserv. **39**, 229–244 (2000).
66. L. S. Harrison, *Report on the Deteriorating Effects of Modern Light Sources* (Metropolitan Museum of Art, 1953).
67. G. S. Hilbert, S. Aydinli, and J. Krochmann, “Zur Beleuchtung musealer Exponate,” Restauro **97**, 313–321 (1991).
68. D. Saunders and J. Kirby, “Wavelength-dependent fading of artists' pigments,” Stud. Conserv. **39**, 190–194 (1994).
69. C. Cuttle, “Damage to museum objects due to light exposure,” Lighting Res. Technol. **28**, 1–9 (1996).
70. C. Cuttle, “Lighting works of art for exhibition and conservation,” Lighting Res. Technol. **20**, 43–53 (1988).
71. M. Scuello and I. Abramov, “Museum lighting: Why are some illuminants preferred,” J. Opt. Soc. Am. A **21**, 306–311 (2004).
72. P. D. Pinto, J. M. M. Linhares, and S. M. C. Nascimento, “Correlated color temperature preferred by observers for illumination of artistic paintings,” J. Opt. Soc. Am. A **25**, 623–630 (2008).

73. P. D. Pinto, J. M. M. Linhares, J. A. Carvalhal, and S. M. C. Nascimento, "Psychophysical estimation of the best illumination for appreciation of Renaissance paintings," Visual Neurosci. **23**, 669–674 (2006).
74. S. M. C. Nascimento and O. Masuda, "Best lighting for visual appreciation of artistic paintings-experiments with real paintings and real illumination," J. Opt. Soc. Am. A **31**, A214–A219 (2014).
75. A. A. Kruithof, "Tubular luminescence lamps for general illumination," Philips Tech. Rev. **6**, 65–73 (1941).
76. F. Viénot, M.-L. Durand, and E. Mahler, "Kruithof's rule revisited using LED illumination," J. Mod. Opt. **56**, 1433–1446 (2009).
77. C. Richardson and D. Saunders, "Acceptable light damage: A preliminary investigation," Stud. Conserv. **52**, 177–187 (2007).
78. M. F. Delgado, C. W. Dirk, J. Druzik, and N. WestFall, "Lighting the world's treasures: Approaches to safer museum lighting," Color Res. Appl. **36**, 238–254 (2011).
79. W. A. Thornton, "The high visual efficiency of prime color lamps," Lighting Des. Appl. **5**, 35–41 (1975).
80. J. M. M. Linhares, P. E. R. Felgueiras, P. D. Pinto, and S. M. C. Nascimento, "Colour rendering of indoor lighting with CIE illuminants and white LEDs for normal and colour deficient observers," Ophthalmic Physiol. Opt. **30**, 618 (2010).
81. A. Žukauskas, R. Vaicekauskas, F. Ivanauskas, R. Gaska, and M. S. Shur, "Optimization of white polychromatic semiconductor lamps," Appl. Phys. Lett. **80**, 234–236 (2002).
82. O. Masuda and S. M. C. Nascimento, "Lighting spectrum to maximize colorfulness," Opt. Lett. **37**, 407–409 (2012).
83. D. Vazquez-Molini, A. Alvarez Fernandez-Balbuena, A. Garcia Botella, J. A. Herraez, M. Del Egido, and R. Ontañon, "Advanced LED lighting system applied to cultural heritage goods," in *Colour and Light in Architecture*, P. Zennaro, ed. pp. 341–348 (2010).
84. S. Muthu, F. J. P. Schuurmans, and M. D. Pashley, "Red, green, and blue LEDs for white light illumination," IEEE J. Select. Topics Quantum Electron. **8**, 333–338 (2002).
85. P. R. Boyce, S. Fotios, and M. Richards, "Road lighting and energy saving," Lighting Res. Technol. **41**, 245–260 (2009).
86. F. Li, D. Chen, X. Song, and Y. Chen, "LEDs: A promising energy-saving light source for road lighting," in *Proceedings of the Asia-Pacific Power and Energy Engineering Conference*, pp. 2798–2800 (2009).
87. A. Žukauskas, R. Vaicekauskas, and P. Vitta, "Optimization of solid-state lamps for photobiologically friendly mesopic lighting," Appl. Opt. **51**, 8423–8432 (2012).
88. T. Taguchi, Y. Uchida, T. Setomoto, and K. Kobashi, "Application of white LED lighting to energy-saving-type street lamps," Proc. SPIE **4278**, 7–12 (2001).
89. Y. A. W. de Kort, A. Haans, L. M. Geerdinck, D. A. P. van Gennip, M. Horst, and J. H. M. Servaes, "Psychological building blocks for dynamic road lighting: Understanding light's role in feelings of safety at night," in *Proceedings of the 12th International Symposium on the Science and Technology of Light Sources and the 3rd International Conference on White LEDs and Solid State Lighting*, M. Haverlag, G. M. W. Kroesen, and T. Tagushi, eds., pp. 529–530 (2010).
90. M. Mendalka, M. Gadaj, L. Kulas, and K. Nyka, "WSN for intelligent street lighting system," in *2nd International Conference on Information Technology*, pp. 99–100 (2010).
91. C. Atici, T. Ozcelebi, and J. J. Lukkien, "Exploring user-centered intelligent road lighting design: a road map and future research directions," IEEE T. Consum. Electr. **57**, 788–793 (2011).
92. D. Schreuder, *Outdoor Lighting: Physics, Vision and Perception: Physics, Vision and Perception* (Springer, 2008).
93. P. R. Boyce, *Lighting for Driving: Roads, Vehicles, Signs, and Signals* (Taylor & Francis, 2008).

94. D. Shinar, *Traffic Safety and Human Behavior* (Elsevier, 2007).
95. R. A. Hargroves, "Road lighting," IEE Review **130**, 420–441 (1983).
96. P. O. Wanvik, "Effects of road lighting: an analysis based on Dutch accident statistics 1987-2006," Accident Anal. Prev. **41**, 123–128 (2009).
97. Commission Internationale de l'Éclairage, "Road lighting as an accident countermeasure," Pub. CIE 93, 1992
98. S. Fotios and C. Cheal, "Predicting lamp spectrum effects at mesopic levels. Part 1: Spatial brightness," Lighting Res. Technol. **43**, 143–157 (2011).
99. S. A. Fotios and C. Cheal, "Predicting lamp spectrum effects at mesopic levels. Part 2: Preferred appearance and visual acuity," Lighting Res. Technol. **43**, 159–172 (2011).
100. P. R. Boyce, N. H. Eklund, B. J. Hamilton, and L. D. Bruno, "Perceptions of safety at night in different lighting conditions," Lighting Res. Technol. **32**, 79–91 (2000).
101. H. Walkey, P. Orreveteläinen, J. Barbur, L. Halonen, T. Goodman, J. Alferdinck, A. Freiding, and A. Szalmás, "Mesopic visual efficiency II: Reaction time experiments," Lighting Res. Technol. **39**, 335–354 (2007).
102. A. L. Lewis, "Visual performance as a function of spectral power distribution of light sources at luminances used for general outdoor lighting," J. Illum. Eng. Soc. **28**, 37–42 (1999).
103. Y. He, M. Rea, A. Bierman, and J. Bullough, "Evaluating light source efficacy under mesopic conditions using reaction times," J. Illum. Eng. Soc. **26**, 125–138 (1997).
104. Y. Lin, W. Chen, D. Chen, and H. Shao, "The effect of spectrum on visual field in road lighting," Build. Environ. **39**, 433–439 (2004).
105. T. Ishida, "Color identification data obtained from photopic to mesopic illuminance levels," Color Res. Appl. **27**, 252–259 (2002).
106. J. Shin, H. Yaguchi, and S. Shioiri, "Change of Color Appearance in Photopic, Mesopic and Scotopic Vision," Optical Review **11**, 265–271 (2004).
107. A. Mayeur, R. Brémond, and J. M. Christian Bastien, "Effects of the viewing context on target detection. Implications for road lighting design," Appl. Ergon. **41**, 461–468 (2010).
108. K. W. Houser and D. K. Tiller, "Measuring the subjective response to interior lighting: Paired comparisons and semantic differential scaling," Lighting Res. Technol. **35**, 183–195 (2003).
109. B. Zhou and Y. Yao, "Evaluating information retrieval system performance based on user preference," J. Intell. Inf. Syst. **34**, 227–248 (2010).
110. E. Cox, "The optimal number of response alternatives for a scale: A review," J. Marketing. Res. **17**, 407–422 (1980).
111. C. H. Coombs, *A Theory of Data* (Wiley, 1964).
112. J. G. Snider and C. E. Osgood, *Semantic Differential Technique: a Sourcebook* (Aldine, 1969).
113. D. K. Tifler and M. S. Rea, "Semantic differential scaling: Prospects in lighting research," Lighting Res. Technol. **24**, 43–51 (1992).
114. W. M. K. Trochim and J. P. Donnelly, *The Research Methods Knowledge Base* (Atomic Dog/Cengage Learning., 2008).
115. L. Loe, K. P. Mansfield, and E. Rowlands, "Appearance of lit environment and its relevance in lighting design: Experimental study," Lighting Res. Technol. **26**, 119–133 (1994).
116. P. R. Boyce, J. A. Veitch, G. R. Newsham, C. C. Jones, J. Heerwagen, M. Myer, and C. M. Hunter, "Lighting quality and office work: two field simulation experiments," Lighting Res. Technol. **38**, 191–223 (2006).
117. S. Mumcu, T. Duzenli, and A. Ozbilen, "Prospect and refuge as the predictors of preferences for seating areas," Sci. Res. Essays **5**, 1223–1233 (2010).
118. S. Fotios and D. Atli, "Comparing judgments of visual clarity and spatial brightness through an analysis of studies using the category rating procedure," Leukos **8**, 261–281 (2012).

119. J. Appleton, *The Experience of Landscape* (Wiley, 1996).
120. K. Lorenz, *King Solomon's Ring: New Light on Animal Ways.* (Methuen, 1964).
121. S. Siegel, *Nonparametric Statistics for the Behavioral Sciences* (McGraw-Hill, 1956).
122. H. Kaiser, "The varimax criterion for analytic rotation in factor analysis," Psychometrika **23**, 187–200 (1958).
123. H. F. Kaiser, "The application of electronic computers to factor analysis," Educ. Psychol. Meas. **20**, 141–151 (1960).
124. J. C. Nunnally and I. H. Bernstein, *Psychometric Theory* (McGraw-Hill, 1994).
125. A. Haans and Y. A. W. de Kort, "Light distribution in dynamic street lighting: Two experimental studies on its effects on perceived safety, prospect, concealment, and escape," J. Environ. Psychol. **32**, 342–352 (2012).
126. E. F. Schubert and J. K. Kim, "Solid-state light sources getting smart," Science **308**, 1274–1278 (2005).
127. International Dark-Sky Association, "Visibility, environmental, and astronomical issues associated with blue-rich white outdoor lighting," 2010.
128. G. C. Brainard, J. P. Hanifin, J. M. Greeson, B. Byrne, G. Glickman, E. Gerner, and M. D. Rollag, "Action spectrum for melatonin regulation in humans: Evidence for a novel circadian photoreceptor," J. Neurosci. **21**, 6405–6412 (2001).
129. K. Thapan, J. Arendt, and D. J. Skene, "An action spectrum for melatonin suppression: evidence for a novel non-rod, non-cone photoreceptor system in humans," J. Physiol.-London **535**, 261–267 (2001).
130. D. M. Berson, F. A. Dunn, and M. Takao, "Phototransduction by retinal ganglion cells that set the circadian clock," Science **295**, 1070–1073 (2002).
131. J. M. Zeitzer, D. J. Dijk, R. E. Kronauer, E. N. Brown, and C. A. Czeisler, "Sensitivity of the human circadian pacemaker to nocturnal light: melatonin phase resetting and suppression," J. Physiol.-London **526**, 695–702 (2000).
132. K. P. Wright, R. J. Hughes, R. E. Kronauer, D. J. Dijk, and C. A. Czeisler, "Intrinsic near-24-h pacemaker period determines limits of circadian entrainment to a weak synchronizer in humans," Proc. Natl. Acad. Sci. U.S.A. **98**, 14027–14032 (2001).
133. S. W. Lockley, G. C. Brainard, and C. A. Czeisler, "High sensitivity of the human circadian melatonin rhythm to resetting by short wavelength light," J. Clin. Endocr. Metab. **88**, 4502–4505 (2003).
134. S. M. Pauley, "Lighting for the human circadian clock: Recent research indicates that lighting has become a public health issue," Med. Hypotheses **63**, 588–596 (2004).
135. G. Glickman, R. Levin, and G. C. Brainard, "Ocular input for human melatonin regulation: Relevance to breast cancer," Neuroendocrinol. Lett. **23**, 17–22 (2002).
136. K. E. West, M. R. Jablonski, B. Warfield, K. S. Cecil, M. James, M. A. Ayers, J. Maida, C. Bowen, D. H. Sliney, M. D. Rollag, J. P. Hanifin, and G. C. Brainard, "Blue light from light-emitting diodes elicits a dose-dependent suppression of melatonin in humans," J. Appl. Physiol. **110**, 619–626 (2011).
137. L. Bellia, F. Bisegna, and G. Spada, "Lighting in indoor environments: Visual and non-visual effects of light sources with different spectral power distributions," Build. Environ. **46**, 1984–1992 (2011).
138. F. Falchi, P. Cinzano, C. D. Elvidge, D. M. Keith, and A. Haim, "Limiting the impact of light pollution on human health, environment and stellar visibility," J. Environ. Manage. **92**, 2714–2722 (2011).
139. C. B. Luginbuhl, P. A. Boley, and D. R. Davis, "The impact of light source spectral power distribution on sky glow," J. Quant. Spectrosc. Radiat. Transfer **139**, 21–26 (2014).
140. K. J. Gaston, T. W. Davies, J. Bennie, and J. Hopkins, "Reducing the ecological consequences of night-time light pollution: options and developments," J. Appl. Ecol. **49**, 1256–1266 (2012).
141. D. Lang, "Energy efficient lighting for the biological clock," Proc. SPIE **7954**, 795402 (2011).

142. P. R. Boyce and C. Cuttle, “Effect of correlated colour temperature on the perception of interiors and colour discrimination performance,” Lighting Res. Technol. **22**, 19–36 (1990).
143. R. G. Davis and D. N. Ginthner, “Correlated color temperature, illuminance level, and the kruithof curve,” J. Illum. Eng. Soc. **19**, 27–38 (1990).
144. A. Zabiliūtė, R. Vaicekauskas, P. Vitta, and A. Žukauskas, “Phosphor converted LEDs with low circadian action for outdoor lighting,” Opt. Lett. **39**, 563–566 (2014).
145. J.-P. Lavalleé and M. Aubé, “Optimized optical filter for LED lighting,” in *Conference on Light Pollution: Theory, Modelling, and Measurements*, pp. 87–97 (2013).
146. Commission Internationale de l’Éclairage, “Recommended system for mesopic photometry based on visual performance,” Pub. CIE 191, 2010.
147. H. F. Ivey, “Color and efficiency of luminescent light sources,” J. Opt. Soc. Am. **53**, 1185–1198 (1963).
148. R. W. Pridmore and M. Melgosa, “Effect of luminance of samples on color discrimination ellipses: Analysis and prediction of data,” Color Res. Appl. **30**, 186–197 (2005).
149. A. Žukauskas and R. Vaicekauskas, “Colour rendering of solid-state sources of light under mesopic conditions,” in *Proceedings of 12th Congress of the International Colour Association*, L. MacDonald, S. Westland, and S. Wuerger, eds., vol. 4., pp. 1737–1740 (2013).
150. R. J. Lucas, S. N. Peirson, D. M. Berson, T. M. Brown, H. M. Cooper, C. A. Czeisler, M. G. Figueiro, P. D. Gamlin, S. W. Lockley, J. B. O'Hagan, L. L. Price, I. Provencio, D. J. Skene, and G. C. Brainard, “Measuring and using light in the melanopsin age,” Trends Neurosci. **37**, 1–9 (2014).
151. D. Gall, “Circadiane Lichtgrößen und deren messtechnische Ermittlung,” Licht **54**, 1292–1297 (2002).
152. M. S. Rea, M. G. Figueiro, A. Bierman, and R. Hamner, “Modelling the spectral sensitivity of the human circadian system,” Lighting Res. Technol. **44**, 386-396 (2012).
153. M. D. Rollag, “Does melanopsin bistability have physiological consequences?” J. Biol. Rhythm. **23**, 396–399 (2008).
154. M. Aube, J. Roby, and M. Kocifaj, “Evaluating potential spectral impacts of various artificial lights on melatonin suppression, photosynthesis, and star visibility,” PLoS One **8**, e67798 (2013).
155. A. Bierman, “Will switching to LED outdoor lighting increase sky glow?” Lighting Res. Technol. **44**, 449–458 (2012).
156. P. L. Turner and M. A. Mainster, “Circadian photoreception: ageing and the eye’s important role in systemic health,” Br. J. Ophthalmol. **92**, 1439–1444 (2008).
157. M. Eloholma, M. Viikari, L. Halonen, H. Walkey, T. Goodman, J. Alferdinck, A. Freiding, P. Bodrogi, and G. Várady, “Mesopic models—from brightness matching to visual performance in night-time driving: A review,” Lighting Res. Technol. **37**, 155–173 (2005).
158. S. Fotios, C. Cheal, and P. Boyce, “Light source spectrum, brightness perception and visual performance in pedestrian environments: A review,” Lighting Res. Technol. **37**, 271–291 (2005).
159. J. D. Bullough and M. S. Rea, “Simulated driving performance and peripheral detection at mesopic and low photopic light levels,” Lighting Res. Technol. **32**, 194–198 (2000).
160. R. Lingard and M. Rea, “Off-axis detection at mesopic light levels in a driving context,” J. Illum. Eng. Soc. **31**, 33–39 (2002).
161. P. R. Boyce and L. D. Bruno, “An evaluation of high pressure sodium and metal halide light sources for parking lot lighting,” J. Illum. Eng. Soc. **28**, 16–32 (1999).
162. P. R. Boyce, “Illuminance, lamp type and performance on a colour discrimination task,” Lighting Res. Technol. **8**, 195–199 (1976).
163. M. P. Royer, K. W. Houser, and A. M. Wilkerson, “Color discrimination capability under highly structured spectra,” Color Res. Appl. **37**, 441–449 (2012).

164. S. Plainis, I. J. Murray, and W. N. Charman, “The role of retinal adaptation in night driving,” Optometry Vision. Sci. **82**, 682–688 (2005).
165. H. R. Blackwell, “Contrast thresholds of the human eye,” J. Opt. Soc. Am. **36**, 624–632 (1946).
166. W. Adrian, “Visibility of targets: Model for calculation,” Lighting Res. Technol. **21**, 181–188 (1989).
167. D. Farnsworth, “The Farnsworth-Munsell 100-hue and dichotomous tests for color vision,” J. Opt. Soc. Am. **33**, 568–574 (1943).
168. K. J. Bowman and B. L. Cole, “A recommendation for illumination of the Farnsworth-Munsell 100-hue test,” Am. J. Optom. Physiol. Opt. **57**, 839–843 (1980).

Curriculum Vitae

Name:	Arūnas
Surname:	Tuzikas
Date of birth;	1983 10 03
Place of birth:	Klaipėda
Nationality:	Lithuanian
E-mail:	arunas.tuzikas@tmi.vu.lt

Education

2000-2002 Klaipėda "Vėtrungė" gymnasium.

2002-2006 Vilnius university, Faculty of physics (Bachelor degree).

2008-2010 Vilnius university, Faculty of physics (Master degree, Cum Laude).

2010-2014 Vilnius university, Faculty of physics, Department of Semiconductor Physics (Ph. D. Student).

Scientific Internships:

2011, 2012 Rensselaer Polytechnic Institute, Centre of Integrated Electronics (Troy, NY, USA).

2013 KaHo Sint-Lieven University, Light and Lighting Laboratory (Ghent, Belgium).